



UNIVERSITÀ DEGLI STUDI DI SALERNO



UNIVERSITÀ DEGLI STUDI DI SALERNO
Dipartimento di Farmacia

Dottorato di ricerca
in Scienze farmaceutiche
Ciclo XIV — Anno di discussione 2016

Coordinatore: Chiar.mo Prof. *Gianluca Sbardella*

***Structural studies, design, identification and
biological evaluation of bioactive compounds***

settore scientifico disciplinare di afferenza: CHIM/06

Dottorando

Dott. *Vincenza Cantone*

Tutore

Chiar.mo Prof. *Giuseppe Bifulco*

Dedicated to the memory of my Father

Preface

My PhD three years course in Pharmaceutical Sciences at the Department of Pharmacy of Salerno University was started in January 2013 under the supervision of Prof. Giuseppe Bifulco. My research activity was mainly focused on structural studies, design, identification and biological evaluation of anti-inflammatory and antitumor molecules potentially utilizable in therapy by means of structure-based drug design, docking studies, QM calculation, cell-free assay and cell-based assay.

These approaches were successfully applied to the identification of new chemical platforms targeting microsomal prostaglandin E₂ synthase (mPGES-1), 5-lipoxygenase (5-LOX), cyclooxygenase-1 (COX-1), cyclooxygenase-2 (COX-2) and G-protein-coupled purinergic receptors (P2Y₁₂R), acting as anti-inflammatory and anti-cancer agents.

The entire work was carried out under the direct supervision of Prof. Giuseppe Bifulco. Furthermore, to improve my knowledge in the biological field, I moved to the Department of Pharmaceutical and Medicinal Chemistry of the Friedrich-Schiller University in Jena (June 2015 until February 2016) under the supervision of the Prof. Oliver Werz. During this period in his research laboratory, my research work was focused on the modulation of 5-LOX activity in the cell-based and cell-free assay, induction of mPGES-1 and determination of PGE₂ synthase activity in microsomes of A549 cells.

In addition to PhD course activities, I was involved in different side projects, mainly regarding the characterization of specific ligand-target interactions involved in inflammation and cancer pathologies.

List of publications related to the scientific activity performed during the three years PhD course in Pharmaceutical Sciences:

1. Chini, M. G.; Ferroni, C.; Cantone, V.; Dambruoso, P.; Varchi, G.; Pepe, A.; Fischer, K.; Pergola, C.; Werz, O.; Bruno, I.; Riccio, R.; Bifulco, G. *Med Chem Comm* **2015**, 6, 75-79.
2. Maione, F.; Cantone, V.; Chini, M. G.; De Feo, V.; Mascolo, N.; Bifulco, G. *Fitoterapia* **2014**, 100C, 174-178.
3. Masullo, M.; Cantone, V.; Cerulli, A.; Lauro, G.; Messano, F.; Russo, G. L.; Pizza, C.; Bifulco, G.; Piacente, S. *J Nat Prod* **2015**, 78, 2975-82.

Table of Contents

Abstract	I-III
		Page
Introduction	1-17
Chapter 1	Cancer-related inflammation	2
1.1	Inflammation and cancer	3
1.1.1	Inflammation: From Acute to Chronic	4-5
1.1.2	Cancer Development: An Overview	5-6
1.1.3	Connecting inflammation and cancer	6-12
1.1.3.1	Mutagenic Potential of Inflammation	12-13
1.1.3.2	Role of Inflammatory Cells in Tumor Development	13
1.1.3.3	Key Molecular Players in Linking Inflammation to Cancer	14-17
Result and Discussion		18-132
Chapter 2	Microsomal Prostaglandin E ₂ Synthase-1 and 5- lipoygenase: drug targets in inflammation and cancer	18-43
2.	Derived-NSAIDs side effects and the necessity to discover new safe targets	19-21
2.1	mPGES-1 as new molecular target for the treatment of inflammation and cancer	21-24
2.1.1	The solved mPGES-1 crystal structures	24-28

2.1.2	Known mPGES-1 inhibitors	28
2.1.2.1	Endogenous lipid, fatty acids and PGH ₂ analogs	29
2.1.2.2	Known anti-inflammatory drugs and/or inhibitors of leukotrienes (LTs) biosynthes	30-31
2.1.2.3	Natural compounds	31
2.1.3	Future challenge	32-33
2.2	Dual inhibition of 5-LOX/mPGES-1 as new molecular target for the treatment of inflammation and cancer	33-35
2.2.1	Human 5-LOX stabilized crystal structure	35-36
2.2.2	Known 5-LOX inhibitors	36-38
2.2.3	Dual inhibitors of mPGES-1 and 5-LOX	38-39
2.3	Scope and outline	39-43
Chapter 3	Determination of new synthetic molecular platforms as mPGES-1 inhibitor	44-84
3.1	Determination of new synthetic molecular platforms as mPGES-1 inhibitors: structure-based discovery	45-47
3.1.1	Elucidating new structural features of the triazole scaffold for the development of mPGES-1 inhibitors	47-59
3.1.2	Rationalization of the binding mode of a small synthetic library as mPGES-1 inhibitors	59-66
3.1.3	Libraries development of a series of 71- 244 derivates as mPGES-1 inhibitors.	66-74

Chapter 4	Determination of new synthetic molecular platforms as mPGES-1 inhibitor	86-121
4.1	Determination of new synthetic molecular platforms as mPGES-1 inhibitors: structure-based discovery	87-88
4.1.1	Virtual screening of focused library, pilot study on natural bioactive compounds by means of molecular docking	88-92
4.1.2	In vivo and <i>in vitro</i> biological evaluation of anti-inflammatory response of carnosol and carnosic acid and in silico analysis of their mechanism of action	93-111
4.1.3	The molecular mechanism of tanshinone IIA and cryptotanshinone in platelet anti-aggregating effects: an integrated study of pharmacology and computational analysis	111-121
Chapter 5	Structural studies of Natural Products	122-132
5.1	QM/NMR integrated approach: a valid support to the determination	123-126
5.1.1	Assignment of the relative configuration of giffonins J- P	126-132
Conclusions		133-139

Appendix A	Experimental section	140- 164
A.1	Molecular docking	141- 144
A.1.1	Autodock Vina: an Overview	145- 148
A.1.2	Glide: an Overview	148- 149
A.2	Biological evaluation and assay systems	150
A.2.1	Induction of mPGES-1 and determination of PGE ₂ synthase activity in microsomes of A549 cells	151
A.2.2	Isolation of polymorphonuclear leukocytes and peripheral blood mononuclear cells from buffy coats	152
A.2.3	Determination of product formation by 5-LOX in the cell-based assay by HPLC	153
A.2.4	Determination of product formation by 5-LOX in the cell-free assay by HPLC	155
A.2.5	Determination of eicosanoids production in PMNL and monocytes by LC-MS/MS	156
A.2.6	Induction and assessment of carrageenan-induced hyperalgesia	157
A.2.7	Formalin test	158
A.2.8	In vitro platelet aggregation assay	159
A.2.9	Cell culture and viability assay	159
A.3	Quantum Mechanical calculation of NMR Parameters in the Stereostructural Determination of Natural Products	160- 161

A.3.1	Computational details in determination of relative configuration of giffonins J-P	162- 164
References		165- 177

Abstract

Computational methodologies in combination with experimental biological assay represent fundamental key tools in the drug discovery process. The study of ligand-macromolecule interactions has a crucial role for the design, the identification and the development of new chemical platforms as anti-inflammatory and anti-cancer agents. In this project, different aspects of interaction and recognition processes between ligand and targets, and stereostructure assignment of natural compounds has been studied through different *in silico* approaches with the determination of their biological activities, which allow to corroborate the predicted results.

In particular, the strong interconnection between the tumoral and inflammatory pathology has led to the identification of new promising targets involved in essential cellular processes and acting at diverse levels and phases of the tumor and inflammation diseases. In this project, the drug design and identification of new compounds able to inhibit microsomal prostaglandin E synthase mPGES-1, 5-lipoxygenase5-LOX, cicloxygenase-1 COX-1, cicloxygenase-2 COX-2 and G-protein-coupled purinergic receptors P2Y₁₂R will be described. The results obtained during my PhD three years course can be summarized in four main areas of activity, whose relative weight was varied according to the development of the overall project:

1) The support in the design of original scaffolds for the generation of libraries potentially utilizable in therapy. This work was conducted *in silico* by molecular docking technique in order to direct the design of the new molecules basing on the analysis of ligand-target interactions and the synthetic possibilities. This kind of approach was successfully applied leading to the identification of new potential inhibitors for mPGES-1 enzyme. The good qualitative accordance between the calculated and experimental data has made

possible the identifications of new lead compounds, rationalizing the molecular basis of the target inhibition.

2) The rationalization of the biological activity of compounds by the study of the drug-receptor interactions. Molecular docking was used for the detailed study of anti-inflammatory and anticancer compounds whose biological activities are known a priori. In fact, thanks to this procedure, in this thesis several rationalizations of binding modes were reported related to a small pool of natural products as mPGES-1 inhibitors, such as carnosol and carnosic acid, and cryptotanshinone and tanshinone IIA as P2Y₁₂R inhibitors. Through the *in silico* methodology the putative binding modes for the reported molecules was described offering a complete rationalization of the observed biological activities, e.g. evaluating the specific influence of the ligand target interactions (e.g. hydrophobic, hydrophilic, electrostatic contacts).

3) The determination of relative configuration of natural products. The complete comprehension of the three dimensional structure of synthetic or isolated molecules is fundamental to design and characterize new platform potentially utilizable in therapy. On this basis, the combined approach basing on the comparison of the predicted NMR parameters (e.g. chemical shifts, computed through quantum mechanical (QM) calculations) and the related experimentally determined values was employed to assigning the relative configuration of giffonins J-P. Moreover, the assignment of relative and absolute configuration of giffonins Q-S is ongoing by a combined approach that consider the quantum mechanical calculations of circular dichroism spectra and quantum mechanical calculations of chemical shifts to be compared with the related experimental data.

4) The biological evaluation and assay systems. The determination of PGE₂ synthase activity in microsomes of A549 cells, the determination of product formation by 5-LOX in the cell-based and cell-free assay and the determination of eicosanoids production by LC-MS/MS in monocytes and

polymorphonuclear leucocytes were performed at the Department of Pharmaceutical and Medicinal Chemistry of the Friedrich- Schiller University in Jena. Moreover, the preparation of plasma through isolation of monocytes, polymorphonuclear leucocytes and platelets was carried out.

-INTRODUCTION-

-CHAPTER 1-

Cancer-related inflammation

1.1 Inflammation and cancer

The link between inflammation and cancers, rather than a recent concern, was noticed ~150 years ago. As early as 1863, Virchow indicated that cancers tended to occur at sites of chronic inflammation.¹

Although it is now clear that proliferation of cells alone does not cause cancer, sustained cell proliferation in an environment rich in inflammatory cells, growth factors, activated stroma, and DNA-damage-promoting agents, certainly potentiates and/or promotes neoplastic risk.

During tissue injury associated with wounding, cell proliferation is enhanced while the tissue regenerates; proliferation and inflammation subside after the assaulting agent is removed or the repair completed. In contrast, proliferating cells that sustain DNA damage and/or mutagenic assault (for example, initiated cells) continue to proliferate in microenvironments rich in inflammatory cells and growth/survival factors that support their growth. In a sense, tumors act as wounds that fail to heal.²

Today, the causal relationship between inflammation, innate immunity and cancer is more widely accepted; however, many of the molecular and cellular mechanisms mediating this relationship remain unresolved. Furthermore, tumor cells may usurp key mechanisms by which inflammation interfaces with cancers, to further their colonization of the host. Moreover, it was clear that the acquired immune response to cancer is intimately related to the inflammatory response.^{3,4}

Here, the critical points and the pathways connections between these two kinds of pathologies will be described.

1.1.1 Inflammation: From Acute to Chronic

Inflammation is a physiologic process in response to tissue damage resulting from microbial pathogen infection, chemical irritation, and/or wounding.⁵ At the very early stage of inflammation, neutrophils are the first cells to migrate

to the inflammatory sites under the regulation of molecules produced by rapidly responding macrophages and mast cells pre-stationed in tissues.⁶ As the inflammation progresses, various types of leukocytes, lymphocytes, and other inflammatory cells are activated and attracted to the inflamed site by a signaling network involving a great number of growth factors, cytokines, and chemokines. All cells recruited to the inflammatory site contribute to tissue breakdown and are beneficial by strengthening and maintaining the defense against infection.

There are also mechanisms to prevent inflammation response from lasting too long.⁷ A shift from antibacterial tissue damage to tissue repair occurs, involving both proinflammatory and anti-inflammatory molecules. Prostaglandin E₂,⁸ transforming growth factor- α ,⁹ and reactive oxygen and nitrogen intermediates⁶ are among those molecules with a dual role in both promoting and suppressing inflammation. The resolution of inflammation also requires a rapid programmed clearance of inflammatory cells: neighboring macrophages, dendritic cells, and backup phagocytes do this job by inducing apoptosis and conducting phagocytosis.¹⁰ The phagocytosis of apoptotic cells also promotes an anti-inflammatory response, such as enhancing the production of anti-inflammatory mediator transforming growth factor- β ¹¹ However, if inflammation resolution is dysregulated, cellular response changes to the pattern of chronic inflammation. In chronic inflammation, the inflammatory foci are dominated by lymphocytes, plasma cells, and macrophages with varying morphology.⁵ Macrophages and other inflammatory cells generate a great amount of growth factors, cytokines, and reactive oxygen and nitrogen species that may cause DNA damage.^{6a} If the macrophages are activated persistently; they may lead to continuous tissue damage.¹² A microenvironment constituted by all the above elements inhabits the sustained cell proliferation induced by continued tissue damage, thus predisposes chronic inflammation to neoplasia.¹

1.1.2 Cancer Development: An Overview

Cancer defines malignant neoplasms characterized by metastatic growth. It may occur in almost every organ and tissue relating to a variety of etiologic factors, such as genomic instability and environmental stress.⁵ A two-stage carcinogenesis model is first conceptualized in a mouse model of skin cancer.¹³ In this model, carcinogenesis is initiated by carcinogen-triggered irreversible genetic alteration and then promoted by dysregulated gene expression of initiated cells that resulted from epigenetic mechanisms and host-selective pressure.^{6^a} Once the proliferation advantage is obtained, cancer cells enter the progression stage in which their population expands rapidly.^{6^b} This model was subjected to criticism because it oversimplifies and failed to apply to all types of cancer.¹⁴

However, cancer development is still accepted as a multistep process, during which genetic alterations confer specific types of growth advantage; therefore, it drives the progressive transformation from normal cells to malignant cancer cells.¹⁵ Malignant growth is characterized by several key changes: self-sufficiency of growth signals, insensitivity to antigrowth signals, escaping from apoptosis, unregulated proliferation potential, enhanced angiogenesis, and metastasis.¹⁵ Each of these shifts is complicated and accomplished by combined efforts of various signaling processes, and moreover it will find out that inflammation may contribute to the formation of these cancer phenotypes.

1.1.3 Connecting inflammation and cancer

Common wisdom says “most things in life are a double-edged sword”. While they are in our favor at one dose or under one condition; they may be disfavor at another dose or under another condition. Inflammation is a part of the host response to either internal or external environmental stimuli. This

response serves to counteract the insult incurred by these stimuli to the host. This response can be pyrogenic, as indicated by fever. When acute inflammation or fever is manifested for a short period of time, it has a therapeutic consequence. However, when inflammation becomes chronic or lasts too long, it can prove harmful and may lead to disease. How is inflammation diagnosed and its biomarkers is not fully understood, however, the role of proinflammatory cytokines, chemokines, adhesion molecules and inflammatory enzymes have been linked with chronic inflammation (Figure 1.1). Chronic inflammation has been found to mediate a wide variety of diseases, including cardiovascular diseases, cancer, diabetes, arthritis, Alzheimer's disease, pulmonary diseases, and autoimmune diseases.¹⁶ Chronic inflammation has been linked to various steps involved in tumorigenesis, including cellular transformation, promotion, survival, proliferation, invasion, angiogenesis, and metastasis.^{17,18} That inflammation is a risk factor for most type of cancers is now well recognized.¹⁹

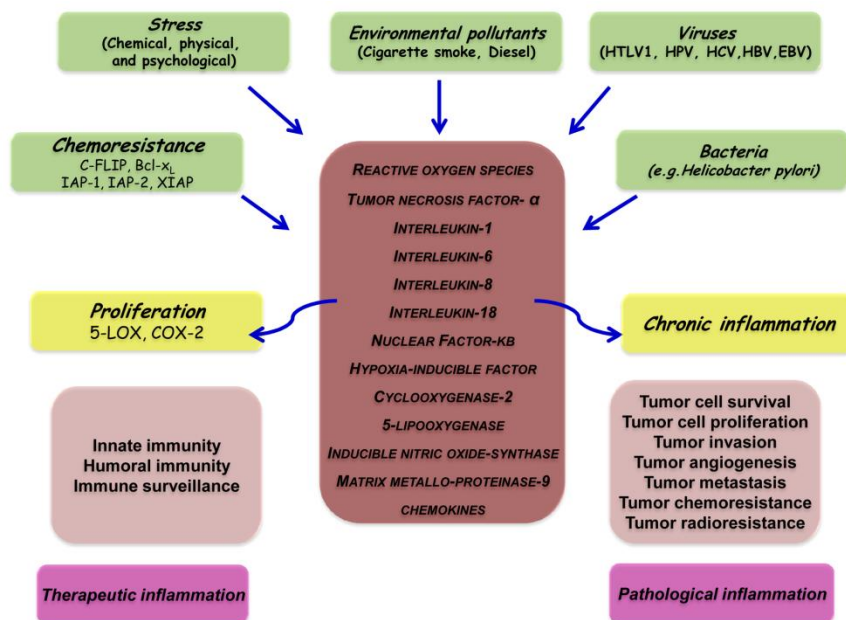


Figure 1. 1 Different faces of inflammation and its role in tumorigenesis.

As already reported, the links between cancer and inflammation were first made in the nineteenth century, on the basis of observations that tumors often arose at sites of chronic inflammation and that inflammatory cells were present in biopsied samples from tumors,¹ but there has been a recent resurgence in interest.

Several lines of evidence²⁰ (Table 1.1) — based on a range of findings, from epidemiological studies of patients to molecular studies of genetically modified mice — have led to a general acceptance that inflammation and cancer are linked. Epidemiological studies have shown that chronic inflammation predisposes individuals to various types of cancer. It is estimated that underlying infections and inflammatory responses are linked to 15–20% of all deaths from cancer worldwide.¹ There are many triggers of chronic inflammation that increase the risk of developing cancer. Such triggers include microbial infections (for example, infection with *Helicobacter pylori* is associated with gastric cancer and gastric mucosal lymphoma), autoimmune diseases (for example, inflammatory bowel disease is associated with colon cancer) and inflammatory conditions of unknown origin (for example, prostatitis is associated with prostate cancer). Accordingly, treatment with non-steroidal anti-inflammatory agents decreases the incidence of, and the mortality that results from, several tumor types.²¹

Table 1. 1 The evidence that links cancer and inflammation

1	Inflammatory diseases increase the risk of developing many types of cancer (including bladder, cervical, gastric, intestinal, oesophageal, ovarian, prostate and thyroid cancer)
2	Non-steroidal anti-inflammatory drugs reduce the risk of developing certain cancers (such as colon and breast cancer) and reduce the mortality caused by these cancers.

3	Signaling pathways involved in inflammation operate downstream of oncogenic mutations (such as mutations in the genes encoding RAS, MYC and RET).
4	Inflammatory cells, chemokines, and cytokines are present in the microenvironment of all tumors in experimental animal models and humans from the earliest stages of development.
5	The targeting of inflammatory mediators (chemokines and cytokines, such as TNF- α and IL-1 β), key transcription factors involved in inflammation (such as NF- κ B and STAT3) or inflammatory cells decreases the incidence and spread of cancer.
6	Adoptive transfer of inflammatory cells or overexpression of inflammatory cytokines promotes the development of tumors.

The hallmarks of cancer-related inflammation include the presence of inflammatory cells and inflammatory mediators (for example, chemokines, cytokines and prostaglandins) in tumor tissues, tissue remodeling and angiogenesis similar to that seen in chronic inflammatory responses, and tissue repair. These signs of ‘smouldering’ inflammation^{20a} are also present in tumors for which a firm causal relationship to inflammation has not been established (for example, breast tumors). Indeed, inflammatory cells and mediators are present in the microenvironment of most, if not all, tumors, irrespective of the trigger for development.

In the tumor microenvironment, inflammatory cells and molecules influence almost every aspect of cancer progress, including the tumor cells’ability to metastasize.²² Thus, whereas there were previously six recognized hallmarks of cancer — unlimited replicative potential, self-sufficiency in growth signals, insensitivity to growth inhibitors, evasion of programmed cell death, ability to develop blood vessels, and tissue invasion and metastasis²³ — cancer related inflammation now emerges as number seven (Figure 1.2). In 2000, Hanahan and Weinberg²³ proposed a model to define the six properties that a tumor acquires.

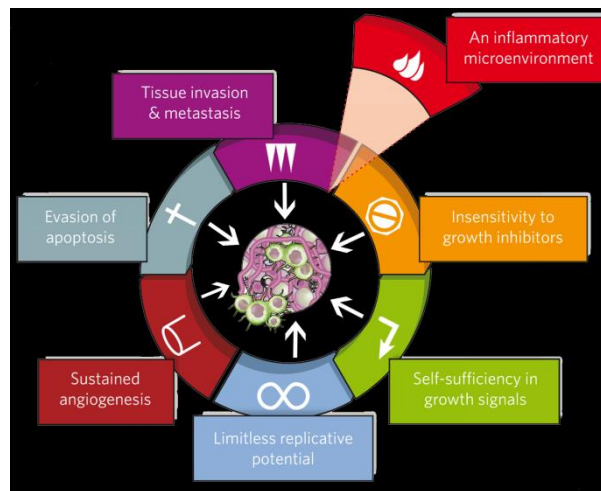


Figure 1. 2The hallmarks of cancer.

These are unlimited replicative potential, ability to develop blood vessels (angiogenesis), evasion of programmed cell death (apoptosis), self-sufficiency in growth signals, insensitivity to inhibitors of growth, and tissue invasion and metastasis. Kim and colleagues' findings,²⁴ together with those of other studies,^{22,18} indicate that this model should be revised to include cancer-related inflammation as an additional hallmark.²³

The connection between inflammation and cancer can be viewed as consisting of two pathways: an extrinsic pathway, driven by inflammatory conditions that increase cancer risk (such as inflammatory bowel disease); and an intrinsic pathway, driven by genetic alterations that cause inflammation and neoplasia (such as oncogenes) (Figure 1.3).

The intrinsic pathway was uncovered when addressing why inflammatory cells and mediators are present in the microenvironment of most, if not all, tumors and therefore are present in cases for which there is no epidemiological basis for inflammation. This finding raised the question of whether the genetic events that cause neoplasia in these cases are responsible for generating an inflammatory environment. This question has been addressed only recently, by

using preclinical and clinical settings in which various oncogenic mechanisms can be assessed.

The intrinsic pathway is activated by genetic events that cause neoplasia. These events include the activation of various types of oncogene by mutation, chromosomal rearrangement or amplification, and the inactivation of tumor-suppressor genes. Cells that are transformed in this manner produce inflammatory mediators, thereby generating an inflammatory microenvironment in tumors for which there is no underlying inflammatory condition (for example, breast tumors). By contrast, in the extrinsic pathway, inflammatory or infectious conditions augment the risk of developing cancer at certain anatomical sites (for example, the colon, prostate and pancreas).

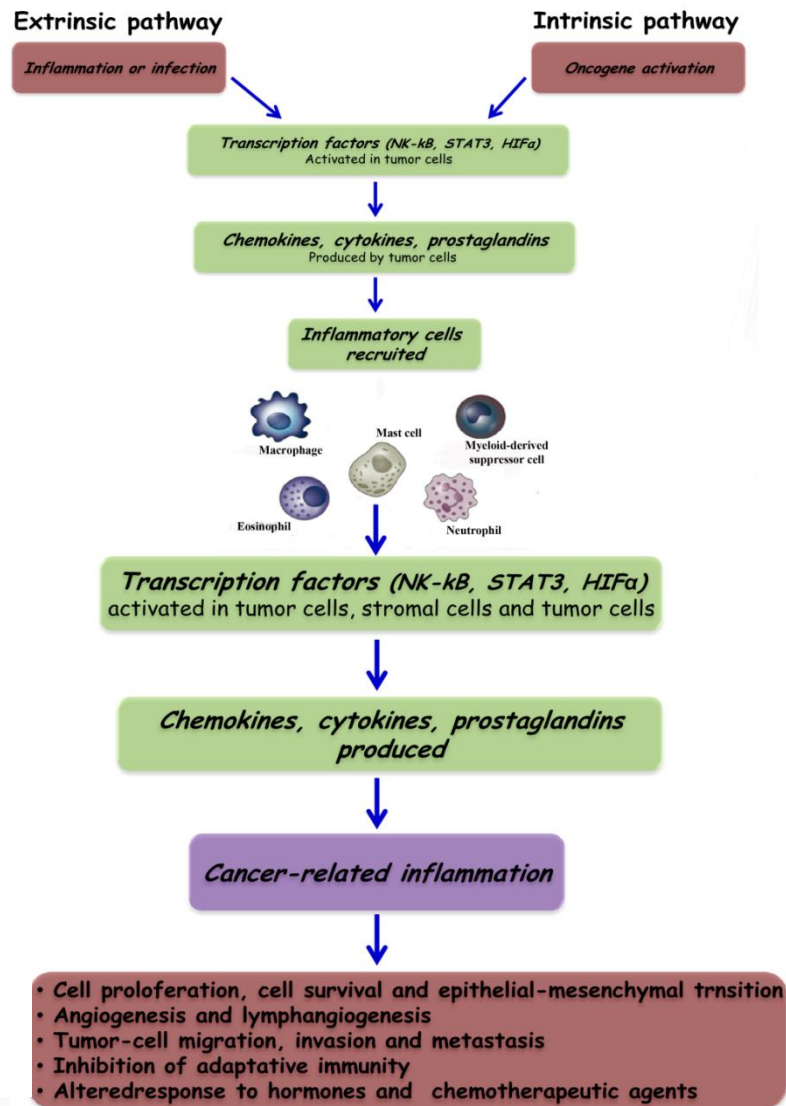


Figure 1. Pathways that connect inflammation and cancer. Cancer and inflammation are connected by two pathways: the extrinsic and the intrinsic pathway.

The two pathways converge, resulting in the activation of transcription factors, mainly nuclear factor-kB (NF-kB), signal transducer and activator of transcription 3 (STAT3) and hypoxia-inducible factor 1 (HIF1 α), in tumor cells. These transcription factors coordinate the production of inflammatory mediators, including cytokines and chemokines, as well as the production of cyclooxygenase 2 (COX₂) (which, in turn, results in the production of

prostaglandins). These factors recruit and activate various leukocytes, most notably cells of the myelomonocytic lineage. The cytokines activate the same key transcription factors in inflammatory cells, stromal cells and tumor cells, resulting in more inflammatory mediators being produced and a cancer-related inflammatory microenvironment being generated. Smouldering cancer-related inflammation has many tumor-promoting effects.

1.1.3.1 Mutagenic Potential of Inflammation

The chronic inflammation microenvironment is predominated by macrophages.⁶ Those macrophages, together with other leukocytes, generate high levels of reactive oxygen and nitrogen species to fight infection.²⁵ However, in a setting of continuous tissue damage and cellular proliferation, the persistence of these infection-fighting agents is deleterious.^{6b} They may produce mutagenic agents, such as peroxynitrite, which react with DNA and cause mutations in proliferating epithelial and stroma cells.^{25,26} Macrophages and T lymphocytes may release tumor necrosis factor- α (TNF- α) and macrophage migration inhibitory factor to exacerbate DNA damage.²⁷ Migration inhibitory factor impairs p53-dependent protective responses, thus causing the accumulation of oncogenic mutations.²⁸ Migration inhibitory factor also contributes to tumorigenesis by interfering Rb-E2F pathway.²⁹ Within an ileocolitis-associated mouse cancer model, the high susceptibility to inflammation and cancer in hydroperoxide-reducing enzyme-deficient mice suggested that intracellular hydroperoxides might also contribute to tumor initiation.³⁰

1.1.3.2 Role of Inflammatory Cells in Tumor Development

Other than a single mutation, more genetic and epigenetic events are required to drive from initiated cells to malignant tumors.²³ Some of these

events are also found to be related to chronic inflammation. For instance, angiogenesis, a critical process in tumor progression,³¹ associates with chronic inflammation, such as psoriasis, rheumatoid arthritis, and fibrosis.²³ In addition, the tumor inflammatory microenvironment can facilitate the breakage of the basement membrane, a process required for the invasion and migration of tumor cells.^{6^a} A wide population of leukocytes and other types of immune cells infiltrate to the developing tumor site and establish the tumor inflammatory microenvironment.^{6^c} Macrophages, neutrophils, eosinophils, dendritic cells, mast cells, and lymphocytes are also found to be key components in the epithelial-originated tumors.^{6^{c,12,32}} The infiltration of immune cells to tumors may repress tumor growth.³³ However, the increasing concern is that inflammatory cells act as tumor promoters in inflammation-associated cancers.^{6^{a,34,35}} Accumulated mutations in epithelial cells lead to dysregulation of their growth and migration. These dysregulated epithelial cells may also signal to recruit leukocytes.³¹ In addition, tumor cells may also produce cytokines and chemokines to attract immune cells to facilitate cancer development.^{6^{a,c,31}}

1.1.3.3 Key Molecular Players in Linking Inflammation to Cancer

To address the details of transition from inflammation to cancers and the further development of inflammation-associated cancers, it is necessary to investigate specific roles of key regulatory molecules involved in this process. In fact, in the panoply of molecules involved in cancer-related inflammation, key endogenous (intrinsic) factors can be identified. These include transcription factors (such as NF- κ B and signal transducer and activator of transcription 3 (STAT3)) and major inflammatory cytokines (such as IL-1 β , IL-6, IL-23 and TNF- α)^{36,37,38} (Table 1.2).

Table 1. 2Key Molecular Players Linking Cancer to Inflammation.

Potential linkers	Functions in linking inflammation to cancer
Cytokines	
IL-6	Promote tumor growth
TNF- α	Induce DNA damage and inhibit DNA repair Promote tumor growth Induce angiogenic factors
Chemokines	Promote tumor cell growth Facilitate invasion and metastasis by directing tumor cell migration and promoting basement membrane degradation
NF- κ B	Mediate inflammation progress, promoting chronic inflammation Promote the production of mutagenic reactive oxygen species Protect transformed cells from apoptosis Promote tumor invasion and metastasis Feedback loop between proinflammatory cytokines
iNOS	Downstream of NF- κ B and proinflammatory cytokines Induce DNA damage and disrupt DNA damage response Regulate angiogenesis and metastasis
COX-2	Produce inflammation mediator prostaglandins Promote cell proliferation, antiapoptotic activity, angiogenesis, and metastasis
HIF-1 α	Promote chronic inflammation Induced by proinflammatory cytokines through NF- κ B Enhance the glycolytic activity of cancer cells Contribute to angiogenesis, tumor invasion, and metastasis by transactivating VEGF
STAT3	Activated by proinflammatory cytokines Promote proliferation, apoptosis resistance, and immune tolerance
Nrf2	Anti-inflammatory activity

	Protect against DNA damage
NFAT	Regulate proinflammatory cytokine expression Required in cell transformation

For sake of simplicity, between the molecular players involved in inflammatory networking cancer, the tumor necrosis factor (TNF- α) and NF- κ B will be described. The TNF- α was first isolated as an anticancer cytokine than two decades ago.³⁹ Experience since then has indicated that when expressed locally by the cells of the immune system, TNF- α has a therapeutic role. However, when dysregulated and secreted in the circulation, TNF- α can mediate a wide variety of diseases, including cancer.³⁹ TNF- α has itself been shown to be one of the major mediators of inflammation.⁴⁰ Induced by a wide range of pathogenic stimuli, TNF- α induces other inflammatory mediators and proteases that orchestrate inflammatory responses. TNF- α is also produced by tumors and can act as an endogenous tumor promoter.⁴⁰ The role of TNF- α has been linked to all steps involved in tumorigenesis, including cellular transformation, promotion, survival, proliferation, invasion, angiogenesis, and metastasis, as outlined below (Figure 1.4).

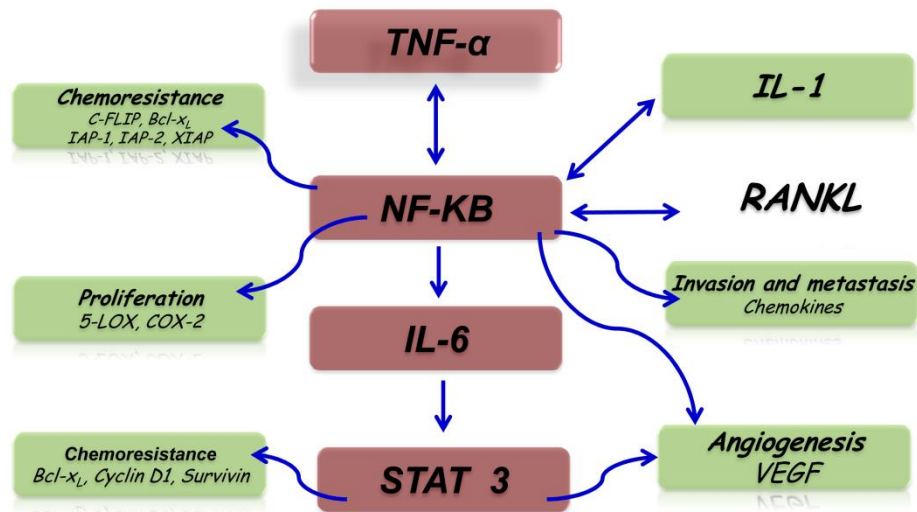


Figure 1. Inflammatory networking in cancer.

On the other hand, NF-κB is a key coordinator of innate immunity and inflammation, and has emerged as an important endogenous tumor promoter.³⁶ NF-κB is crucial both in the context of tumor or potential tumor cells and in the context of inflammatory cells. In these cell types, NF-κB operates downstream of the sensing of microorganisms or tissue damage by the Toll-like receptor (TLR)–MyD88 signaling pathway, and by signaling pathways mediated by the inflammatory cytokines TNF-α and IL-1β. In addition, NF-κB can be activated as a result of cell-autonomous genetic alterations (amplification, mutations or deletions)⁴¹ in tumor cells. In tumor cells and epithelial cells at risk of transformation by carcinogens, as well as in inflammatory cells, NF-κB activates the expression of genes encoding inflammatory cytokines, adhesion molecules, enzymes in the prostaglandin-synthesis pathway (such as COX₂), inducible nitric oxide synthase (iNOS; also known as NOS2) and angiogenic factors.

In addition, one of the important functions of NF-κB in tumor cells or cells targeted by carcinogenic agents is promoting cell survival, by inducing the expression of anti-apoptotic genes (such as BCL2). There is also accumulating

evidence of interconnections and compensatory pathways between the NF- κ B and HIF1 α systems,⁴² linking innate immunity to the response to hypoxia. There is unequivocal evidence that NF- κ B is involved in tumor initiation and progression in tissues in which cancer-related inflammation typically occurs (such as the gastrointestinal tract and the liver).⁴³ The NF- κ B pathway is tightly controlled by inhibitors that function at various stages of the pathway. An example is TIR8 (also known as SIGIRR), a member of the IL-1-receptor family. TIR8 has a single immunoglobulin domain, a long cytoplasmic tail, and a Toll/IL-1 receptor (TIR) domain that differs from that of other members of the IL-1-receptor family. Deficiency in the gene that encodes TIR8 is associated with increased susceptibility to intestinal inflammation and carcinogenesis.⁴⁴ Thus, the balance of inhibitors and activators tunes the extent to which the NF- κ B pathway operates as an endogenous tumor promoter. Support for the connection between cancer and inflammation is further strengthened by studies of the role of NF- κ B in tumor-infiltrating leukocytes. In established, advanced tumors, which typically have a microenvironment of smouldering inflammation,²⁰ tumor-associated macrophages (TAMs) have delayed and defective NF- κ B activation.⁴⁵ Evidence suggests that homodimers of the p50 subunit of NF- κ B (a negative regulator of the NF- κ B pathway) are responsible for this sluggish activation of NF- κ B in TAMs and for the protumor phenotype of these cells.⁴⁶ Thus, NF- κ B seems to function as a 'rheostat' whose function can be tuned to different levels, a property that enables the extent of inflammation to be regulated. Such regulation allows the vigorous inflammation (for example, in inflammatory bowel disease) that predisposes individuals towards developing cancer to be sustained, and enables TAMs to sustain the smouldering inflammatory microenvironment present in established metastatic neoplasia.

Briefly, the mediators and cellular effectors of inflammation are important constituents of the local environment of tumors.

-CHAPTER 2-

Microsomal Prostaglandin E Synthase-1 and 5-lipoxygenase: drug targets in inflammation and cancer

2. Derived-NSAIDs side effects and the necessity to discover new safe targets

Non steroidal anti-inflammatory drugs (NSAIDs) represent so far the pivot of inflammation therapy as a consequence of their potent effect in the suppression of prostaglandins (PGs), prominent bioactive mediators involved in key physiological functions and also implicated in several pathologic conditions like inflammation and tumorigenesis. However, especially for long-term treatments - like those required for chronic pathologies such as rheumatoid arthritis - their use comprises severe side effects; in particular NSAIDs are well known to be endowed with relevant gastric toxicity due to the efficient suppression of constitutively generated PGs involving the COX-1 pathway with gastro-protection function. Not long ago, the introduction of coxibs in therapy was initially considered as a solution of all the problems connected with the use of NSAIDs, as these selective COX-2 inhibitors showed to exhibit potent anti-inflammatory activity without causing significant gastrointestinal injury. Unfortunately, several clinical evidences indicated their implication in serious cardiovascular accidents. Given the known effects of PGs on cardiovascular function, there has been concern of the potential for cardiotoxicity with any inhibitor of PG biosynthesis as anticancer agents. For example, prostacyclin synthase is expressed in endothelial cells, its product, PGI₂, is known for its cardio-protective properties that cause platelet de-aggregation and vessel dilation.⁴⁷ For example, a study in patients taking selective COX-2 inhibitors showed that the increased risk of myocardial infarction (MI) and stroke,^{48,49} and increased mortality after MI⁵⁰ may be due to an imbalance of prothrombotic eicosanoids (increased TXA₂) and antithrombotic eicosanoids (decreased PGI₂).⁵¹

In this perspective, there is an ever growing need for the research of safer anti-inflammatory drugs. Recently, great attention has been focused on the mPGES-1 enzyme involved in the last step of the arachidonic acid cascade; this

enzyme is over-expressed in several inflammatory disorders as well as in many human tumors. Elevated levels of mPGES-1, in fact, are often observed concomitantly with COX-2 over-expression. In fact, *in vitro* studies have demonstrated that mPGES-1 is localized at the perinuclear membrane and endoplasmic reticulum and is in general functionally coupled with COX-2, thereby enabling efficient generation of PGE₂ during inflammation. Moreover, recent studies have shown that mPGES-1 expression can be specifically induced by lipopolysaccharide (LPS) in rat peritoneal macrophages, interleukin-1 β (IL-1 β) and tumor necrosis factor (TNF)- α in a human lung carcinoma cell line, A549 with or without induction of COX-2.^{52,53,54} However, studies with these diverse stimuli have clearly shown that mPGES-1 can also be functionally activated in the absence of induced COX-2 levels, providing evidence that these two enzymes can be independently regulated. This latter observation is important from the standpoint of drug targeting. It suggests the possibility that the enzymatic activity of mPGES-1 can be pharmacologically targeted with resultant suppression of PGE₂ production by mechanisms that circumvent the toxicity associated with inhibition of COX-2 activity. Interestingly, the deletion of mPGES-1 did not have impact on blood pressure when the mice were crossed with low-density lipoprotein receptor (LDLR) knockout mice.⁵⁵ Moreover, Wu et al.⁵⁶ demonstrated absence or reduced levels of myocardial damage after coronary occlusion in mice lacking mPGES-1 compared to mice given COX-2 inhibitor (celecoxib).⁵⁷ However, in contrast to work with COX-2 inhibitors mice with targeted deletion of the gene encoding mPGES-1 did not show any alteration the levels of TXA₂ or PGI₂ in the heart after MI. Therefore, pharmacological inhibition of mPGES-1 may not be associated with the perturbations in TXA₂ and PGI₂ metabolism that increase the risk of arterial thrombosis in patients taking COX-2 inhibitors. Moreover, it was recently reported by Cheng et al.⁵⁸ that mPGES-1 deletion, in contrast to deletion, disruption, or inhibition of COX-2, does not result in

hypertension or a predisposition to thrombosis in normolipidemic mice.⁵⁸ The controversial discussion about the pharmacological potential of mPGES-1 as safe drug target reached its peak after inhibition of mPGES-1 has been shown to redirect the COX product and mPGES-1 substrate PGH₂ towards the biosynthesis of other PGs. The blockage of mPGES-1 either elevated levels of thromboxane (Tx)B₂, PGI₂ and/or PGD₂ or was without effect depending on the cell type- and tissue-specific expression pattern of PGs synthases. The redirection of PGH₂ is not necessarily detrimental. The increase of PGI₂ production, for example, might even be advantageous for the cardiovascular safety of mPGES-1 inhibitors. Meanwhile, multiple cellular and animal studies have drawn a more complete picture about the physiological interrelations of mPGES-1 as described in several excellent reviews. These important findings suggest that selective mPGES-1 inhibitors should have very low, if any, cardiotoxic side effects typically associated with COX-2 inhibitors.

2.1 mPGES-1 as new molecular target for the treatment of inflammation and cancer

mPGES-1 is the terminal inducible synthase responsible for the production of protumorigenic PGE₂ and it is overexpressed in a variety of cancers.^{59,60,61,62,63,64} It is a member of the membrane-associated proteins involved in eicosanoid and glutathione metabolism (MAPEG) superfamily and exhibits a significant sequence homology with microsomal glutathione-S-transferase (GST)-1-like 1 (MGST-1), 5-lipoxygenase (LOX)-activating protein (FLAP) and leukotriene C₄ synthase (LTC4S). All MAPEG proteins are small proteins of 14–18 kDa and have a similar 3D structure. Hence, mPGES-1 is the terminal enzyme in the biosynthesis of PGE₂ (Figure 2.1). In the first step, membrane-bound and secretory phospholipase A₂ (PLA₂) isoforms convert phospholipids (PL) to arachidonic acid (AA). Next, the COXs convert AA into the unstable intermediate, PGH₂. Finally, terminal PGESs

isomerize PGH₂ into PGE₂. PGH₂ is the precursor for several structurally related PGs, which are formed by the action of specialized prostaglandin synthases. The PGs synthesized by this pathway include the before-mentioned PGE₂, as well as prostaglandin D₂ (PGD₂), prostaglandin F_{2α} (PGF_{2α}), prostaglandin I₂ (PGI₂, also known as prostacyclin) and thromboxane A₂ (TXA₂) (Figure 2.3). Consequently, it is thought that inhibition of COX-2 activity affects the synthesis of all prostanoids down-stream of PGH₂, whereas selective targeting of mPGES-1 would only reduce PGE₂ production. It should be noted that shunting towards other PG has been observed and that dual inhibitors for the 5-LOX and mPGES-1 are considered as a novel excellent avenue to inhibit the pathway.

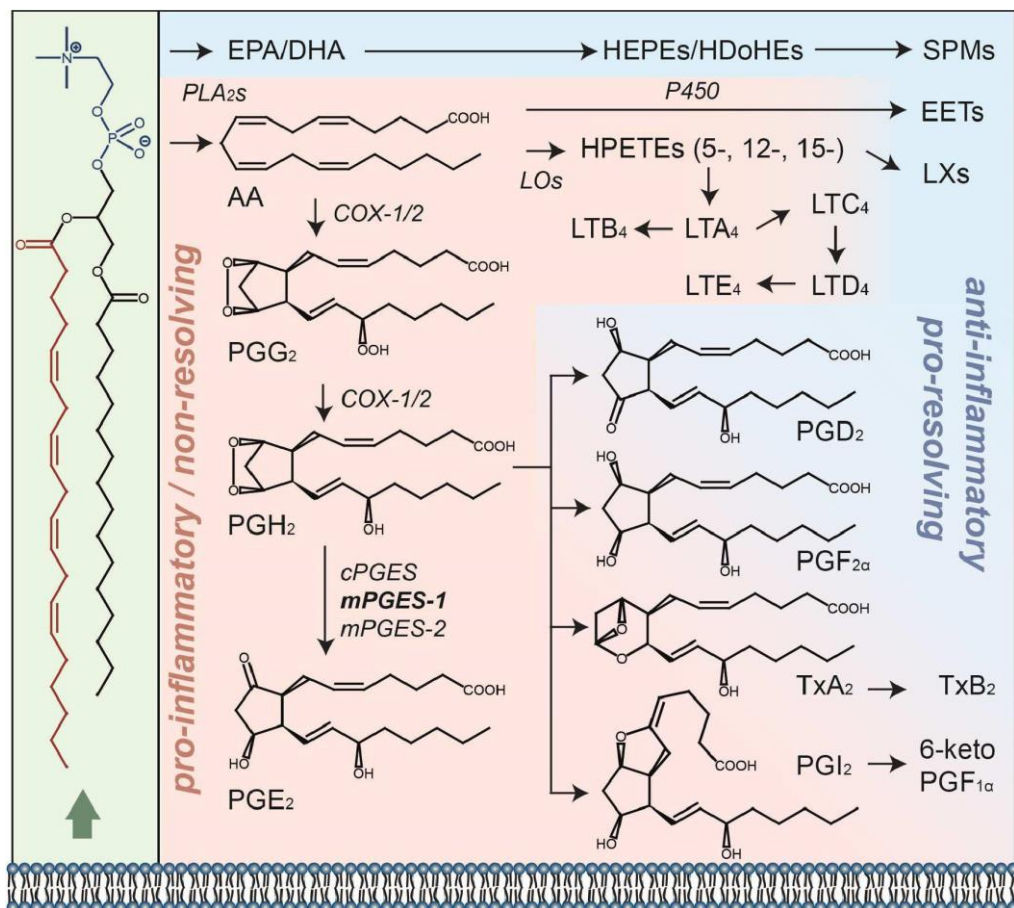


Figure 2. 1. Biosynthetic pathway of arachidonic acid.

Microsomal prostaglandin E synthase-1 expression is low in most normal tissues, although abundant and constitutive expression is detected in a limited number of organs, such as the lung, kidney and reproductive organs. The induction of COX-2 and mPGES-1 by pro-inflammatory factors and their cooperation in converting AA to PGE₂ *in vitro* suggests that both enzymes are important for PGE₂ biosynthesis and that inhibition of either is sufficient to inhibit PGE₂ production. The kinetics of induction of mPGES-1 and COX-2 has been reported⁶⁵ to be different suggesting a differential regulation of the enzymes. mPGES-1 expression can be specifically induced by LPS, IL-1 β and TNF- α in various cell types with or without induction of COX-2. The putative promoter of human mPGES-1 gene is GC-rich, lacks a TATA box and contains binding sites for C/EBP and AP-1, two tandem GC boxes, two progesterone receptor and three GRE elements.⁶⁶ Of these sites, the GC boxes are critical for the promoter activity where the transcription factor early growth response protein 1 (Egr-1) binds to the proximal GC box and triggers mPGES-1 transcription. Mice genetically deficient in mPGES-1 have shown that the enzyme is a key mediator of inflammation, pain, angiogenesis, fever, bone metabolism and tumorigenesis, thus making this protein an attractive target for the treatment of osteoarthritis, rheumatoid arthritis, acute or chronic pain and cancer, which is the focus of this review. In 2003, the role of mPGES-1 in inflammatory and pain response was first studied.⁶⁷ The authors generated mPGES-1-deficient trans-genic mice and showed that reduced expression of mPGES-1 leads to decrease in writhing, an indicator of inflammatory pain. Other reports have further concluded that mPGES-1 is indeed involved in various types of inflammation, including pain hyperalgesia, granulation associated with angiogenesis, and inflammatory arthritis accompanying bone destruction. However, using the acetic acid stretching test with or without LPS stimulation, Kamei et al.⁶⁸ demonstrated that mPGES-1 contributes more

profoundly to LPS-primed inflammatory hyper-algesia than to basal acute pain perception.⁶⁸

2.1.1. The solved mPGES-1 crystal structures

An electron crystallographic structure (3.5 Å) of mPGES-1 was published in 2008 (PDB code: 3DWW)⁶⁹ and confirmed the trimeric structure of the protein as predicted by Xing et al.⁷⁰ and suggested by Hetu et al.⁷¹. The enzyme might switch between two conformations⁴⁵ as previously described for LC4S. Similarly to MGST-1, FLAP and LTC4S, the protein folds into four transmembrane helices (TM1–4). The centre of the mPGES-1 trimer consists of a funnel-shaped cavity, which opens towards the cytoplasm and expands well into the transmembrane region. Subsequently, the protein was crystallized in the presence of GSH (PDB: 4AL1),⁷² which binds in the active site of the enzyme defined mostly by TM1 and TM4 for each of the subunits (Figure 2.1.1 and 2.1.2). GSH interacts in a ‘U-shape’ mainly with Arg126, Arg110 and Glu77 from TM4 and His72 from TM1 of another subunit. Since COX generates PGH₂ at the luminal side of the endoplasmic reticulum, PGH₂ has to diffuse through the membrane for transfer to mPGES-1. PGH₂ is believed to enter the active site pocket with its peroxofuran head group. The two flexible aliphatic chains of PGH₂ protrude from the pocket and might be inserted into the membrane, or they interact with the membrane/cytosol interface.

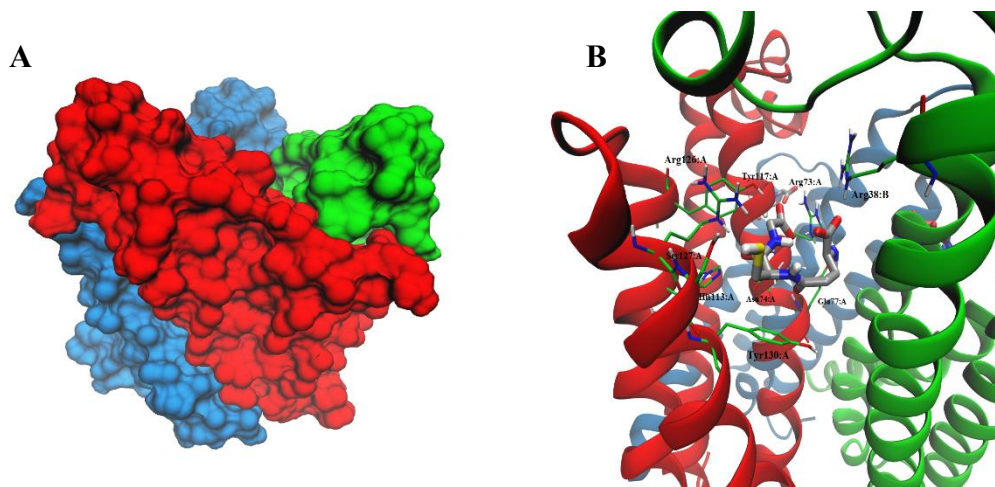


Figure 2. 1. 1Tridimensional model of mPGES-1 in complex with GSH.

It should be stressed that the mPGES-1 structure obtained by Jegerschöld et al.⁶⁹ represents a closed conformation of the protein. A model of the open conformation reveals that prostaglandin endoperoxide (PGH₂) could fit into the cleft defined by TM1 and TM4, allowing the synthesis of PGE₂.

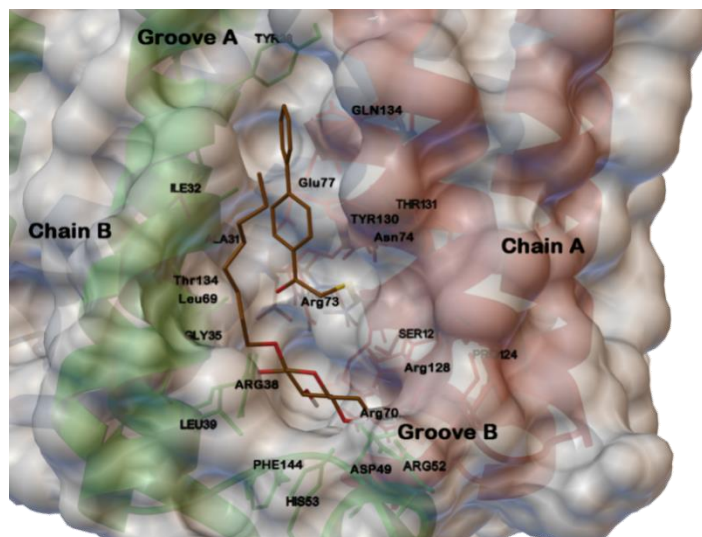


Figure 2. 1. 2Tridimensional model of mPGES-1 in complex with GSH analogue and b-octyl glucoside.

The homology model published by Xing et al.⁷⁰ predicted a 3:3 binding stoichiometry of mPGES-1 and its substrate. A co-crystal of mPGES-1 with a small-molecule inhibitor LVJ (**I**) (PDB code: 4BPM)⁷³ would confirm these previous predictions and facilitate drug design for this interesting therapeutic target (Figure 2.1.3).

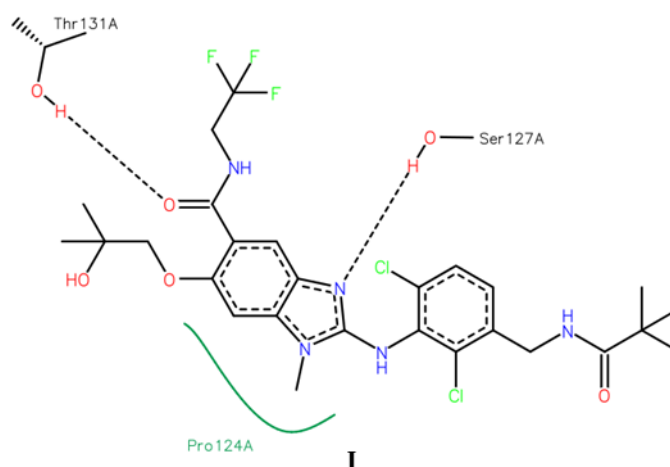


Figure 2. 1. 3 Chemical structure of LVJ (**I**) in 4BPM.

The most recent crystal structures of mPGES-1 bound to four distinct specific potent small molecule inhibitors (Figure 2.1.4), providing a rationale for understanding the associated structure–activity relationships and a structural context for species-associated selectivities.⁷⁴ The four scaffolds presented in complex with mPGES-1 are a biarylimidazole (**II**),⁷⁵ a phenanthrene imidazole (MF63, **III**),⁷⁶ and two biarylindoles (**IV**, **V**).^{77,78} A general binding mode is observed in which inhibitors pack against the fourth helix of the first monomer while placing head groups into a critical pocket formed above the GSH. While a strong tendency to interact with α -4 of monomer 1 is observed, there is clear potential to access contacts with α -1 of monomer 2 in a possible alternative binding mode. Aside from the conservative substitution of valine for isoleucine at position 32, the residues of

α -1 that could potentially contribute to ligand binding are conserved between the rat and human sequences, implying that inhibitors utilizing such interactions might be less species-dependent with respect to potency. The tail end of the inhibitors, opposite the head group which binds in the pocket above GSH, is largely exposed to solvent in the crystal structures, implying that modifications of the inhibitor tails likely improve potency through nonspecific means.

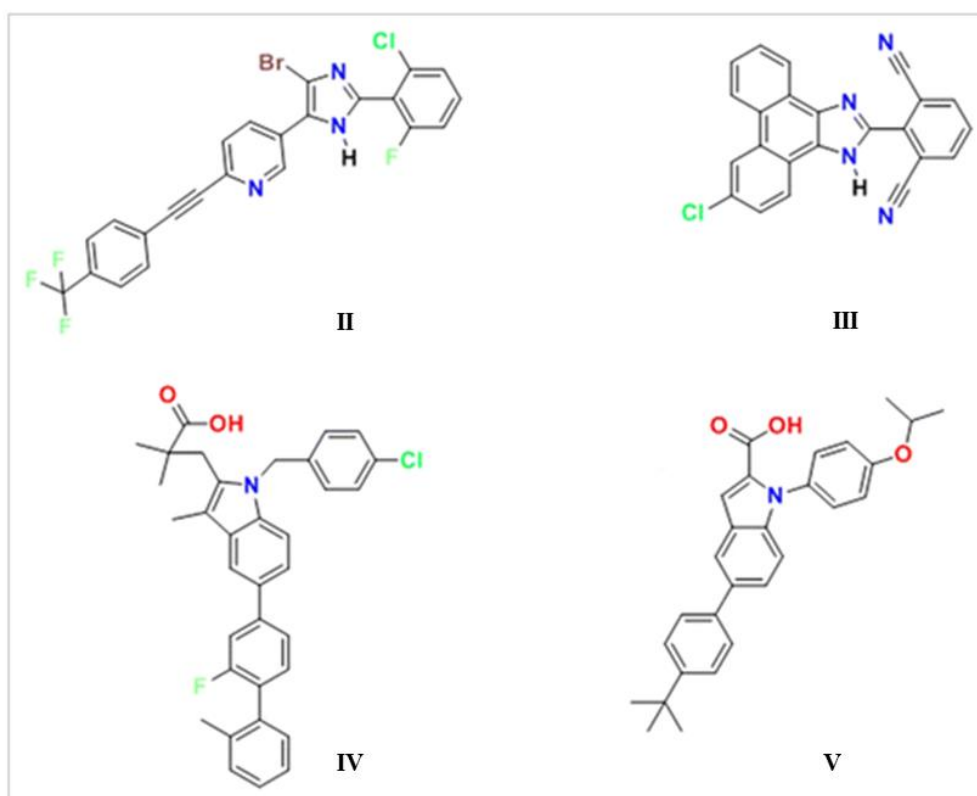


Figure 2. 1. 4 Structures of co-crystallized inhibitors biarylimidazole (**II**), MF63 (**III**), and two biarylindoles (**IV-V**) in 4YK5.

Of note are also the structural similarities with other crystallized proteins) such as the Huntingtin interacting protein 12 (PDB code: 1R0D), the V-type sodium ATP syn-thase subunit K (PDB code: 2BL2), or the protein tyrosine

kinase 2 β (β 3GM3). Part of these structural similarities should be taken in consideration perhaps when selective inhibitor design is undertaken.

2.1.2. Known mPGES-1 inhibitors

There are several examples of compounds that were identified and developed to target mPGES-1, that have been described in the literature classified into three different categories: endogenous lipid, fatty acids and PGH₂ analogs; known anti-inflammatory drugs and/or inhibitors of leukotrienes (LTs) biosynthesis; and natural compounds.⁷⁹ Compounds that were further improved based on their structure and cellular activities are also described in the next section.

2.1.2.1. Endogenous lipid, fatty acids and PGH₂ analogues

It has been reported that mPGES-1 is weakly inhibited ($IC_{50} = 5 \mu M$) by cysteinyl leukotriene C₄ (LTC₄), which also inhibits the structurally related MGST-1 with higher potency ($IC_{50} = 50 \text{ nM}$). With a GSH moiety, LTC₄ has been shown to inhibit MGST-1 by competing with GSH. Because of the structural homology between the members of MAPEG family of enzymes, inhibition of mPGES-1 activity by LTC₄ may be due to a similar mechanism. Other lipid mediators such as PGs have also been tested for mPGES-1 inhibition. The anti-inflammatory 15-deoxy- Δ 12,14-PGJ₂ is found to be the most potent inhibitor of mPGES-1 ($IC_{50} = 0.3 \mu M$) compared with PGE₂, PGF_{2 α} , TXB₂ and PGJ₂. The fact that 15-deoxy- Δ 12,14-PGJ₂ is much more potent than its analogs PGJ₂ or Δ 12-PGJ₂ ($IC_{50} > 50 \mu M$) suggests that the hydroxyl group at C15 position impairs mPGES-1 inhibition. Besides naturally occurring PGs, stable PGH₂ analogs have also been tested as potential mPGES-1 inhibitors, among which U-51605 inhibits mPGES-1 activity to some extent. However, the potency is inconsistent between the studies. Unlike U-51605, two other stable PGH₂ analogs U-44069 and U-46619 fail to inhibit mPGES-1. The

activity of mPGES-1 is also inhibited by a number of fatty acids such as AA, docosahexaenoic acid (DHA), eicosapentaenoic acid (EPA) ($IC_{50} = 0.3 \mu\text{M}$ for each), and palmitic acid ($IC_{50} = 2 \mu\text{M}$). These results suggest that the anti-inflammatory properties of 15-deoxy- Δ 12,14-PGJ₂, DHA and EPA can be partly attributed to mPGES-1 inhibition.

2.1.2.2. Known anti-inflammatory drugs and/or inhibitors of leukotrienes (LTs) biosynthesis

The only traditional nonsteroidal anti-inflammatory drug (NSAID) that exhibits inhibitory effect for mPGES-1 is sulindac. Its active metabolite sulindac sulfide has been shown to weakly inhibit mPGES-1 activity ($IC_{50} = 80 \mu\text{M}$). There are several examples of selective COX-2 inhibitors that also found to inhibit mPGES-1 activity. For instance, NS-398 is a COX-2 inhibitor that also inhibits mPGES-1 with an IC_{50} value of $20 \mu\text{M}$. Similarly, some other coxibs such as celecoxib ($IC_{50} = 22 \mu\text{M}$), lumiracoxib ($IC_{50} = 33 \mu\text{M}$), and valdecoxib ($IC_{50} = 75 \mu\text{M}$) also moderately inhibit mPGES-1 activity, whereas the other tested coxibs (etoricoxib and rofecoxib) fail to inhibit mPGES-1 activity even when used up to $200 \mu\text{M}$. Interestingly, the celecoxib derivative dimethylcelecoxib (DMC) loses the COX-2 inhibitory effect, while obtaining slightly better potency for mPGES-1 inhibition ($IC_{50} = 16 \mu\text{M}$) as measured in a cell-free assay. MK-886, an LT suppressor acting through inhibition of FLAP ($IC_{50} = 26 \text{ nM}$), is also found to inhibit mPGES-1 *in vitro* ($IC_{50} = 1.6 \mu\text{M}$).^{80,81} This result reinforces the similarity among the members of MAPEG (mPGES-1 versus FLAP). In intact cells, however, MK-886 has limited inhibitory effects on PGE₂. At $100 \mu\text{M}$, MK-886 only slightly reduces (~20%) LPS-induced PGE₂ in human whole-blood, and does not show further inhibition with higher concentration. In cytokine-stimulated gingival fibroblasts, MK-886 does not significantly reduce PGE₂ synthesis at 2–4 μM , although the protein level of

mPGES-1 is slightly reduced. When used at higher concentration (8 μM), it even increases PGE₂ production in these gingival fibroblasts, with a concomitant upregulation of COX-2 protein. In Caco-2 and HT-29 colon cancer cells, 10 μM of MK-886 significantly increases PGE₂ production, which may be due to a shunt of AA metabolism to the PG pathway, since MK-886 is an inhibitor targeting the 5-LOX pathway. Taken together, the lack of inhibitory effect of MK-886 on cellular PGE₂ synthesis suggests that this compound is unlikely to serve as an mPGES-1 inhibitor *in vivo* to reduce PGE₂ production. Nevertheless, MK-886 has been used as a basis for the development of more potent and selective mPGES-1 inhibitors.

2.1.2.3. Natural compounds

Another anti-inflammatory drug licofelone (ML3000), originally identified as a dual inhibitor blocking both COX and 5-LOX pathways, has also been shown to inhibit mPGES-1 activity with an IC₅₀ value of 6 μM . It dose-dependently reduces PGE₂ production (EC₅₀ = 0.1 μM) in IL-1 β -stimulated A549 cells, a system where COX-1 is undetectable, without affecting the generation of PGI₂ (as detected by its stable metabolite 6-keto PGF_{1 α} using an ELISA assay). However, the *in vivo* effect of licofelone on PGE₂ reduction is also contributed by COX-1 inhibition, because licofelone is a potent COX-1 inhibitor as tested *in vitro* (IC₅₀ = 0.8 μM) and in intact human platelets (EC₅₀ = 0.24 μM) for 12-hydroxy-5,8,10-heptadecatrienoic acid (12-HHT) reduction. Interestingly, it has been shown by flexible alignment that licofelone shares pharmacophore features with MK-886. In line with this observation, it acts primarily on FLAP rather than 5-LOX itself. Licofelone is currently evaluated as a treatment for osteoarthritis, as it can suppress both PGE₂ and LTs biosynthesis, which offers benefits over traditional NSAIDs and selective COX-2 inhibitors. In fact, licofelone derivatives have also been developed as

selective mPGES-1 inhibitors by further structure–activity relationship (SAR) studies.

2.1.3. Future challenge

An exponential increase in the number of papers on mPGES-1 can be noticed since its discovery and clearly the pathway and the enzyme have generated a great interest in the field of research. Papers that describe small molecules that inhibit the activity of the enzyme have increased dramatically over the past 5 years. This observation can further be followed in the number of patents issued over these past 5 years as well. GRC27864 is the only potent, selective, orally bioavailable inhibitor that has successfully completed pre-clinical and phase 1 enabling studies. However, and interestingly, compounds that are subsequently found to inhibit mPGES-1 in cell-free assays and/or *in vitro* cellular assays, have been reported to exhibit *in vivo* anti-inflammatory activity only in rare cases in various animal models. One may wonder as to the explanation of such observation. There are several facts that could explain this. First, selectivity could be one of them, thus, compounds that will inhibit the target will likely hit the other members of the family. The fact that one subunit of mPGES-1 also resembles other proteins such as the Huntingtin interacting protein 12 (PDB: 1R0D), the V-type sodium ATP synthase subunit K (PDB: 2BL2) or the protein tyrosine kinase 2 β (b3GM3) is also concerning. Only MK-886 has been demonstrated to exhibit some anticancer properties *in vivo*, mostly due to its FLAP inhibitory properties. However, increasing evidences suggest that dual inhibitors such as 5-LOX/mPGES-1 inhibitors would work well but clinical trials will further validate this novel concept. Second, amino acid sequence disparities between human, mouse and rat may have impaired research. Finally, from a modeling as well as a drug design point of view, the trimeric target possess a very hydrophobic active site and has been proposed to exist in an open and closed conformation. The two facts increase the

complications encountered during the development and/or discovery of novel selective inhibitors for mPGES-1.⁸²

In conclusion, it is clear that mPGES-1 represents an attractive therapeutic target for cancer as well as other disease in which inflammation plays a role. How soon will a mPGES-1 inhibitor be identified and tested in clinical trials will depend on the co-crystallization of a lead compound within the active recently gained and the selectivity that can be achieved within the MAPEG family of enzymes.

2.2 Dual inhibition of 5-LOX/mPGES-1 as new molecular target for the treatment of inflammation and cancer

Although high selectivity is generally one of the primary aims in the development of mPGES-1 inhibitors, the targeted discovery of agents that besides mPGES-1 also interfere with 5-LOX has been pursued in parallel, and various chemical scaffolds have been identified that dually suppress mPGES-1 and 5-LOX. Such simultaneous suppression of PGE₂ and leukotrienes might be a valuable pharmacological strategy to intervene with inflammatory disorders and is expected to have beneficial effects over single interference, not only in terms of better efficacy but also in view of a reduced incidence of side effects.^{83,84} The well-recognized shunting of arachidonic acid derived lipid mediator biosynthesis towards leukotrienes due to suppression of PG formation by COX inhibitors (which cause NSAID-induced asthma) can be circumvented by dual COX/5-LOX inhibitors that had been developed already 20 years ago. The disadvantage of dual COX/5-LOX inhibitors, however, concerns the suppression of beneficial prostanoids such as antithrombotic and vasodilatory PGI₂, but also of gastrointestinal-protective PGE₂. Accordingly, agents that mainly suppress the formation of pro-inflammatory ones (i.e., “inducible” PGE₂, leukotriene B₄ and cysteinyl-leukotrienes) among all eicosanoids may ideally have an exceptional benefit for a safe therapy of inflammation; dual

mPGES-1/5-LOX inhibitors may have this potential. On this basis, the increasing evidences suggest that dual inhibitors such as 5-LOX/mPGES-1 inhibitors would work well but clinical trials will further validate this novel concept. 5-Lipoxygenase (5-LOX), a non-haeme iron-containing dioxygenase, initiates the biosynthesis of leukotrienes (LTs) from arachidonic acid (AA) and it is responsible of the synthesis of anti-inflammatory lipoxins. LTs are involved in the pathogenesis of asthma and allergic rhinitis, but may also play a role in atherosclerosis and cancer. Upon cell stimulation, the cytosolic PLA₂ (cPLA₂) releases AA that is converted by the enzyme 5-LOX into LTA₄. The conversion of AA induced by 5-LOX is facilitated by the nuclear membrane bound 5-LOX-activating protein (FLAP), which will ultimately determine the biosynthesis of the LTs. LTA₄ is then converted to other LTs (i.e. LTB₄ or cysteinyl-LTs) by LTA₄ hydrolase or LTC₄ synthase, depending on the cell type. LTB₄ acts as potent pro-inflammatory agent by inducing chemotaxis and activation of leukocytes, whereas the cys-LTs essentially cause vaso and bronchoconstriction. Because of the significant pathophysiological role of LTs, pharmacological concepts have been developed to either block the action of LTs or to inhibit their biosynthesis. Inhibition of cPLA₂ or of 5-LOX as well as competition with FLAP are effective pharmacological strategies that interfere with LT biosynthesis and there are currently novel 5-LOX and FLAP inhibitors undergoing clinical trials. Similar to mPGES-1, the expression and activity of 5-LOX have been found to be up-regulated in many cancer cell lines, and closely related to tumor size, depth and vessel invasion. It is evident from recent studies that 5-LOX and its downstream products leukotriene B₄ (LTB₄) and 5-hydroxyeicosatetranoic acid (5- HETE) could enhance cell proliferation and suppress apoptosis, thereby promoting the development of carcinogenesis. It seems likely that mPGES-1 and 5-LOX may represent an integrated system that regulates the proliferation, metastatic and proangiogenic potential of cancer cells. Therefore, dual inhibition of mPGES-1 and 5-LOX constitutes a

rational concept for the design of more efficacious anti-inflammatory and antitumoral agents with an improved safety profile. Dual inhibitors that block both mPGES-1 and 5-LOX metabolic pathways of arachidonic acid are expected to possess clinical advantages over the selective inhibitors of enzyme

2.2.1. Human 5-LOX stabilized crystal structure

5-LOX activity is short-lived, apparently in part due to an intrinsic instability of the enzyme. The 5-LOX-specific destabilizing sequence is involved in orienting the carboxy-terminus which binds the catalytic iron. The crystal structure at 2.4 Å resolution of human 5-LOX stabilized was reported by replacement of this sequence.⁸⁵ Leukotrienes (LT) and lipoxins are potent mediators of the inflammatory response derived from arachidonic acid (AA). When leukocytes are activated, arachidonic acid is released from the nuclear membrane by the action of cytosolic phospholipase A₂ and binds 5-lipoxygenase-activating protein (FLAP). The increased Ca²⁺ concentration of the activated cells simultaneously promotes translocation of 5-LOX to the nuclear membrane where it acquires its substrate from FLAP. Arachidonic acid (AA) is converted to leukotriene (LTA₄) in a two-step reaction which produces the 5S-isomer of hydroperoxyeicosatetraenoic acid (5S-HPETE) as an intermediate. Auto-inactivation of 5-LOX activity has been described, and this loss of activity is perhaps important in limiting the synthesis of its pro- and anti-inflammatory products. Previous reports indicate that non-turnover based inactivation is a consequence of an O₂ sensitivity linked to the oxidation state of the catalytic iron. However, not all LOXs display this hypersensitivity to O₂. For example, 8R-LOX activity is stable despite a solvent exposed iron coordination sphere equivalent to that in 5-LOX. In similar conditions 50% of 5-LOX activity is lost in 10 hours. We reasoned that 5-LOX specific destabilizing features may confer susceptibility to non-turnover based

inactivation. Regulatory mechanisms that facilitate transient activation include targeted degradation, phosphorylation, and allosteric control of enzyme activities. Auto-inactivation as a consequence of intrinsic protein instability may play a similar role. For example, the instability of the tumor suppressor protein p53, relative to its orthologs such as p73, has been proposed to have a functional role.

2.2.2. Known 5-LOX inhibitors

5-LOX inhibitors are classified into: redox-type inhibitors that interfere with the redox cycle of the active-site iron; iron ligand-type inhibitors that chelate the active-site iron; non-redox-type inhibitors that compete with AA and/or fatty acid hydroperoxides and ‘novel type’ 5-LOX inhibitors with distinct modes of action. However, only zileuton, an iron ligand-type 5-LOX inhibitor of the N-hydroxyurea series developed by Abbott, has been approved as a LT synthesis inhibitor for pharmacotherapy. Zileuton reportedly inhibits 5-LOX via iron chelation but is devoid of 12- and 15-LOX inhibitory activity.⁸⁶ A78773 proved to be more potent than Zileuton both *in vitro* and *in vivo*. A78773 was 30-fold more potent than Zileuton in the ionophore-stimulated neutrophil assay. One of the most widely studied redox inhibitors is docebenone or 2,3,5-trimethyl-6-(12-hydroxy-5,10-dodecadiynyl)-1,4-benzoquinone (AA-861), a lipophilic quinone structurally resembling coenzyme Q developed by Takeda Chemical Industries, Ltd. (Osaka, Japan). AA-861 is a potent competitive inhibitor of 5-LOX but has no effect on either 12-LOX or COX at concentration 10 mM. ZD2138 by Zeneca, a selective, p.o.- active 5-LOX inhibitor of the methoxytetrahydropyran series, is devoid of redox and iron ligand-binding properties. Despite its promising anti-inflammatory profile, Phase II clinical trials carried out in asthmatics had mixed results, halting further clinical development of this compound. Extensive screening of indole compounds

derived from COX inhibitors indomethacin and sulindac led to development of MK-886 by Merck, the first FLAP inhibitor to reach clinical evaluation. MK-886 is believed to work by binding to an arachidonic acid binding site on FLAP, facilitating the transfer of the substrate to 5-LOX. Optimization of the 2-quinolylmethoxy phenyl residue of Revlon's REV 5901 led to BAY-X1005, a potent, p.o. active inhibitor of 5-LOX developed by Bayer AG to treat asthma. BAY-X1005 reportedly lacks 12-LOX or COX inhibitory activity and is devoid of antioxidant activity. SC 41930, a potent first generation LTB₄ receptor antagonist developed by Searle (Monsanto) has demonstrated potency in a variety of inflammatory models. However, the discovery that SC 41930 inhibits f-MLP-induced superoxide release prompted further research to develop agents with greater potency and selectivity. Ultair (Pranlukast, ONO-1078, SB205312) or N-(4-oxo-2-(1H-tetrazol-5-yl)-4H-1-benzopyran-8-yl)-4-(4-phenylbutoxy)-benzamide, licensed from Ono Pharmaceuticals by Smithkline Beecham, is the first LTD₄ antagonist to be introduced in the world, having been approved to treat asthma in Japan in 1995; it is now in Phase III clinical trials in the United Kingdom and United States.

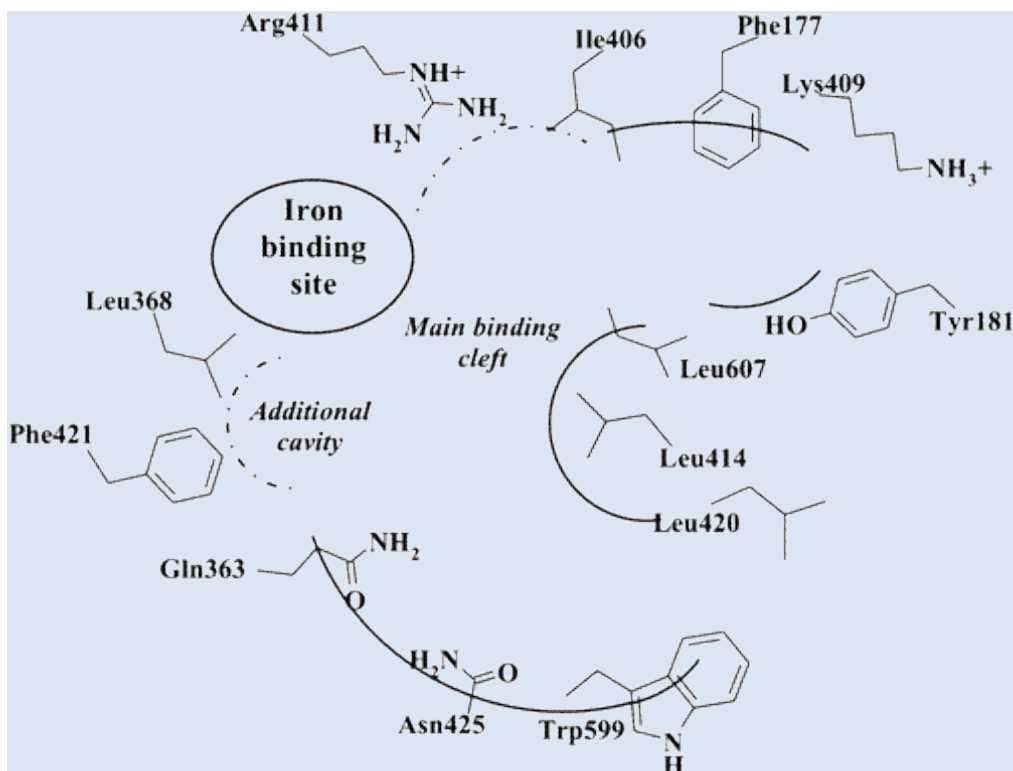


Figure 2. 1. 1 Binding site of 5-LOX.

2.2.3. Dual inhibitors of mPGES-1 and 5-LOX

As mentioned before, suppression of both LTs and PGs biosynthetic pathways might be more advantageous than single interference with prostaglandins formation, in terms of anti-inflammatory effectiveness and of reduced incidence of gastrointestinal and cardiovascular side-effects showed by the traditional NSAIDs and coxibs, respectively. This assumption paved the way for the development of a new class of molecules able to inhibit both mPGES-1 and 5-LOX. Within this class we can include MK-886⁸⁰ and related derivatives⁸¹, pirinixic acid analogues and acylphloroglucinols. MK-886 and its derivatives seem to interfere with cellular PGE₂ biosynthesis also through other mechanisms different from a direct inhibition of mPGES-1. For example, they were proved to interfere with several members of the MAPEG family (FLAP, mPGES-1, and LTC₄ synthase) that might result from a conserved

amino acid motif within this family, in the MK-886 binding pocket of FLAP. Furthermore, licofelone, currently undergoing phase III trials for osteoarthritis, showed potent anti-inflammatory properties in clinical and pre-clinical studies lacking gastrointestinal toxicity. This activity has been related to the simultaneous inhibition of COX-1, mPGES-1 and 5-LOX. The dual mPGES-1 and 5-LOX pirinixin acid derivatives inhibitors were synthesized starting from the PPAR γ agonist WY-14,643. The structural optimization of this lead compound led to the discovery of the potent carboxylic acid which represents the most potent dual inhibitor within this series (mPGES-1: IC₅₀ = 1.3 μ M; 5-LOX: IC₅₀ = 2 μ M). Finally among the acylphloroglucinols noteworthy are myrtucommulone (mPGES-1: IC₅₀ = 1.0 μ M; 5-LOX: IC₅₀ < 30 μ M) from myrtle, hyperforin (mPGES-1: IC₅₀ = 1.2 μ M; 5-LOX: IC₅₀ = 0.09 μ M) from St. John's wort and garcinol (mPGES-1: IC₅₀ = 0.3-1.2 μ M; 5-LOX: IC₅₀ = 0.1 μ M). Their activity seems to be connected with the presence of acylphloroglucinol core which itself is hardly active (IC₅₀ > 30 μ M).

2.3 Scope and outline

The study of ligand-macromolecule interactions has a fundamental role for the design and the development of new and more powerful platforms as anti-inflammatory and anticancer drugs. In this project, different aspects of interaction and recognition processes between ligand and macromolecule has been studied through a combined approach based on computational chemistry techniques and biological assays. In particular, the computational aspects regard the employment and elaboration of screening methods, the analysis of structural determinants responsible of drug-macromolecule interaction and the design and development of new potent bioactive compounds by means of docking calculations. For what concern the biological part, the determination of PGE₂ synthase activity in microsomes of A549 cells, the determination of product formation by 5-LOX in the cell-based and cell-free assay and the

determination of eicosanoids production by LC-MS/MS in monocytes and polymorphonuclear leucocytes were performed at the Department of Pharmaceutical and Medicinal Chemistry of the Friedrich- Schiller University in Jena. Moreover was carry out the preparation of plasma through isolation of monocytes, polymorphonuclear leucocytes and platelets.

Several and different proteins, involved in essential cellular processes, have been investigated as biological targets taking into account their implication in tumor and inflammation initiation and progress with the aim to identify and rationalize new molecules potentially utilizable in therapy. As already reported, in some types of cancer, inflammatory conditions are present before a malignant change occurs. Conversely, in other types of cancer, an oncogenic change induces an inflammatory microenvironment that promotes the development of tumors. Regardless of its origin, inflammation in the tumor microenvironment has many tumor-promoting effects. It aids in the proliferation and survival of malignant cells, promotes angiogenesis and metastasis, subverts adaptive immune responses, and alters responses to hormones and chemotherapeutic agents. The molecular pathways of this cancer-related inflammation are now being unraveled, resulting in the identification of new target molecules that could lead to improved diagnosis and treatment. In particular, the inhibition of mPGES-1 has been proposed as a more promising approach for the development of safer drugs for cancer suppression and in inflammatory disorders^{87,88} devoid of classical NSAID side effects, as this inducible enzyme affects the biosynthesis of massive PGE₂ generation as a response to inflammatory stimuli.⁸⁹ Among the three isoforms so far identified for PGES, it is mPGES-1, functionally coupled with COX-2, which seems to be the isoform primarily involved in pathologies.⁸⁹ Increasing evidences suggest that farther dual inhibitors such as 5-LOX/mPGES-1 inhibitors would work well but clinical trials will further validate this novel concept. Between them, in this project, the attention was focused on targets

(microsomal prostaglandin E synthase, mPGES-1; 5-lipoxygenase, 5-LOX; cyclooxygenase-1, COX-1; cyclooxygenase-2, COX-2; G-protein-coupled purinergic receptors, P2Y₁₂R) with different mechanisms of action involved in diverse levels and phases of tumor and inflammation process.

mPGES-1⁹⁰ is becoming a target for cancer suppression thanks to its inhibitory ability to suppress the PGE₂ synthesis offering the potential for therapeutic benefit without the potential toxicity associated with COXs inhibition. In particular, in the chapter 3 the results obtained by the design and the biological evaluation of new synthetic platforms targeting mPGES-1 and/or acting as dual inhibitor of mPGES-1/5-LOX were discussed. The elucidation of new structural features of the triazole scaffold through docking calculations on the basis of a structure-based analysis was reported.⁹¹ Moreover, was achieved the identification of four synthetic lead compounds from a small library by molecular docking, three of them showed also 5-LOX inhibitory activity. Two of them, acting as weak inhibitors, were further optimized to develop new possible mPGES-1 inhibitors. Finally in this chapter, by means of a structure-based drug design strategy, from a series of novel biphenylic derivatives two potent inhibitors were identified.

The chapter 4 is related to the theoretical and biological evaluation of natural molecular platforms targeting mPGES-1 and/or acting as dual inhibitors of mPGES-1/5-LOX. As first step, we reported the virtual screening of a focused library of natural bioactive compounds by means of molecular docking as potential mPGES-1 inhibitors and the *in vitro* assay of the selected compounds. Afterwards, the *in vivo* and *in vitro* biological evaluation of anti-inflammatory response of carnosol and carnosic acid and *in silico* analysis of their mechanism of action were studied. The biological effects are mainly due to the inhibitory activity on arachidonic related metabolites production, these effects might contribute for the anti-nociceptive, anti-inflammatory and antitumoral property of others *Salvia spp.* containing these diterpenoids, supported by *in silico*

computational analysis. Another study has concerned the molecular mechanism of tanshinone IIA and cryptotanshinone in platelet anti-aggregating effects.⁹² Until now, the molecular mechanisms of action of these two diterpenoids on platelets are partially known. To clarify this aspect, here we utilized an integrated study of pharmacology and computational analysis determining that they are able to inhibit in a concentration dependent manner the rat platelet aggregation and act as antagonist of Gi-coupled P2Y₁₂R.

In the chapter 5, the relative configurations of the giffonins J-P⁹³ were assigned by a combined QM/NMR approach, comparing the experimental ¹³C/¹H-NMR chemical shift data and the related predicted values.

Finally, after a brief conclusions of our studies, the adopted computational techniques, the employed biological evaluation, assay systems and the use of quantum mechanical calculation of the NMR parameters (e.g. chemical shifts) will be described in the appendix.

-CHAPTER 3-

*Determination of new synthetic molecular
platforms as mPGES-1 inhibitors*

3.1 Determination of new synthetic molecular platforms as mPGES-1 inhibitors: structure-based drug discovery

mPGES-1 has emerged as an attractive target for the discovery and development of new anti-inflammatory and anti-cancer drugs. Interestingly, no selective inhibitors targeting mPGES-1 have been identified and, despite the high number of published patents, only one of these drugs has yet made it to the clinic. In this framework, the first X-ray crystal structure of human mPGES-1 (4AL1) published by Geschwindner and co-workers⁷² represents a powerful tool for the rational *in silico* design of potent and efficient mPGES-1 inhibitors. It was crystallized in the presence of GSH in the active site of the enzyme defined mostly by TM1 and TM4 for each of the three subunits. GSH interacts in a 'U-shape' mainly with Arg126, Arg110 and Glu77 from TM4 and His72 from TM1 of another subunit. A model of the open conformation reveals that prostaglandin endoperoxide (PGH₂) could fit into the cleft defined by TM1 and TM4, allowing the synthesis of PGE₂. Moreover, further high-resolution X-ray structures of human mPGES-1 have been reported in complex with several potent inhibitors acting both as substrate (available crystal structures with PDB codes: 4BPM⁷³ 4YK5, 4YL0, 4YL1, 4YL3).⁷⁴ This new structural information, and the retrospective analysis of the mode of interaction of the already developed inhibitors, are useful to confirm the pharmacophoric portions of potential mPGES-1 blocking agents. Thus, the focus of this research is the identification of new synthetic and natural platforms targeting mPGES-1 as anti-inflammatory and anti-cancer agents. AutodockVina¹²⁹ and Glide were chosen as the tool to conduct the computational studies.

Therefore, we report initially the elucidation of new structural features of the triazole scaffold through docking calculations on the basis of a structure-based analysis.⁹¹ In the course of previous studies, we identified a novel class of 1,4-disubstituted 1,2,3-triazoles that inhibited mPGES-1 in a cell-free assay with IC₅₀ values in the low mM range.^{95,96} Afterwards, based on these

considerations, we have undertaken a new structure drug design with the aim of investigating the influence of the ring-substituent topological position and simplifying the mPGES-1 inhibitor structure. The reported results led to the identification of compound **24** that showed efficient inhibitory activity and has proved the importance of halogen bonding as new key interaction useful for the design of this novel triazole derivatives as mPGES-1 inhibitors.⁹¹

Moreover, we achieved the identification of four synthetic lead compounds from a small library by molecular docking, three of them showed also 5-LOX inhibitory activity. **36** and **38**, acting as weak inhibitors were further optimized to develop new possible mPGES-1 inhibitors. In this way, a series of available building blocks to decorate the selected scaffolds were determined to render the ligand more affine and selective for the active pocket. The design of these potential new scaffolds was carried out *in silico* by virtual screening on the basis of a drug-receptor analysis, and were identified the compounds **41** and **42** from spiro[indoline-3,2'-thiazolidine]-2,4'-dione series displaying an increase of the inhibitory activity (mPGES-1 inhibition of 30% and 50% respectively) with respect to the lead compound and the compound **43** from nitrofurans displaying highest inhibitory activities with an IC_{50} of $1.37 \pm 0.7 \mu M$.

Finally in this chapter, by means of a structure-based drug design strategy, from a series of novel biphenylic derivatives two potent inhibitors were identified.⁷⁴ It has guided to the identification of 2 potent inhibitors of the enzyme **44** and **47** showing the strongest inhibitory activity, validated with biological assay. These results encouraged us to start a focused SAR exploration to define the effect of the fluorine atom and the importance of nitro groups, which can influence the cytotoxicity and the pharmacokinetic properties. *In vitro* biological test of the new designed compounds show that the fluorine atom and nitro groups are essential for the inhibitory activity.

Some of them have an action on other enzymes within the arachidonic acid cascade, such as 5-LOX. In fact, interference with 5-LOX, the key enzymes in

the formation of leukotrienes (LTs) from arachidonic acid, is considered a valuable characteristic of a given mPGES-1 inhibitor, because dual suppression of PGE and LT formation might be superior over single interference in terms of higher anti-inflammatory efficacy as well as in terms of reduced side effects.⁹⁴

3.1.1. Elucidating new structural features of the triazole scaffold for the development of mPGES-1 inhibitors

As confirmed by Geschwindner's work,⁷² the mPGES-1 active site is subdivisible in cofactor (GSH) and substrate (PGH₂) binding sites. Moreover, it includes the N-terminal (helices II and IV), the C-terminal (helix I) and an adjacent monomeric cytoplasmic domain. In more detail, the major portion of the active site is occupied by GSH while only the PGH₂ ring interacts with it. This pattern of binding is well represented by the co-crystallized structure of mPGES-1 with the GSH analogue, 1-(4-phenylphenyl)-2-(S-glutathionyl)-ethanone and a β -octyl glucoside, which discloses key interactions for the rational design of substrate's competitors (Figure 3.1.1).

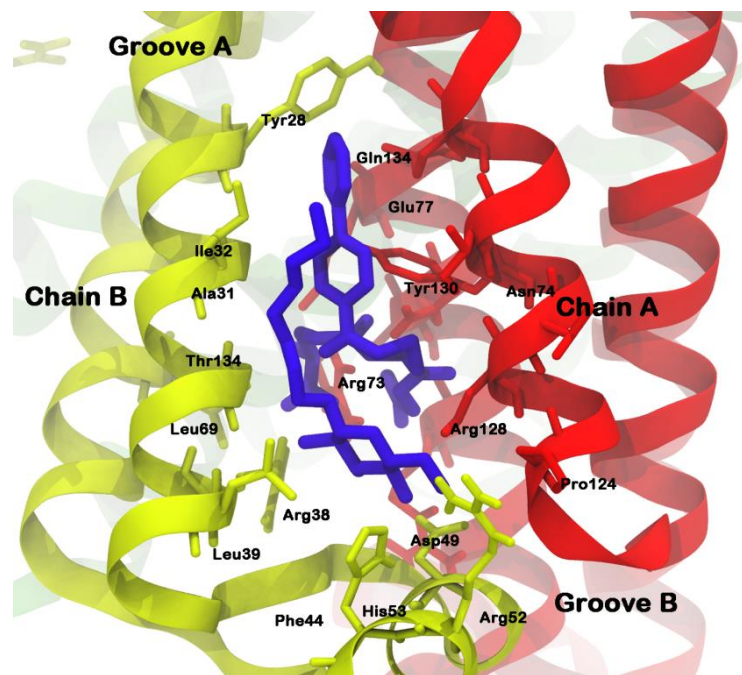


Figure 3.1.1.1 Three dimensional model of mPGES-1 in complex with GSH analogue and β -octyl glucoside depicted by violet stick and balls. The crucial amino acids of mPGES-1 receptor are depicted by stick and balls, and ribbon colored by chains (A, red; B, green; C, light blue).

In the course of previous studies, we identified a novel class of 1,4-disubstituted 1,2,3-triazoles that inhibited mPGES-1 in a cell-free assay with IC_{50} values in the low mM range.⁹⁵ In particular, compound **4** (Figure 3.2) showed the most promising activity with an IC_{50} of 0.7 mM in the microsomal fraction of A549 cells that was used as a source for the human mPGES-1 enzyme.⁹⁶ These active compounds were disclosed by means of structure-based studies using the microsomal glutathione transferase 1 (MGST-1) as the model enzyme.^{97,98,99,100,101,102,103,104} Thanks to the 4AL1 human mPGES-1 X-ray structure resolution and studies, we have used Glide software (version 9.6)¹⁰⁵ with extraprecision (XP) mode, and we have designed the triazole compounds for an optimal placement in the substrate's binding site. On this basis, we analysed our previous results in relation to the model reported above (Figure

3.1.1). As shown by Geschwindner, a competitive inhibitor of mPGES-1 should be able to interact with Ile32 and Tyr28 of chain B, and Gln134 and Tyr130 of chain A in groove A, as well as with the cofactor, with Arg126, Ser127 of chain A, and with Asp49, His53, Arg38, Phe144 of chain B in groove B (Figure 3.1.1). The best binding modes of compounds 1–5 are in agreement with the key interactions reported for the putative mPGES-1 inhibitor (Figure 3.1.2).

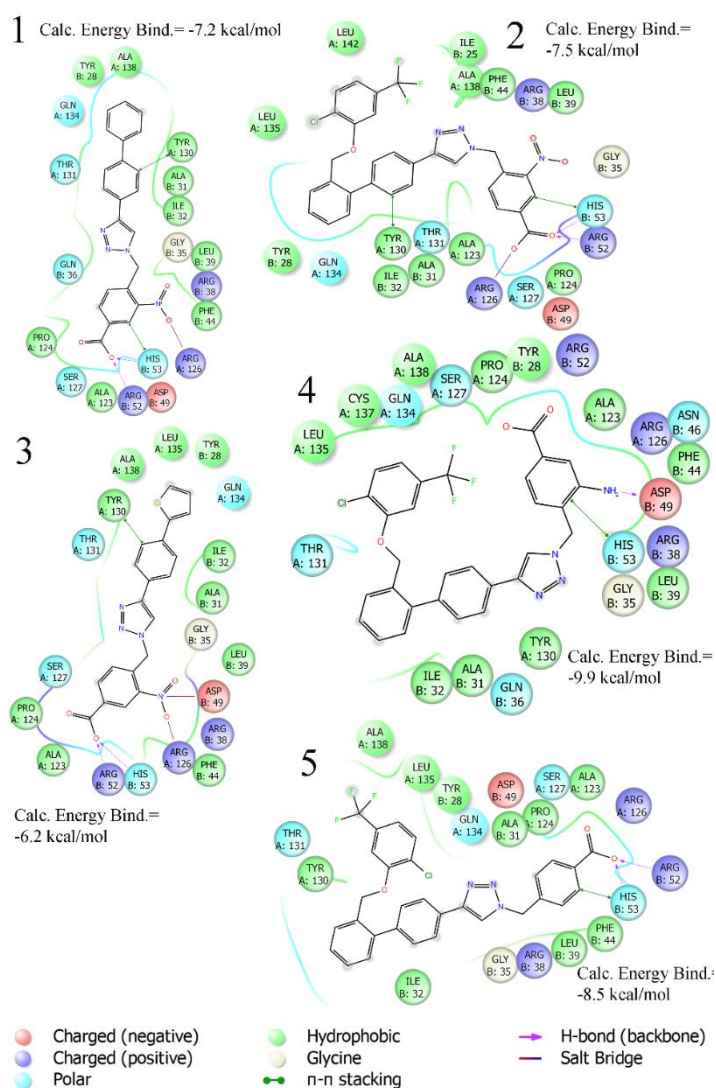


Figure 3.1.1.2 2D diagram interactions of active triazole-based inhibitors 1–5.

Based on these considerations, we have undertaken a new structure drug design with the aim of investigating the influence of the ring-substituent topological position and simplifying the mPGES-1 inhibitor structure. In fact, as can be seen from the 2D diagram interactions (Figure 3.1.2), in our previous triazole inhibitors, the key features were represented by a benzyl group at the N1 position bearing a para hydrogen bond acceptor able to interact with groove B, responsible for PGH₂ recognition and involved in its isomerisation into PGE₂; and bis-aryl substituents at the C4 position, which establish hydrophobic and π - π interactions with groove A. Interestingly, in the crystallized model of the GSH analogue (Figure 3.1) only the first aromatic ring of the biphenyl portion directly bonded at position 4 is involved in π - π interactions with the key amino acid Tyr130 (A), while the second aromatic ring is involved in hydrophobic interactions with groove A (e.g. Gln134 (A) and Tyr 117 (A)).

Based on this, we present herein the effect of the substituents inversion on the triazole ring. Thus, a phenyl ring was positioned on N1, while a phenoxy-methyl group was attached at the C4 position (scaffold II, Figure 3.1.3). Moreover, as an effort to improve the activity with respect to the previous molecules, we also explored the substitution at position C5 (R₇, Figure 3.1.3 and 3.1.4). The first step towards the scaffold optimization was the introduction of a p-substituent on ring B (II, Figure 3.1.3). Docking studies performed on compounds 6–8 revealed that none of them was able to interact with groove B. Therefore, in order to improve the interaction with its amino acids (e.g. Ser127 and Arg126), we introduced another hydrogen bond acceptor, namely a CF₃ group, at R₃ of ring B (scaffold II, Figure 3.1.3), in analogy to the ring B of scaffold I (Figure 3.1.3) of the previously reported molecules (Figure 3.1.2).

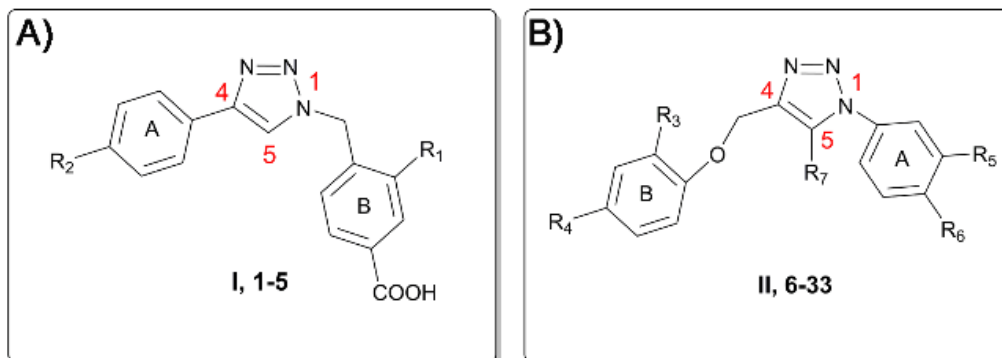


Figure 3.1.1.3 Scaffold hopping of the triazole pharmacophore. (A) Scaffold I, compounds **1-5**. (B) Scaffold II, compounds **6-33**.

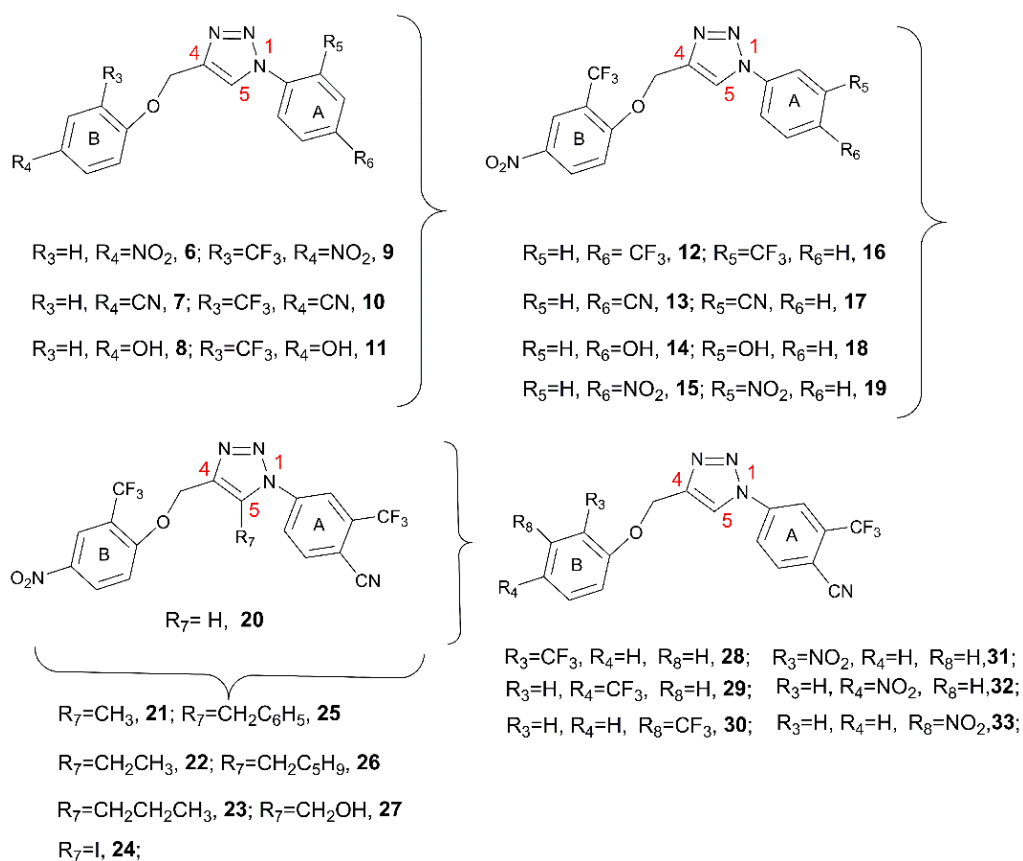


Figure 3.1.1.4 Triazoles **6-33** structures.

Docking studies on derivatives **9–11** showed that, with respect to **10** and **11**, scaffold **9** strongly interacts with groove B, being able to simultaneously interact with Arg126 (A), Arg38 (B), Asp49 (B) and Ser127 (A) (Figure 3.1.5), thus **9** was selected for further optimization. By superimposing the binding mode of **9** with respect to the lead compound **4** in the mPGES-1 structure, the para and meta positions of ring A (II, Figure3.1.3) were identified as the most suitable and attractive for modifications. For this reason, compound **9** was functionalized with four different hydrogen bond acceptors (e.g. CF₃, NO₂, OH and CN) at meta and para positions, respectively (Figure3.1.4, compounds **12–19**). From the analysis of the docking results (Figure3.1.6), the best substitutions were represented by the CF₃ group at meta and para positions (**12**, predicted energy of binding = -7.4 kcal mol⁻¹ and **16**, predicted energy of binding = -7.2 kcal mol⁻¹), and by the CN group at the para position (**17**, predicted energy of binding = -6.4 kcal mol⁻¹), displaying an energy gain of ca. 1.5 kcal mol⁻¹ in comparison to those of the other complexes.

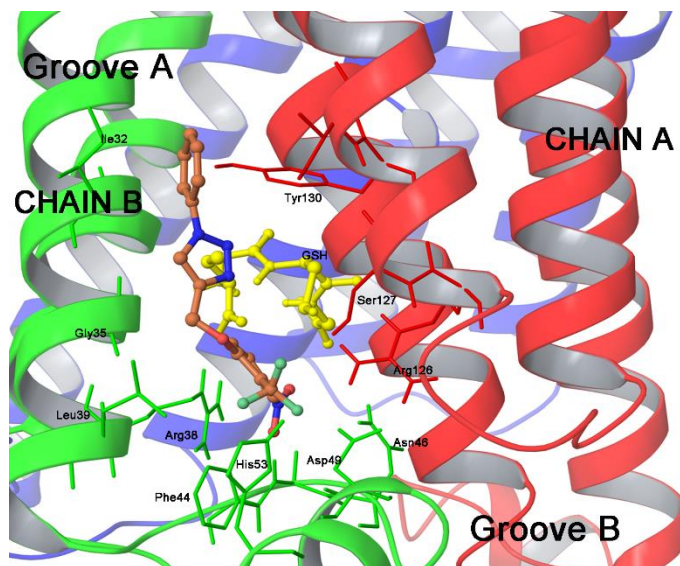


Figure 3.1.1.5 Three dimensional model of scaffold **9** (orange sticks) in mPGES-1 binding site.

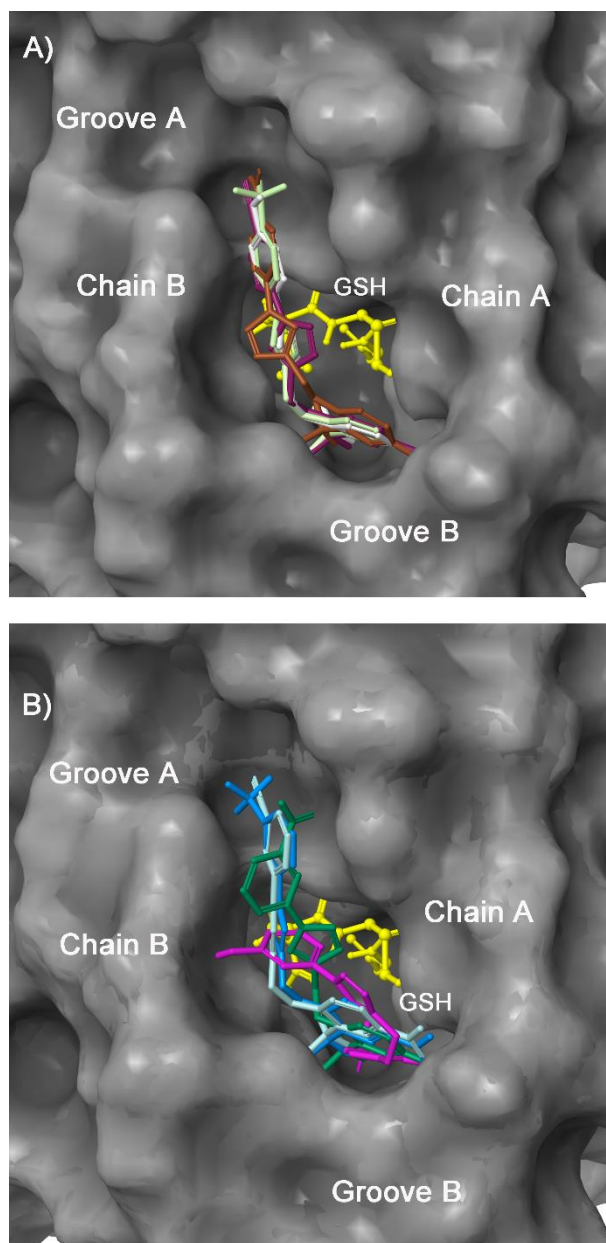


Figure 3.1.1.6 Superimposition of **12** (light green), **13** (purple), **14** (white), and **15** (brown) (panel A), and **16** (light blue), **17** (cyan), **18** (magenta), and **19** (dark green) (panel B) in the mPGES-1 binding site.

In order to further extend the compounds' virtual library, we inserted a chimeric substituent at N1 of the triazole scaffold with CF_3 at meta and a CN group at para position of ring A (compound **20**, Figure 3.1.4), which provided

a calculated binding energy of 7.6 kcal mol⁻¹. Moreover, the analysis of the binding mode of **20** (Figure3.1.7) suggested that a substituent at position C5 of the triazole ring should protrude towards a left hydrophobic side (Ile32, Ala31 chain B) and a right side where the polar amino acids Thr131 and Ser127 of chain A are located. As a consequence, we explored the effect on the binding energy of properly selected substitutions at this position (compounds **21–27**, Figure3.1.4). As a result of the docking studies, derivative **24**, which bears an iodine atom at C5, displayed the most promising binding mode (Figure3.1.8).

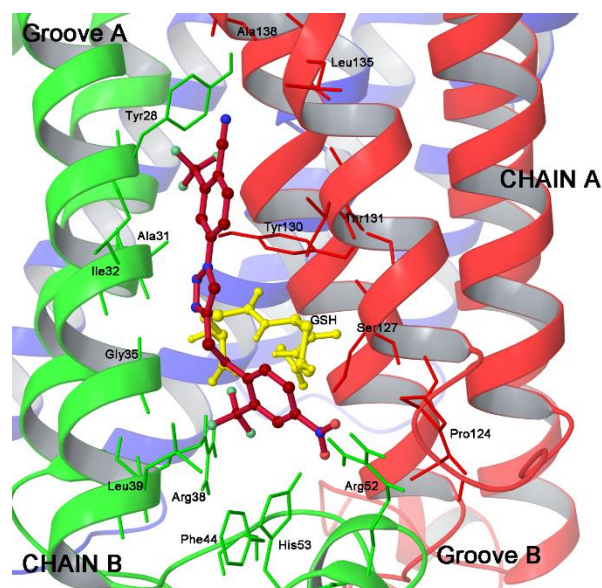


Figure 3.1.1.7 Three dimensional model of scaffold **20** (red sticks) in mPGES-1 binding site.

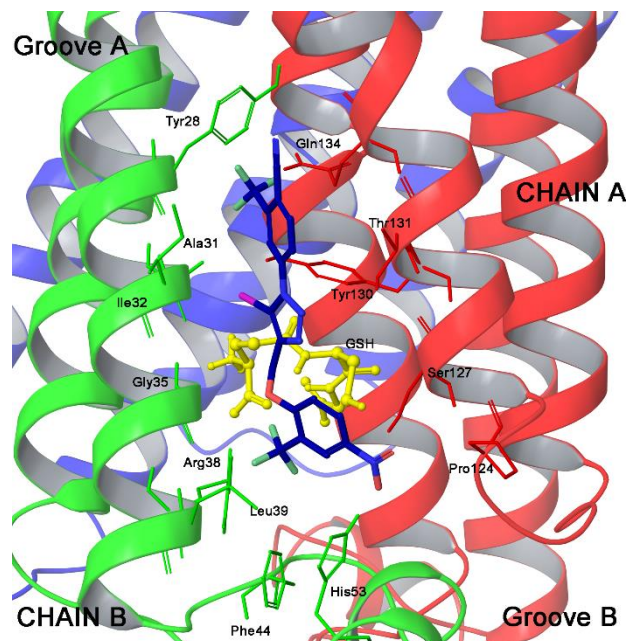


Figure 3.1.1.8 Three dimensional model of **24** (blue sticks) in the mPGES-1 binding site.

In more detail, the portions at C1 and C4 of the triazole ring maintained similar binding modes of **20** (Figure3.1.8), while the iodine atom at C5 is involved in a halogen bond with CO of Ala31 (B). These optimal interactions were associated with a calculated binding energy of $8.8 \text{ kcal mol}^{-1}$ for **24**, which was in good agreement with the calculated affinities of our lead compound **15** (Figure3.1.2). Moreover, the iodine atom at position C5 presents several advantages with respect to the other halogens especially in terms of halogen bonding strength, which decreases from iodine to chlorine. In summary, our docking studies suggested that this revisited version of triazole based inhibitors should be able to interact with mPGES-1 in the same manner of the previously reported **2**, **4** and **5** inhibitors, and that the halogen atom should play a fundamental role in the inhibition activity.

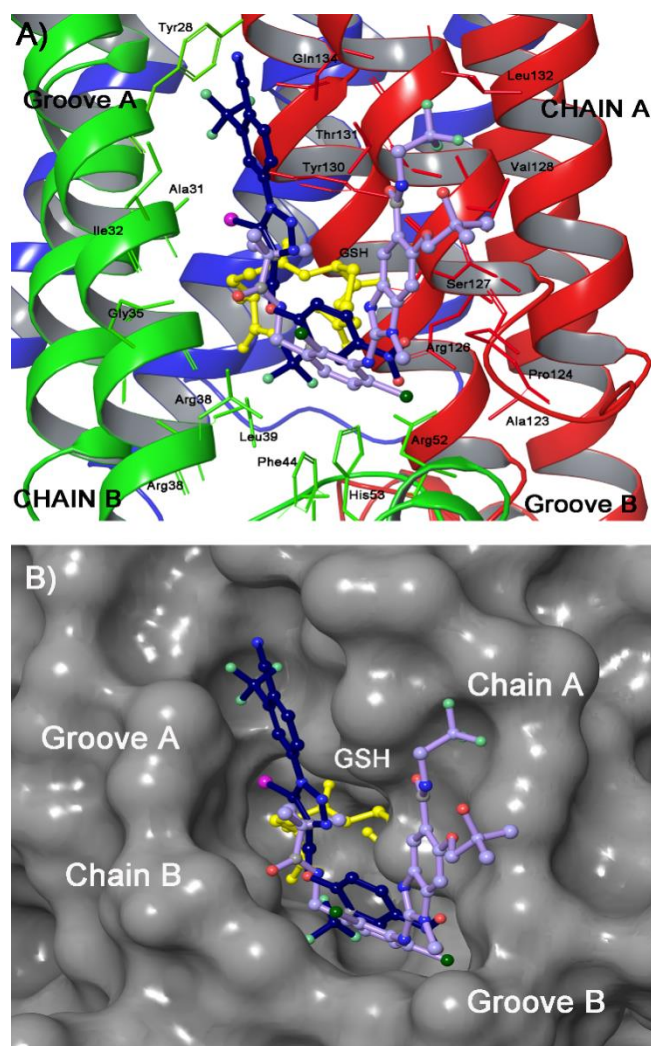


Figure 3.1.1.9 Superimposition of **24** (blue sticks) with LVJ (light violet) (panel B) in the mPGES-1 binding site.

To prove our hypothesis, starting from compound **20**, we have synthesized compounds **16**, **20** and **24**. Moreover, starting from scaffold **20**, to prove the influence of topology of selected hydrogen bond acceptors on ring B (NO₂ and CF₃ group), we have designed another small pool of compounds (**28–33**), and synthesized among them the most significant compounds (**29** and **30**). The biological evaluation of the representative compounds (**16**, **20**, **24**, **29**, and **30**) on the mPGES-1 activity in a cell-free assay showed efficient inhibitory

activity for **24** ($IC_{50} = 0.7 \pm 0.2$ mM) (Figure 3.1.10) and significant but incomplete suppression of mPGES-1 activity by the other compounds (20% inhibition at 10 mM, $IC_{50} > 30$ mM).

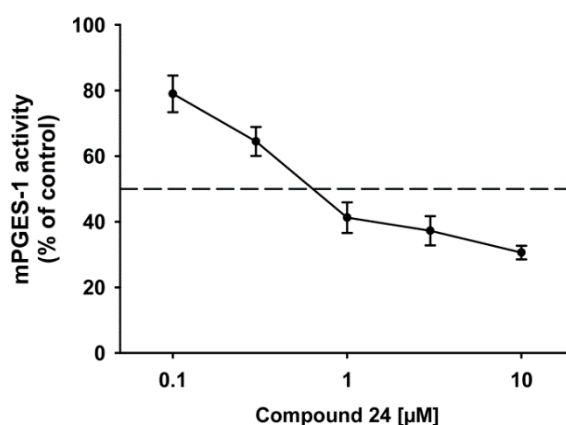


Figure 3.1.1.10 Inhibition of mPGES-1 activity by compound **24** in a cell-free assay. Data are means \pm S.E.M., $n = 3$.

To further corroborate the influence of an iodine atom at C5 on a triazole scaffold on the biological activity, we have compared the putative binding mode of **24** with respect to the known inhibitor LVJ recently co-crystallized with the mPGES-1 enzyme by Caffrey and co-workers (4BPM).⁷³ Figure 3.9 clearly shows the good superimposition of the aromatic ring B of **24** with respect to the bischlorophenyl ring of LVJ in groove B of the mPGES-1 surface, even if a more potent inhibitor (2.4 nM) makes an optimal π - π stacking with Phe44. On the other hand, peculiar interactions of the benzimidazole portion of LVJ with Ile132, Val128, Ala123, and Arg52 are partially balanced by the halogen bonding of **24** with Ala31, and by the contacts with Tyr28, Gln134 accounting for the minor inhibitory potency of **24** with respect to LVJ. Even if **24** shows a relatively simple skeleton in comparison to LVJ, the docking results suggest that the different patterns of interactions established

with mPGES-1 are sufficient to support its biological activity in occupying and inhibiting the enzyme binding site. In conclusion, thanks to the recent disclosure of the mPGES-1 X-ray crystal structure, we were able to perform a structure-based design of a novel class of potential mPGES-1 triazole inhibitors. In particular, compound 24 was identified as the most promising of the series, enabling the interaction with the membrane protein and occupying the PGH₂ binding site, and inhibiting mPGES-1 activity in a cell-free assay with IC₅₀ = 0.7 mM. The smaller dimension and different interactions of the rings A and B with respect to the lead compound (**4**) are balanced by the presence of an iodine atom at position C5 and of precise positions of the substituents on these two rings. In fact, the halogen bonding of the iodine atom with the receptor backbone resulted as a new key interaction suitable for the design of new mPGES-1 inhibitors, proved by the complete inactivity of compounds lacking this atom.⁹¹

3.1.2. Evaluation of a small synthetic library acting as mPGES-1 inhibitors

The computational study on this small synthetic library was structured in two main tasks: identification of new compounds showing activity against mPGES-1, and the progressive optimization of the identified lead compounds (**36-38**) with improved potency and, eventually, improved efficacy. In the first task, the identification of leads was carried out by virtual screening of a small synthetic library. We performed the molecular docking of the potential candidates using Autodock Vina¹²⁹ in presence or absence of GSH, taking into account the possibilities that the potential inhibitor would displace the substrate PGH₂ or it would compete with GSH for the binding. The 150 compounds were selected by affinity average ($-10.1 < \Delta G < -9.5$ kcal/mol) and by crucial interactions. In more details, the interaction with Ile32 and Tyr28 of chain B, and Gln134 and Tyr130 of chain A in groove A, as well as with the cofactor,

with Arg126, Ser127 of chain A, and with Asp49, His53, Arg38, Phe144 of chain B in groove B were considered essential for the inhibitory activity. This step allows to select candidates with an high docking score and a rational binding mode. Previous studies have demonstrated that the hydrogen bond between inhibitor and Ser127 or His53 or Thr131 was necessary for mPGES-1 inhibitory activity which was consistent with our analysis. Both van der Waals and electrostatic components play key roles in the binding. In particular the analysis of docking results (Figure 3.1.2.1) led us to choose seven compounds (34-40), which are shown in the Figure 3.1.1.2.

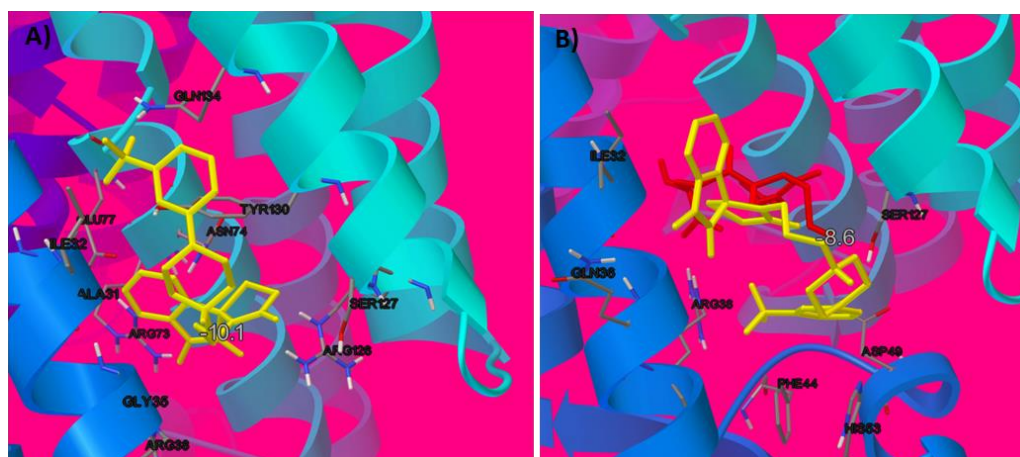


Figure 3.1.2.1 Three-dimensional model of the interactions between **36** and mPGES-1 in absence of GSH (A) and in presence of GSH (B). The protein is depicted by ribbons and tube. **36** is represented by sticks (yellow). GSH is represented by sticks (red).

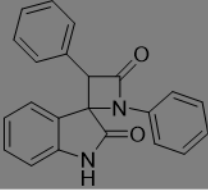
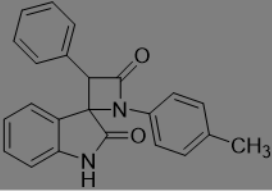
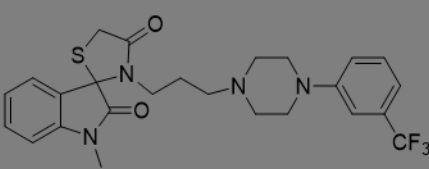
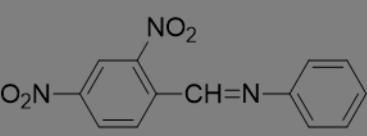
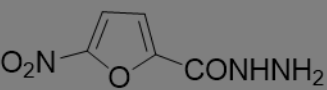
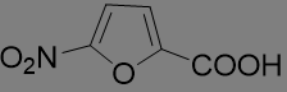
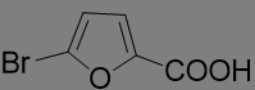
34	
35	
36	
37	
38	
39	
40	

Figure 3.1.2.2 Chemical structures of the selected compounds.

The hits selected via virtual screening were then validated using an *in vitro* mPGES-1 activity assay. The inhibition of mPGES-1 activity by the test compounds was assessed in cell-free assays using overexpressed mPGES-1 in microsomal preparations of interleukin-1 β -stimulated A549 cells.¹⁰⁶ In particular, the determination of product formation by mPGES-1 demonstrated that the compounds **34-38** exhibited weak inhibitory activity (Figure 3.1.2.3). Analysis of the inhibition of mPGES-1 activity (i.e., the transformation of PGH₂ to PGE₂) by a given compound in the cell is not immediately feasible, since other enzymes than mPGES-1 are involved in PGE₂ formation in stimulated cells (i.e. COX-1/2, cPGES and mPGES-2), and an appropriate test system is not available. The mPGES-1 inhibitor MK-886 (3-(3-(tert-butylthio)-1-(4-chlorobenzyl)-5-isopropyl-1H-indol-2-yl)-2,2-dimethylpropanoic acid), was used as reference compound.

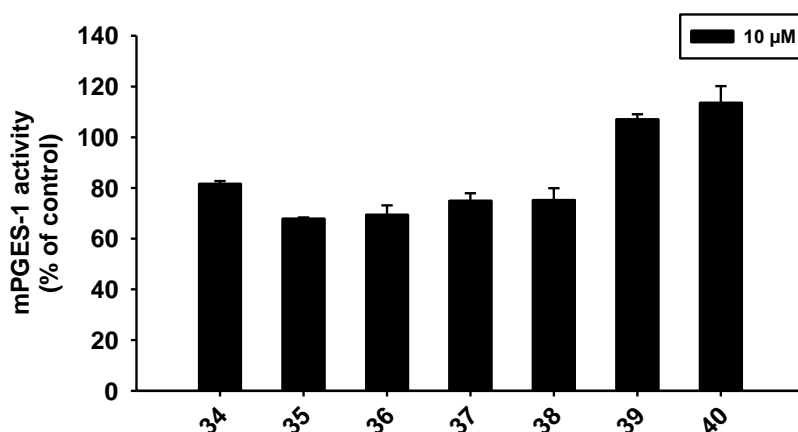


Figure 3.1.2.3 Effect of the selected compounds on mPGES-1 activity. Data are given as means \pm SE, n = 3.

A promising approach to enhance the efficacy is offered by targeting with a single agent more than one component of the inflammatory cascade. Furthermore, in order to find dual inhibitor of mPGES-1/5-LOX or to investigate the selectivity profile, the selected compounds were also tested

against 5-LOX enzyme. The inhibition of 5-LOX activity by the test compounds was assessed in cell-based assays using ionophore A23187-stimulated human polymorphonuclear leukocytes (PMNL) in the presence of exogenous AA (20 mM) as 5-LOX substrate.¹⁰⁷

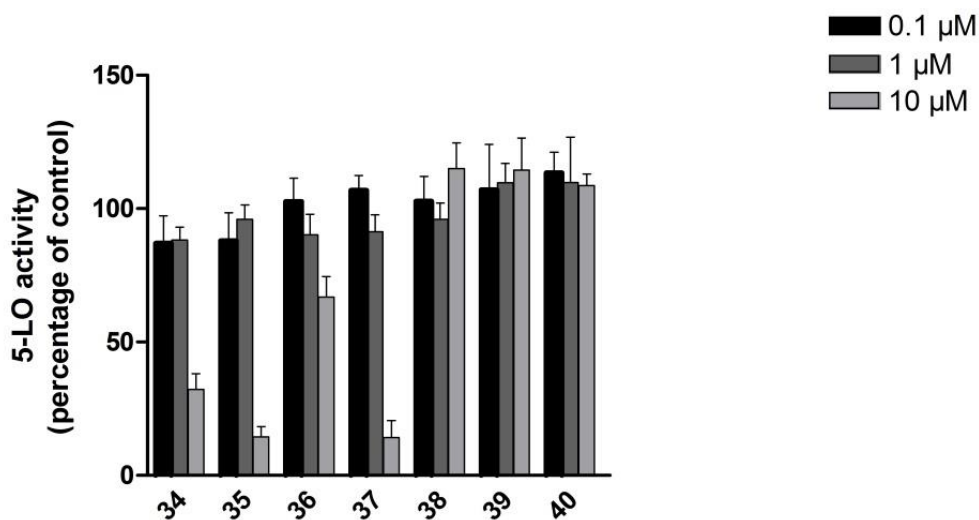


Figure 3.1.2.4 Effect of selected compounds on 5-LOX activity. Data are given as means \pm SD, n = 3.

5-LOX activity was suppressed by **34-35** and **37** in intact cells (Figure 3.1.2.4). Of interest, the compounds **35-37** showed the lower IC₅₀ values of 3.76 ± 1.2 and 3.63 ± 0.9 μM μM respectively (Figure 3.1.2.5), which have good mPGES-1 inhibitory activity as well.

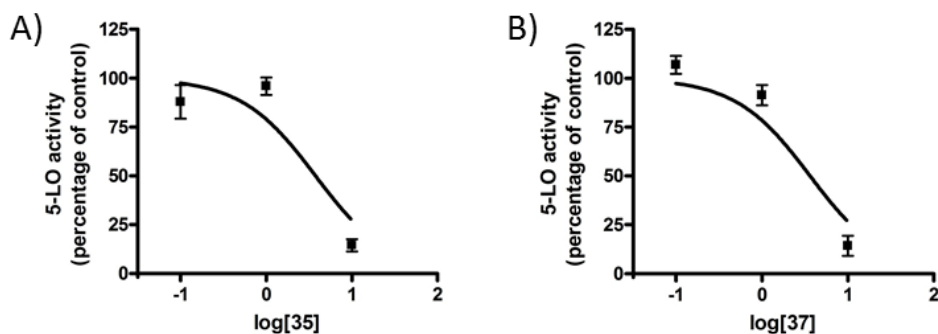


Figure 3.1.2.5 Concentration-response curves of compounds **35** (A) and **37** (B) for inhibition of 5-LOX activity. Data are given as means \pm SD, n = 3.

Note that in intact PMNL a given test compound may suppress 5-LOX product synthesis without inhibiting 5-LOX directly, for example by modulating cellular co-factors of 5-LOX or by targeting other enzymes involved in LT synthesis (e.g., FLAP, LTA4H, LTC₄S). The 5-LOX inhibitor BWA4C ((E)-N-hydroxy-N-(3-(3- phenoxyphenyl)-allyl)acetamide) was used as control). Considering the frequent co-expression of these two enzymes and the striking analogy of their biological functions, dual inhibitors of mPGES-1 and 5-LOX may present a superior anticancer profile in carcinogenesis. And notably, there is a cross-talk between mPGES-1 and 5-LOX pathways, inhibition of only one of them would shunt AA metabolism to the other pathway, thereby inducing potential side effects. Hence the dual mPGES-1/5-LOX inhibitors would be safer under the anti-inflammatory profile.

The reported weak inhibitors represent promising starting points for further medicinal chemistry optimization. Therefore, we are confident that we can design and optimize the leads based on the predicted binding mode to improve the potency.

3.1.3. Optimization of 36-38 derivatives as mPGES-1 inhibitors

Continuing the studies described in the previous paragraph, some interesting molecules able to inhibit mPGES-1 as well as other key enzymes of the arachidonic acid cascade such as 5-lipoxygenase (5-LOX) were identified. The good accordance between the biological results and the predictions of molecular docking calculations for the compound **36** and **38** has prompted us to develop some derivatives of these two compounds. The identification of the most promising binding poses represented the starting point for the design of

optimized compounds, able to bind the protein with higher affinity with respect to the parent compound covering further regions thanks to the additional chemical groups. In more detail, the previous investigations have disclosed **36** and **38** able to efficiently interact with key aminoacid residues in the catalytic site.

Furthermore, the crystal structures of mPGES-1 reveals the standard requirements and key features needed for the enzyme inhibition. Firstly, a binding groove is between the GSH binding site and a molecular surface nearby the cytoplasmic part of the protein, mainly composed by aromatic (B:Phe44, B:His53) and polar (B:Arg52) residues. A potential ligand could establish π - π contacts with these aromatic groups, as occurred for the co-crystallized LVJ inhibitor. Moreover, Ser127 on chain A represents another fundamental residue, since it was supposed to be involved in the catalytic process behind the isomerization of PGH₂ to PGE₂. Finally, moving from the external part of endoplasmic reticulum membrane to the cytoplasmic part of the protein, an external binding groove is identifiable at the intersection between helix 1 of chain B and helix 4 of chain A, with polar (A:Gln134), aliphatic (B:Val24) and aromatic (B:Tyr28) residues, and could be bound by long molecular functions. Considering the structural requirements for mPGES-1 inhibition, we initially aimed at identifying a potential moiety that can interact with catalytic site and additional substituents to capture such polar and hydrophobic interactions with the external or the upper groove. In line with these considerations, it was decided to leave the spiro[indoline-3,2'-thiazolidine]-2,4'-dione and the nitrofurans moieties unchanged and to variously decorate the right hand portion of the molecule(Figure 3.1.3.2).

Initially we just designed a small pool of 3'-(2-(piperazin-1-yl)ethyl)spiro[indoline-3,2'-thiazolidine]-2,4'-dione derivatives through the introduction of 10 acyl halides in R₁, 2 alkylic halides in R₂ and the reduction by 3 to 2 C atom linker to understanding the influence of this different

substituents in that position and of the length of the linker with respect to the compound **36** (Figure 3.1.3.1).

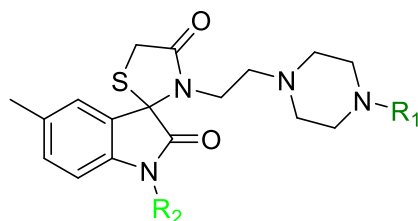


Figure 3.1.3.1 Scaffold structures of **36** with attachment points.

After an accurate design regarding the compound **36** taking into account the spiro[indoline-3,2'-thiazolidine]-2,4'-dione scaffold, we designed two series of compounds: the design of the NH spiro[indoline-3,2'-thiazolidine]-2,4'-dione series was done through the introduction of 80 acyl halides in R_1 ; moreover the design of the NR spiro[indoline-3,2'-thiazolidine]-2,4'-dione series was done through the introduction of 80 acyl halides in R_1 in all possible combination with 12 acyl halides in R_2 . In both, the substitution of the carbonyl group with ester and alcohol groups and the elongation of chain linker by 3 to 5 C atom were investigated; obtaining in total about 66000 compounds (Figure 3.1.3.2).

For what concerns the compound **38**, we also performed the design of two series of nitrofurans: the first series was designed through the introduction of 68 amines in R_1 in all the possible combination with 2 acyl halides in R_2 ; the second series was drawn through the reduction from nitro to amine group and the introduction of 48 acyl halides in R_3 . Moreover the substitution of nitrofurans with benzonitrofurans was explored; obtaining in total about 4800 compounds (Figure 3.1.3.2).

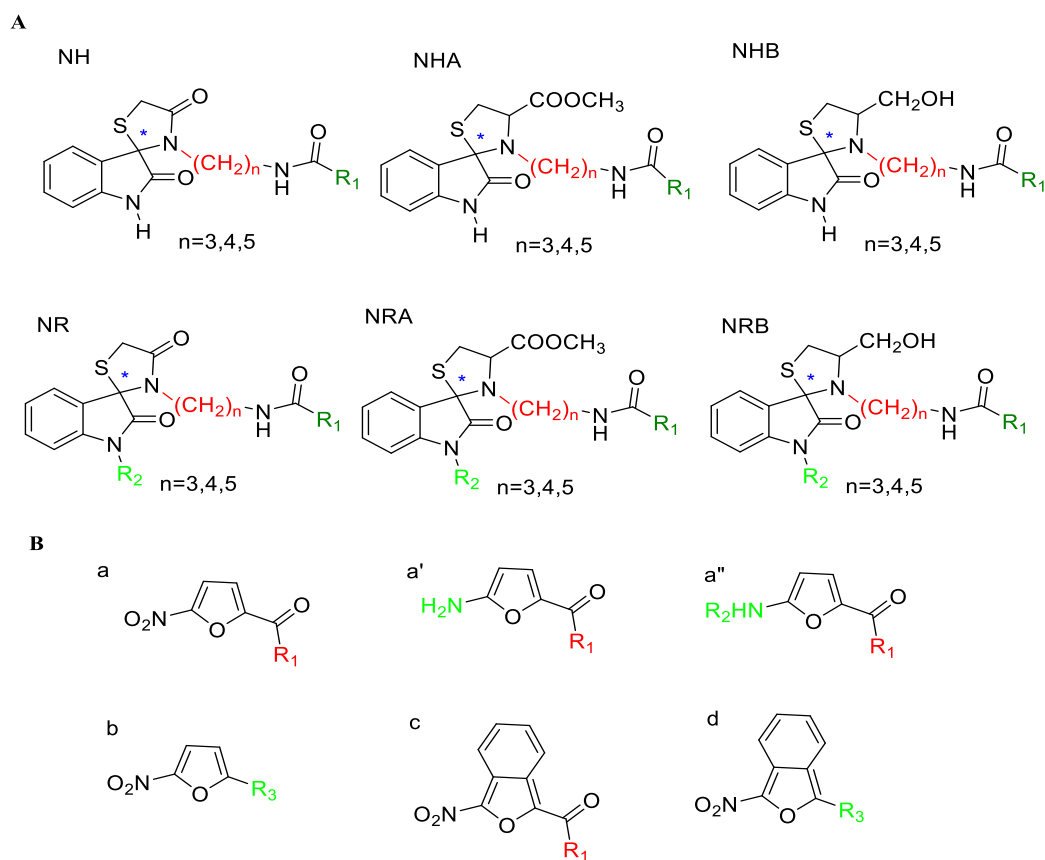


Figure 3.1.3.2 Scaffold structures of **36** and **38** with attachment points.

We performed the molecular docking of the potential candidates' library using Autodock Vina¹⁴⁷ in presence or absence of GSH. After the evaluation of the binding energies, these compounds were inspected to check whether they had interactions with the binding pocket of mPGES-1 and the external upper and lower grooves. The obtained results point out two different docking poses for these two first series as potential mPGES-1 inhibitors: the first one includes molecules which have some interactions with the aminoacids of the external upper groove as Tyr130, Thr131 and Gln134; the second family relates to compounds which show a deep interaction mode strictly closed to the GSH and establish interactions with lower groove like Arg52, His53 and Phe44. However, all the designed molecules accommodate in the ligand pocket

situated in the region at the interface of the two mPGES-1 subunits interacting with the fundamental residues, which guarantee, at least in theory, the mPGES-1 binding (Figure 3.1.3.3). We also investigated the effects of the length of the linker's chain and the effect of the ketone, alcohol or ester groups, identifying 3 atom's linker and ketone group as energetically favourite for the mPGES-1 activity.

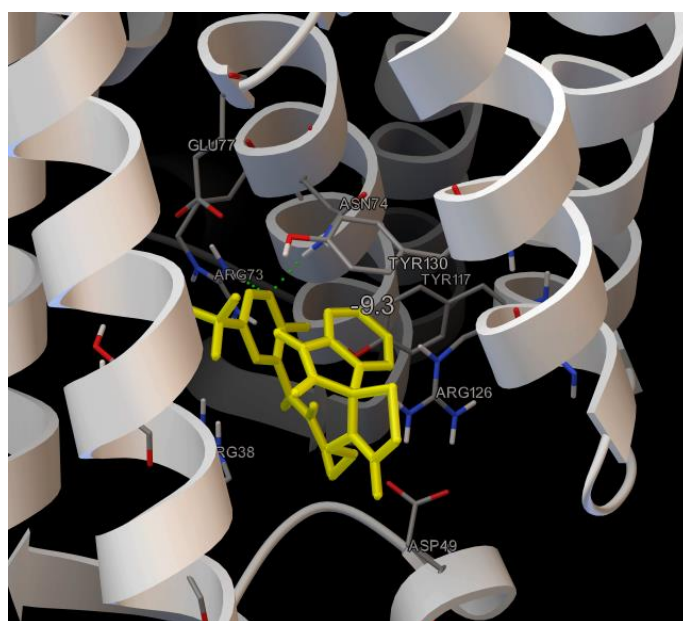


Figure 3.1.3.3 Three-dimensional model of the interactions between **41** and mPGES-1 in absence of GSH. The protein is depicted by ribbons and tube. **41** is represented by sticks (yellow).

We identified two promising candidates by the optimization of compounds **36** (**41** and **42** Figure 3.1.3.4) and one by the optimization of compounds **38** (**43**Figure 3.1.3.5) as mPGES-1 inhibitor after selection by affinity average and by crucial interactions. In the Figure 3 is showed the

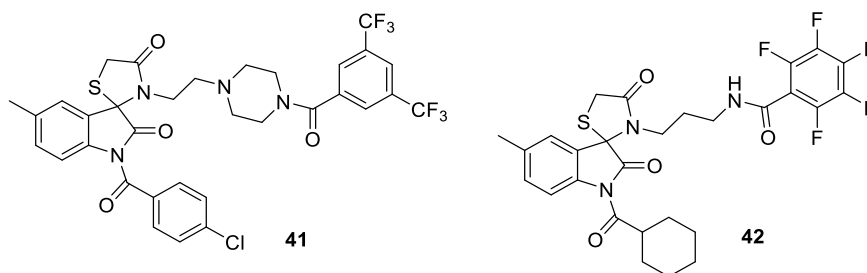


Figure 3.1.3.4 Chemical structures of the selected compounds **41** and **42**.

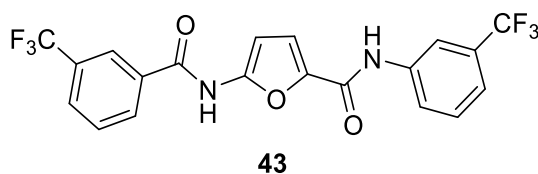


Figure 3.1.3.5 Chemical structures of the selected compound **43**.

This theoretical result can qualitatively explain the biological interaction with the target confirmed by potent inhibitory activity. The predicted activity values are in good agreement with the experimental data. Herein we report the screening results of mPGES-1 inhibitory activity *in vitro* of the two synthesized compounds of the spiro[indoline-3,2'-thiazolidine]-2,4'-dione series. The two compounds **41** and **42** displayed an increase of the inhibitory activity (mPGES-1 inhibition of 30% and 50% respectively) with respect to the lead compound (Figure 3.1.3.6).

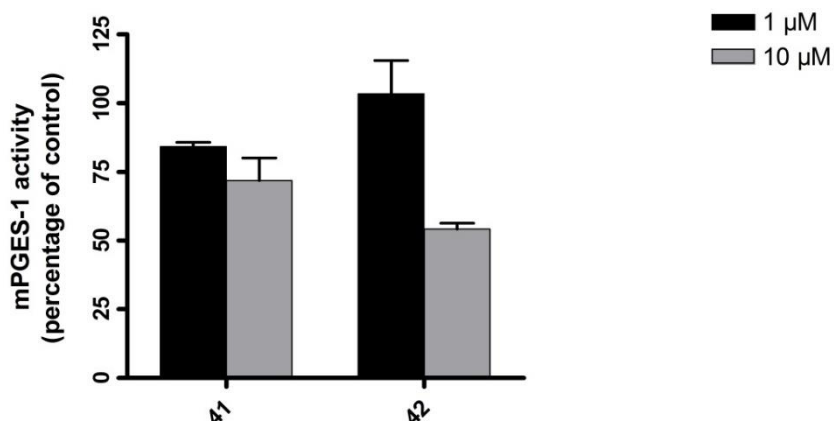


Figure 3.1.3.6 Effect of selected compounds on mPGES-1 activity. Data are given as means \pm SD, n = 3.

The inhibition curve (plot of the inhibition rate vs the concentration) for selected compound **43** of the nitrofurans derivatives is illustrated in Figure 3.1.3.7.

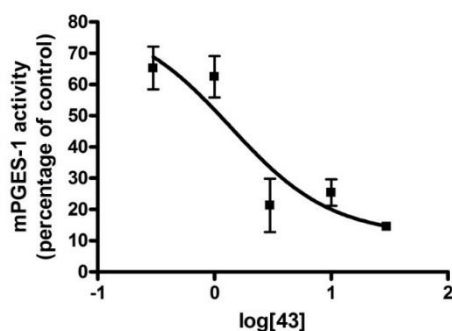


Figure 3.1.3.7 Concentration-response curves of compounds **43** for inhibition of mPGES-1 activity. Data are given as means \pm SD, n = 3.

The compound **43** displayed highest inhibitory activities with an IC_{50} of $1.37 \pm 0.7 \mu\text{M}$ (Figure 3.1.3.8).

The inhibition of 5-LOX activity by the test compounds in cell-based assays using ionophore A23187-stimulated human polymorphonuclear leukocytes (PMNL) in the presence of exogenous AA (20 mM) as 5-LO substrate are under evaluation.

3.1.4. Structure-based rational drug design for the development of new potent mPGES-1 inhibitors

To find a specific inhibitor against mPGES-1, a series of novel biphenylic derivatives has been successfully designed by means of a structure-based drug design strategy. According to co-crystal structural data, mPGES-1 inhibitors interact with transmembrane helix 4 from one monomer and transmembrane helix 1 from the other monomer, place their head groups or cores in a groove above the GSH cofactor and let the hydrophobic tails protrude from the active site cavity.

Hence, based on the fundamental interactions that an inhibitor have to establish in the receptor counterpart and on the hypothesized mechanism of action for the cleavage of the PGH₂ peroxide bond, we have designed five biphenylic derivatives reported in Figure 3.4.2.1. Docking was performed using Autodock Vina¹⁴⁷ in presence of the cofactor GSH, due to the hypothesis that they can compete with the substrate PGH₂ displacing it from the active site.

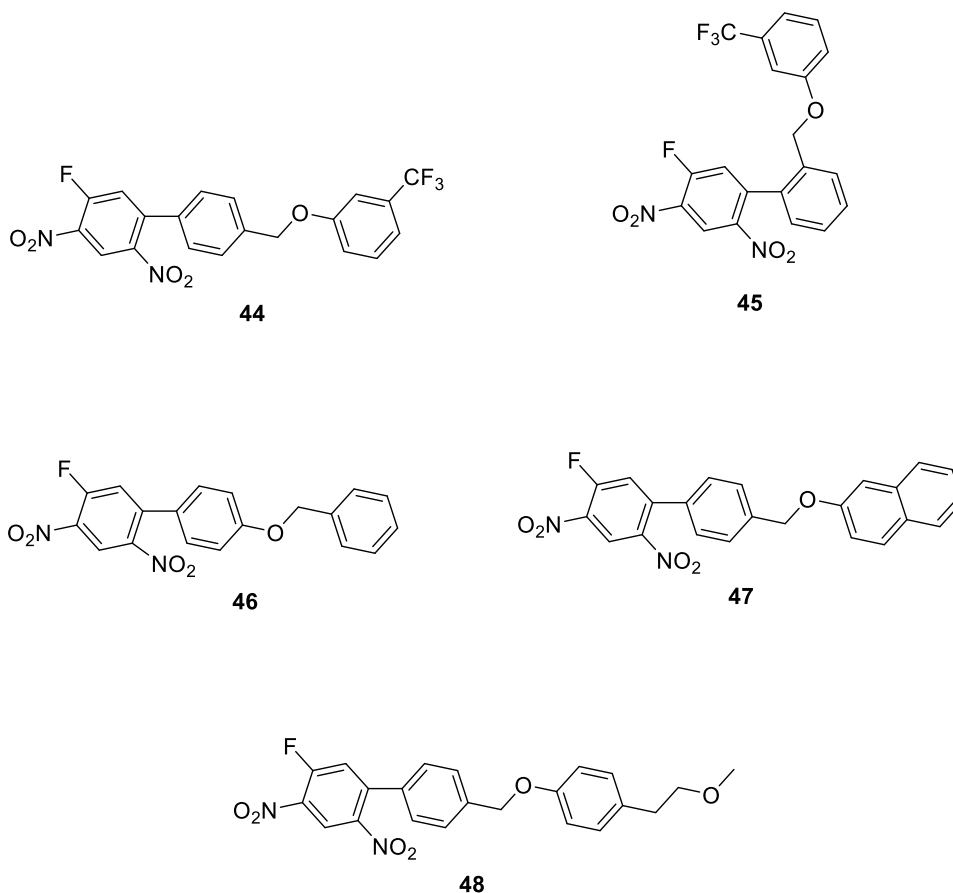


Figure 3.1.4.1 Chemical structures of the designed compounds.

Exploring the best docking poses, the analysis revealed optimal occupancy of substrate binding cavity, high binding energy scores and complete interaction with the fundamental active site aminoacids like the co-crystallized inhibitors. In this case, for the accurate analysis were observed the following interactions: π - π interaction with Phe44, and/or His53, and/or Tyr130 and polar contacts with Arg38, Arg126, Ser127, and/or GSH. As additional interactions were noticed the hydrogen bonds with Ser127, and/or Thr131, and/or His53 the salt bridges with the side chain of Arg52 and some hydrophobic interactions with Ala31, Pro124, Val128, and Leu132 (Figure 3.1.4.2).

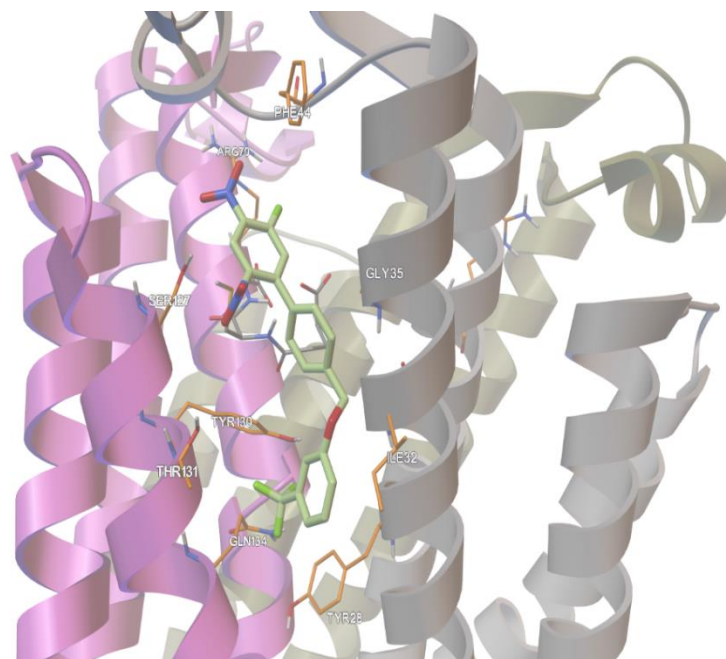


Figure 3.1.4.2 Three-dimensional model of the interactions between **44** and mPGES-1. The protein is depicted by ribbons and tube. **44** is represented by sticks (green).

The synthesized compounds were initially tested for mPGES-1 inhibition at 1 and 10 μM concentration (Figure 3.1.4.3).

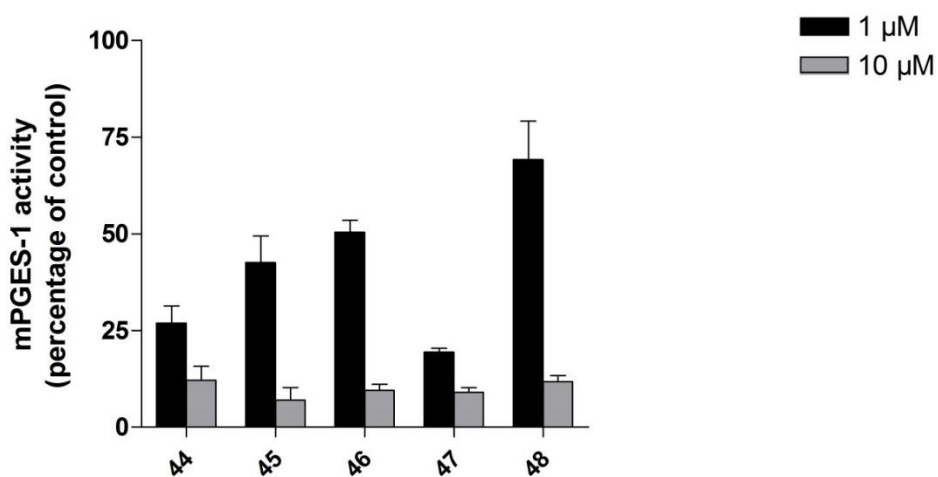


Figure 3.1.4.3 Effect of designed compounds on mPGES-1 activity. Data are given as means \pm SD, $n = 3$.

The percentage of inhibition confirmed our theoretical results and we also tested them at 3-0.1- 0.3- 0.03 μM concentration, the compounds **44** and **47** showed the strongest inhibitory activity. **44** and **47** show a value of $\text{IC}_{50} = 0.26 \pm 0.05$ and $0.18 \pm 0.03 \mu\text{M}$ respectively, higher inhibitions than known inhibitor MK-886 (Figure 3.1.4.4).

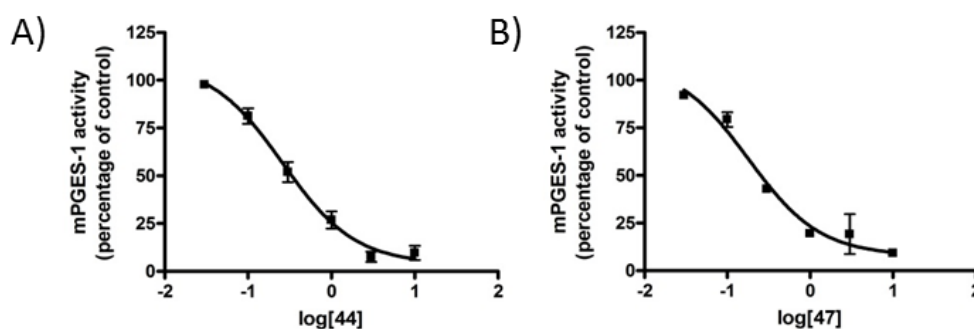


Figure 3.1.4.4 Concentration-response curves of compounds **44** (A) and **47** (B) for inhibition of mPGES-1 activity. Data are given as means \pm SD, $n = 3$.

The enzymatic results suggest that the substituents on the phenoxy portion of the hit compounds can significantly influence the inhibitory activity, the substitution of the 2-trifluoromethyl phenoxy group with 2-naphthol group exhibit an enhancement of the inhibitory activities.

These results encouraged us to initiate a more focused SAR exploration to define the effect of the fluorine atom as pharmacophoric group and the importance of nitro groups, due to the fact that nitro groups can influence the cytotoxicity and the pharmacokinetic effects. Initially, we removed the fluorine atom, then we replaced 4-nitro group with trifluoromethyl group to have the first two derivatives **49** and **51**. We explored the scaffold also replacing 4-nitro group with hydroxyl group and 2-nitro group with methyl group obtaining **50**. At the last we replaced the 4-nitro groups of **50** with amino group obtaining **52** (Figure 3.1.4.5).

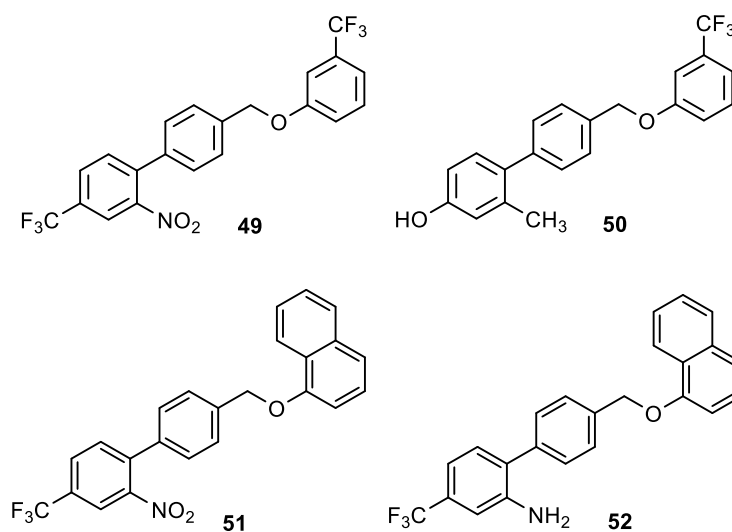


Figure 3.1.4.5 Chemical structures of the new designed compound.

The new synthesized compounds were tested for mPGES-1 inhibition at 1 and 10 μM concentration, *in vitro* biological test shows the lack of the inhibitory activity for the all new designed compounds, establishing in this way the importance of fluorine atom and nitro groups as essential for the binding with receptor counterpart (Figure 3.1.4.6).

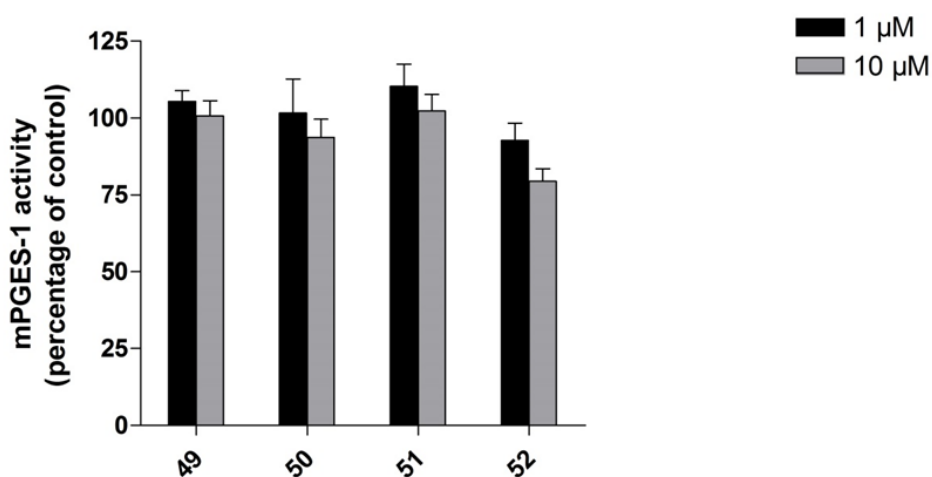


Figure 3.1.4.6 Effect of new designed compounds on mPGES-1 activity. Data are given as means \pm SD, n = 3.

The inhibition of 5-LOX activity by the test compounds in cell-based assays using ionophore A23187-stimulated human polymorphonuclear leukocytes (PMNL) in the presence of exogenous AA (20 mM) as 5-LOX substrate are under evaluation.

-CHAPTER 4-

*Determination of natural molecular platforms
as mPGES-1 and 5-LOX inhibitors*

4.1. Determination of natural molecular platforms as mPGES-1 inhibitors

On the basis of known natural compound reported in literature as mPGES-1 inhibitor: curcumin from turmeric ($IC_{50} = 0.22 \mu\text{M}$), epi-gallocatechin gallate from green tea ($IC_{50} = 1.8 \mu\text{M}$), garcinol from the fruit rind of Guttiferae species ($IC_{50} = 0.3 \mu\text{M}$), myrtucommulone from myrtle ($IC_{50} = 1 \mu\text{M}$), arzanol from *Helichrysum italicum* ($IC_{50} = 0.4 \mu\text{M}$), boswellic acids from frankincense ($IC_{50} = 3\text{--}10 \mu\text{M}$);⁷⁹ here we report the determination of natural molecular platforms targeting mPGES-1.

We reported the virtual screening of a focused library of natural bioactive compounds by means of molecular docking in order to identify new potential mPGES-1 inhibitors. From the *in vitro* assay of the selected compounds, the 12-O-methylsalvipestinoic acid shows significantly inhibitory mPGES-1 activity. This molecule causes dual suppression of PGE₂ and LT formation might be superior over single interference in terms of higher anti-inflammatory efficacy as well as in terms of reduced side effects, the compounds were then tested for inhibition of 5-LOX activity in a cell-based assay using PMNL. As first step, we performed an accurate conformational search at empirical level, combining with Monte Carlo Molecular Mechanics (MCMM) and Molecular Dynamics (MD) simulations to explore the conformational space.

Another line of this project has regarded the *in vivo* and *in vitro* biological evaluation of anti-inflammatory response of carnosol and carnosic acid and *in silico* analysis of their mechanism of action. We investigated the effects of these compounds in different models of inflammatory pain. The compounds displayed at 4h a significant and dose-dependent anti-inflammatory and anti-nociceptive effects in carrageenan-induced hyperalgesia in mice and also inhibited the late phase of formalin test. The biological effects showed significant inhibitory activity on arachidonic related metabolites, these effects might contribute for the anti-nociceptive, anti-inflammatory and antitumoral

property of others *Salvia spp.* containing these diterpenoids. In conclusion, our molecular docking and biological studies have allowed the rationalization of the antinociceptive and anti-inflammatory effects of carnosol and carnosic acid associated to the inflammatory pain, which are related to the biological activity on some key enzymes involved in the arachidonic acid cascade such as mPGES-1, 5-LOX, COX-1 and COX-2. In fact, the multiple suppression might be superior over single inhibition in terms of efficacy as well as in terms of side effects.

Another study has concerned the molecular mechanism of tanshinone IIA and cryptotanshinone in platelet anti-aggregating effects. Until now, the molecular mechanisms of action of these two diterpenoids on platelets are partially known. To clarify this aspect, here we utilized an integrated study of pharmacology and computational analysis. Cryptotanshinone is able to inhibit in a concentration dependent manner the rat platelet aggregation and also is endowed of Gi-coupled P2Y₁₂ receptor antagonist as demonstrated by docking studies. This computational method was also performed for tanshinone IIA demonstrating even for this diterpenoid an interaction with the same receptor. The findings from our study enable a better understanding of TIIA and CRY biological properties, which could ultimately lead to the development of novel pharmaceutical strategies for the treatment and/or prevention of some cardiovascular disease.⁹²

4.1.2. Virtual screening of focused library, pilot study on natural bioactive compounds by means of molecular docking

Numerous natural products from plants with anti-inflammatory properties have long been recognized as efficient repressors of PGE₂ biosynthesis in intact cells. Detailed analysis of their molecular targets and modes of action revealed mPGES-1 as primary point of attack providing unique chemotypes for development of mPGES-1 inhibitors. Most of these mPGES-1-active natural

products include lipophilic acidic molecules including: cyclphloroglucinols such as myrtucommulone A, hyperforin, arzanol; (poly)phenols such as epigallocatechin-3-gallate, curcumin, the depside perlatolic acid and the depsidone physodic acid; quinones such as embelin, and tetra- or pentacyclic triterpene acids such as boswellic, tirucallic and lupeolic acids.⁸³ The IC₅₀ values of most of these natural products for mPGES-1 are in the range of 0.2 to 10 μ M,⁸³ and some of them have been demonstrated to suppress PGE₂ levels *in vivo*, connected to anti-inflammatory activity. Inhibition of mPGES-1 by these natural products may rationalize the anti-inflammatory properties of remedies containing them, and they may also serve as novel templates for drug development.

Our natural small library with approximately 80 compounds was screened through molecular docking and binding free energy evaluation. Initially, we performed an accurate conformational search at empirical level, combining with Monte Carlo Molecular Mechanics (MCMM) and Molecular Dynamics (MD)¹⁷⁷ simulations. The library were then docked by Autodock Vina¹²⁹ software, subsequently the compounds were selected using a binding score range, defined between -9.9 and 8.6 kcal/mol as cut-off, and the key interactions, as reported above (Figure 4.1.2.2). From this analysis, 8 representative compounds were selected for biological assay (Figure 4.1.2.1).

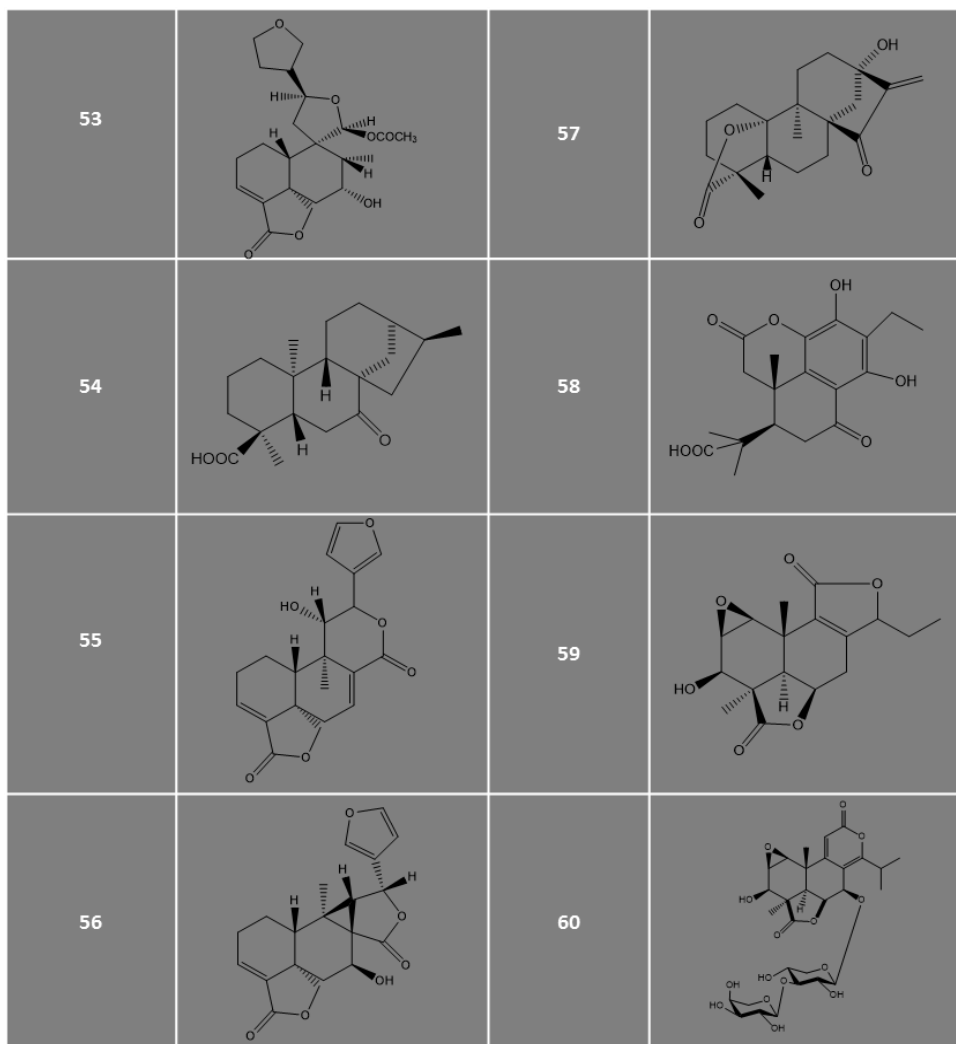


Figure 4.1.2.1 Chemical structures of the selected compounds.

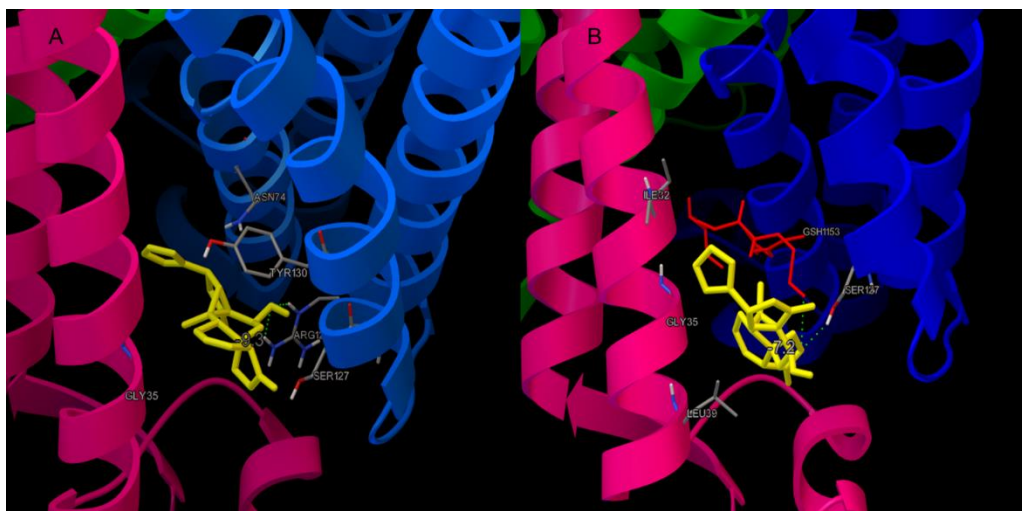


Figure 4.1.2.2 Three-dimensional model of the interactions between **56** and mPGES-1 in absence of GSH (A) and in presence of GSH (B). The protein is depicted by ribbons and tube. **56** is represented by sticks (yellow). GSH is represented by sticks (red).

To assess the ability of the selected compounds to interfere with the activity of mPGES-1, a cell-free assay using the microsomal fractions of interleukin-1 β (IL-1 β)-stimulated A549 cells (as source for mPGES-1) was applied (Figure 4.1.2.3). All compounds, solubilized in dimethyl sulfoxide (DMSO), were tested at concentrations of 1 and 10 μ M. The mPGES-1 inhibitor compound MK886 (IC_{50} = 2.4 μ M) was used as a reference control, and DMSO (0.3%, v/v) was used as a vehicle control.

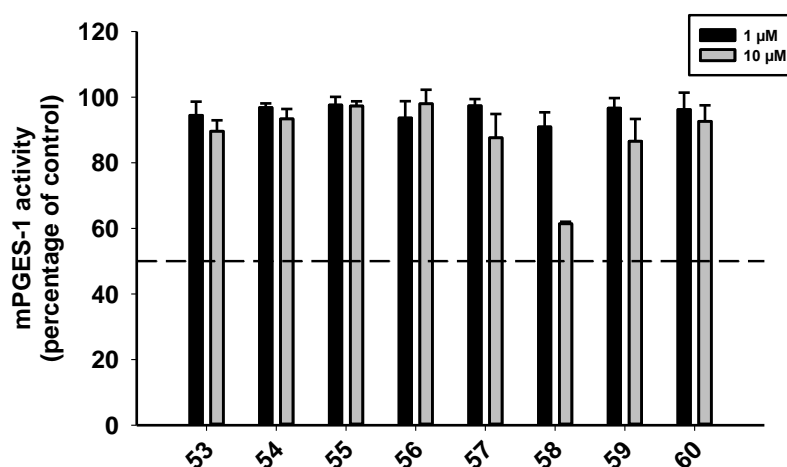


Figure 4.1.1.3 Effect of selected compounds on 5-LO activity. Data are given as means \pm SD, n = 3.

12-O-methylsalvialpalestinoic acid significantly inhibited mPGES-1 activity, whereas all other molecules were not significantly active. Interestingly, these data confirm the results from the docking studies favouring that compounds as mPGES-1 inhibitors.

Previous studies on acid mPGES-1 inhibitors showed that such compounds often interact also with other enzymes within the arachidonic acid cascade, such as 5-LOX or FLAP. In fact, interference with 5-LOX or FLAP, the key enzymes in the formation of leukotrienes (LTs) from arachidonic acid, is considered a valuable characteristic of a given mPGES-1 inhibitor, because dual suppression of PGE₂ and LT formation might be superior over single interference in terms of higher anti-inflammatory efficacy as well as in terms of reduced side effects. Thus, we further analyzed the test compounds (1- 10 μ M, each) for inhibition of 5-LO activity in a cell-based assay using PMNL as the intact cell enzyme source. The well recognized 5-LO inhibitor BWA4C ((E)-N-hydroxy-N-(3-(3-phenoxyphenyl)-allyl)acetamide) was used as a

positive control, and DMSO (0.3%, v/v) was used as a vehicle control. The molecules were not significantly active (Figure 4.1.2.4).

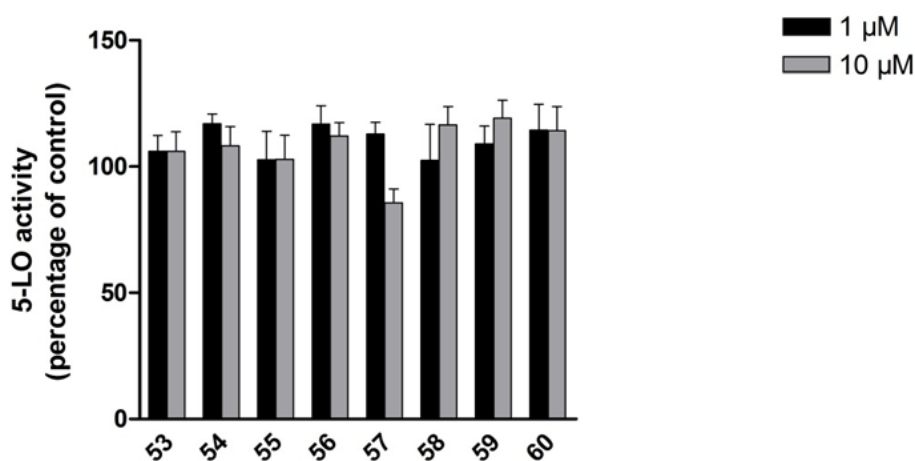


Figure 4.1.1.4 Effect of selected compounds on 5-LO activity. Data are given as means \pm SD, n = 3.

4.1.2. *In vivo* and *in vitro* biological evaluation of anti-inflammatory response of carnosol and carnosic acid and *in silico* analysis of their mechanism of action

Diterpenoids are secondary metabolites that can be found in higher plants, fungi, insects and marine organisms and display a great deal of biological activities.^{108,109} The anti-inflammatory characteristics of some members of diterpenoid family, especially those isolated from plants, have been described and mostly involve the multiple signaling pathways that are deregulated during inflammation and inflammatory pain syndrome, including nuclear factor κ B, p38 mitogen-activated protein kinase and phosphatidylinositol-3-kinase. Among these, much attention has been recently pointed on the diphenolic diterpenoids carnosol and carnosic acid. Recent investigations have demonstrated that these compounds are able to suppress COX-2, IL-1 β and TNF- α expression and leukocyte infiltration in inflamed tissue¹¹⁰ and to

regulate the levels of inflammatory chemokines MMP-9 and MCP-1 on cell migration.¹¹¹ It has been found that *Salvia* spp. (Lamiaceae) that contain these diterpenoids, could act as a mild analgesic. Recent investigations have demonstrated the anti-nociceptive potential of *Salvia officinalis* extract and its isolated compounds carnosol in different *in vivo* models of inflammation. Subsequently it has been validated that the hydroalcoholic extract of *Salvia officinalis* and its constituent carnosol inhibit formalin-induced pain and inflammation in mice.¹¹² One of the most recent specie of *Salvia* that has attracting the attention of the researchers for its high content of carnosic acid is represented by *Salvia solamensis* Vatke¹¹³. In light of the ethno botanical use of *Salvia* species, in which the main constituents are diterpenoids, in the treatment of pain and inflammation, here we have evaluated the potential analgesic activity of diphenolic terpenes carnosol and carnosic acid using *in vivo* models of inflammatory and mechanical pain. Since insufficient data are reported on the antinociceptive effects of mentioned compounds, we have also expanded previous observations taking on account the possibility to investigate their potential arachidonic enzyme related inhibitory activity (cicloxygenase 1 and 2 COXs, microsomal prostaglandin E synthase-1 mPGES-1, and 5-lipoxygenase 5-LOX) by molecular docking studies and biological assay.

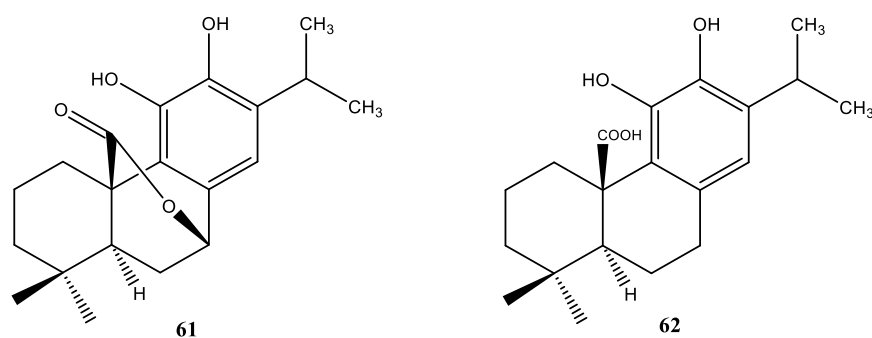


Figure 4.1.2.1 Molecular structures of carnosol (**61**) and carnosic acid (**62**).

Finally, we have evaluated, by molecular docking, the interaction of carnosol and carnosic acid with mPGES-1, 5-LOX, COX-1 and COX-2 enzymes in order to understand at the molecular level the analgesic action related to the inflammatory pain of these two compounds. In particular, carnosol and carnosic acid are accommodated in the pocket situated in the region at the interface of the two mPGES-1 subunits,⁷² establishing good interactions with receptor counterpart. Carnosol respects the fundamental hydrophobic, electrostatic and π - π interactions namely with Arg38, Phe44, Arg52, His53 of the chain A, and Arg126, Pro124, Ser127, Thr131 of the chain B (Figure 4.1.2.4), in analogy to the co-crystallized ligand. Moreover, it makes other interactions with Gly35, Leu39, Asp49 of the chain A, and Ala123, Val128 of the chain B (Figure 4.1.2.4), and it establishes a hydrogen bonds with the side chain of Arg52 (Figure 4.1.2.4). On the other hand, carnosic acid shows the same pattern of hydrophobic, electrostatic and π - π interactions and it establishes an extra hydrogen bond between hydroxyl group at position 11 and Ser127 (Figure 4.1.2.4).

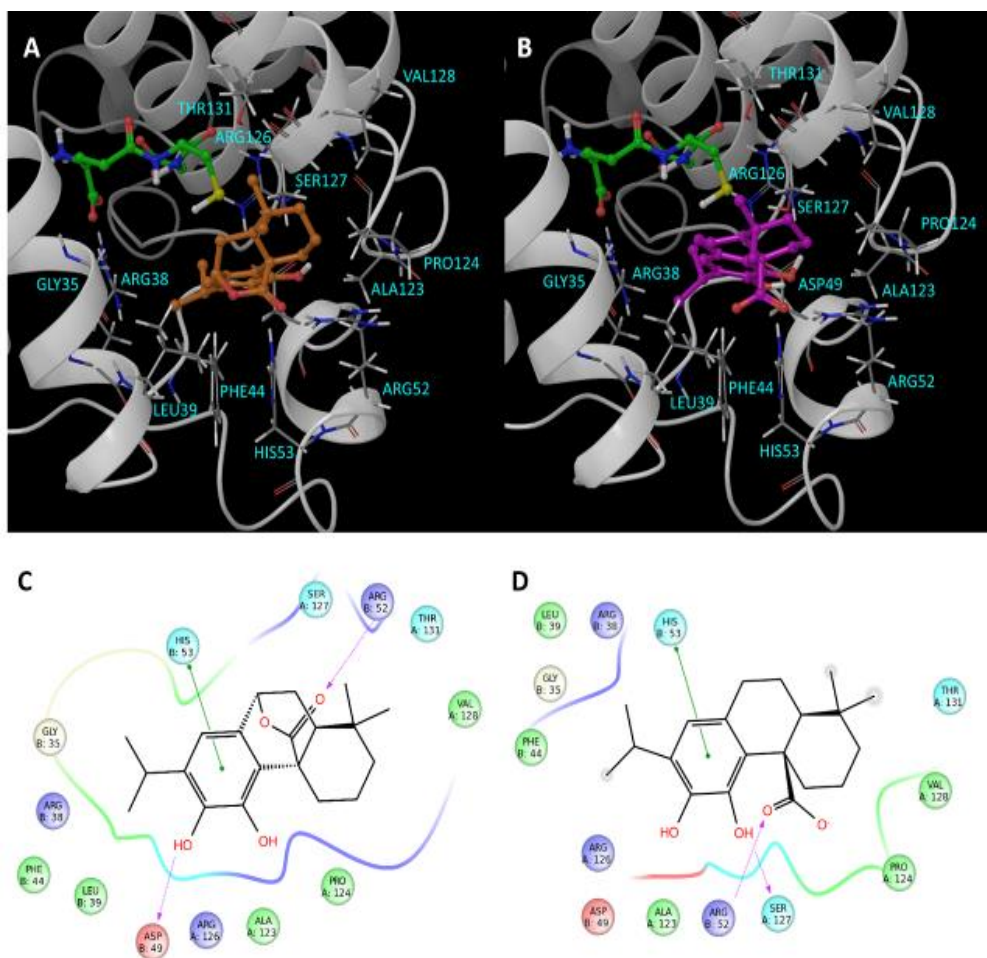


Figure 4.1.2.4 3D models of carnosol (**A**) (orange) and carnosic acid (**B**) (fuchsia) in the binding site of mPGES-1 with GSH (green). Residues in the active site are represented in tubes. 2D panels represent the interactions between carnosol (**C**), carnosic acid (**D**) and the residues of mPGES-1 binding site. Positive charged residues are colored in violet, negative charged residues are colored in red, polar residues are colored in light blue, hydrophobic residues are colored in green. The π - π stacking interactions and H-bond (side chain) are indicated as green lines, and dotted pink arrows respectively.

Regarding the 5-LOX enzyme,⁸⁵ the induced fit docking approach was used to simulate and study the interactions of carnosol and carnosic acid with the residues belongs to the active site close to the catalytic iron of this enzyme. The

analysis of the most representative docking poses of carnosol in the ligand binding site reveals a better accommodation with respect to the carnosic acid, it establishes key interactions with Phe177, Tyr181, Leu368, Ile406, Asn407, Leu414, Leu420, Phe421, His432 and Leu607 (Figure 4.1.2.5). Moreover, it is involved in two hydrogen bonds with Gln363 and the carbonyl oxygen coordinates the metal (Figure 4.1.2.5). Carnosic acid shows an opposite binding mode with respect to carnosol maintaining the metal coordination, a hydrogen bond with His372, and the key interactions with Phe177, Tyr181, Leu368, Ile406, Asn407, Leu414, Phe421, Leu607, with the exception of contacts with Leu420 and His432 (Figure 4.1.2.5).

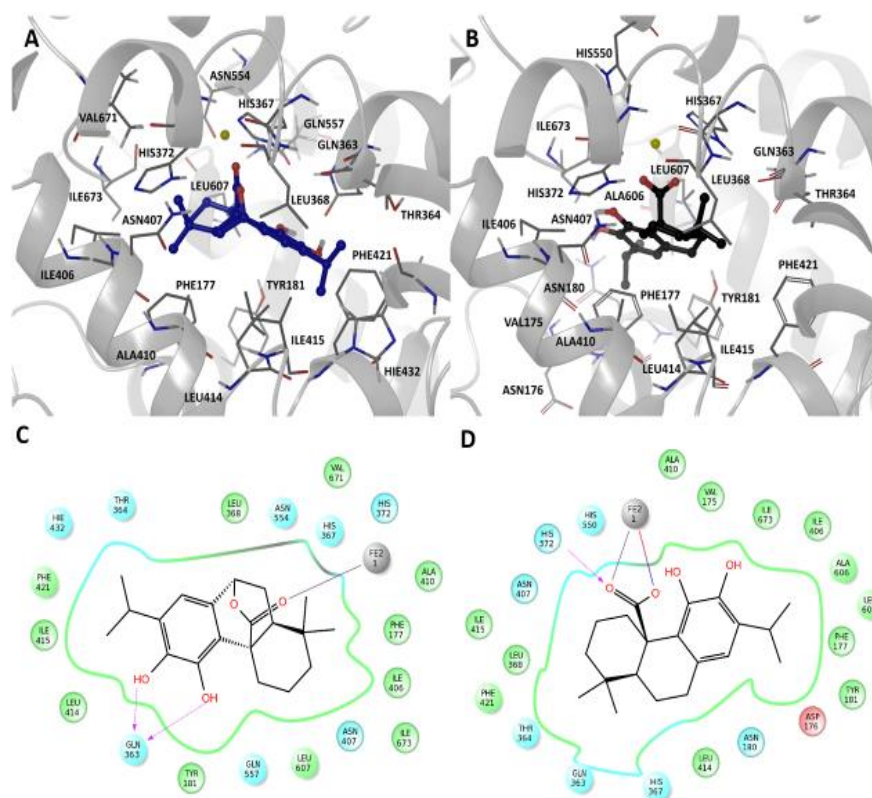


Figure 4.1.2.5 3D models of carnosol (**A**) (green) and carnosic acid (**B**) (fuchsia) in the binding site of 5-LOX. Residues in the active site are represented in tubes and Fe is depicted as yellow cpk. 2D panels represent the interactions between carnosol (**C**), carnosic acid (**D**) and residues of the 5-LOX binding site. Metal coordination and salt bridge are indicated as grey lines, and blue/red lines respectively.

To evaluate the binding modes of carnosol and carnosic acid in the COX-1 and COX-2 pockets, we have performed an induced fit docking calculation. To this aim, we have ascribed the biological activity of both diterpenoids to the carboxylate group, peculiar structural feature of classical COXs inhibitors, and to the lactone moiety. In particular, the carboxylate group of carnosic acid is involved in hydrogen bonds with Arg120 of both COXs enzymes. Moreover, it makes the same hydrophobic interactions in the iso-enzyme catalytic sites, namely with Leu93, Met113, Val116, Val349, Leu352, Tyr355, Leu359, Trp387, Phe518, Gly526, Ala527, Leu531, Leu357_{COX-1} and Phe357_{COX-2}, Ile523_{COX-1} and Val523_{COX-2}, and polar interactions with Ser353 and Ser530. Furthermore, comparing the binding modes of the carnosic acid in COXs ligand binding sites, the natural diterpenoid shows additional contacts with Leu117, Gln350 and Met522 of COX-1, and with Tyr348, Phe381, Tyr385 and Leu534 of COX-2 (Figure 4.2.6). For what concern the lactone moiety of carnosol, it is involved in the same hydrogen bonds with Arg120 of both COXs enzymes; moreover, it establishes the same hydrophobic and polar interactions with respect to carnosic acid in COX-1 binding site, except for contacts with Leu93, Leu117, and Leu384. In COX-2 active site, it makes further interactions with Leu117, Tyr348, Tyr385 and Leu534 (Figure 4.1.2.6).

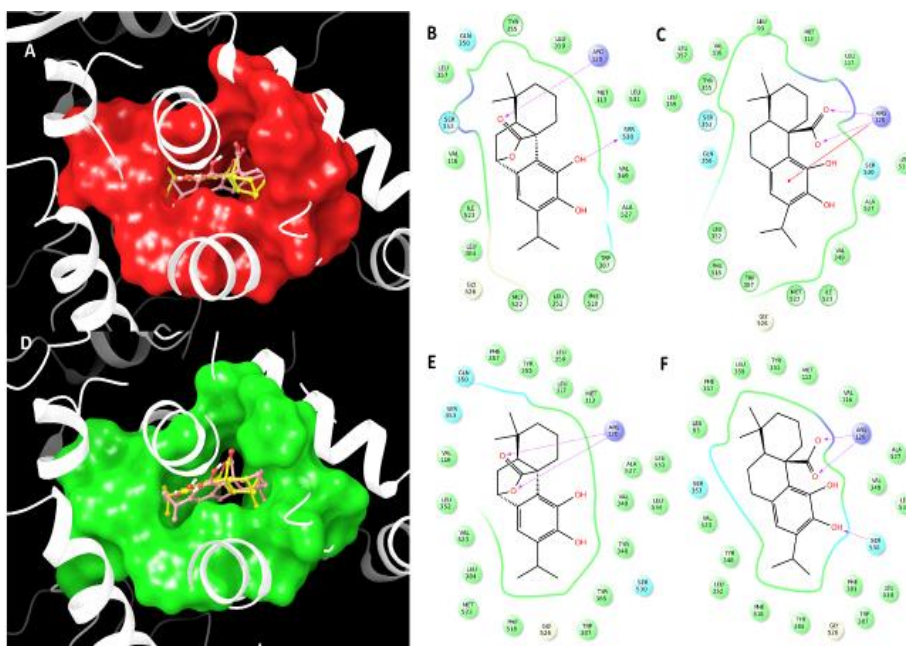


Figure 4.1.2.6 3D models of carnosol (yellow) and carnosic acid (pink) in docking with COX-1 (A) and COX-2 (D). Active binding sites are represented as red (COX-1) and green (COX-2) molecular surfaces. 2D panels represent the interactions between carnosol (B in COX-1 binding site, E in COX-2 binding site) and carnosic acid (C in COX-1 binding site, F in COX-2 binding site).

To verify the predicted binding of carnosol and carnosic acid and to investigate the functional consequences on mPGES-1 and 5-LOX activity, we determined the effect of the test compounds on the enzymatic conversion of PGH₂ to PGE₂ in a cell-free assay using microsomes of interleukin-1b-stimulated A549 cells and on the enzymatic conversion of AA to LTB₄ in cell-free assays using partially purified human recombinant 5-LOX. In these assays, reduced enzymatic activity is most likely due to direct interference of the test compound with the target enzyme.

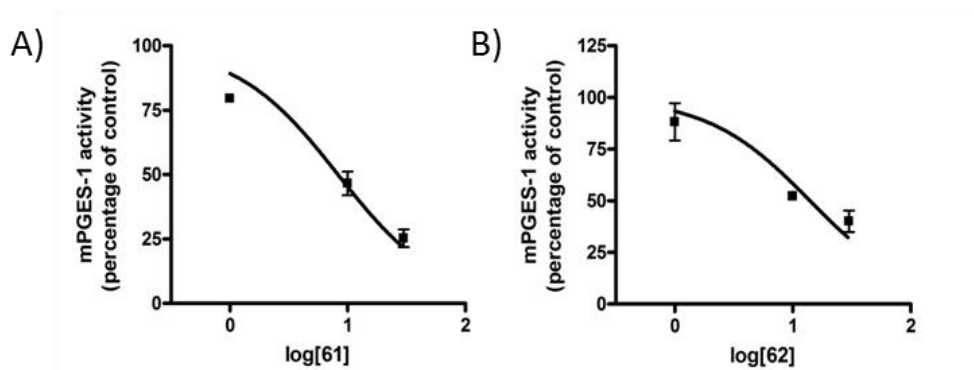


Figure 4.1.2.7 Concentration-response curves of carnosol and carnosic acid for inhibition of mPGES-1 activity. Data are given as means \pm SD, $n = 3$.

In a cell-free mPGES-1 activity assay, carnosol and carnosic acid inhibited the enzymatic conversion of PGH₂ to PGE₂ catalyzed by mPGES-1 in microsomes from stimulated A549 cells¹⁰⁶ with IC₅₀ 10.94 \pm 2.36 and 14.0 \pm 2.95 μ M, respectively (Figure 4.1.2.7).

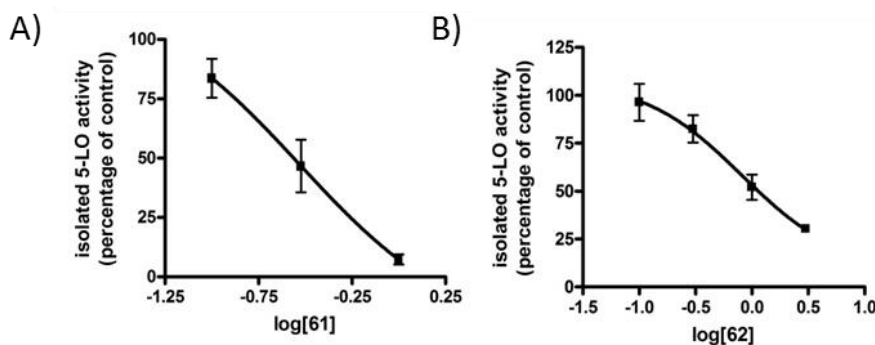
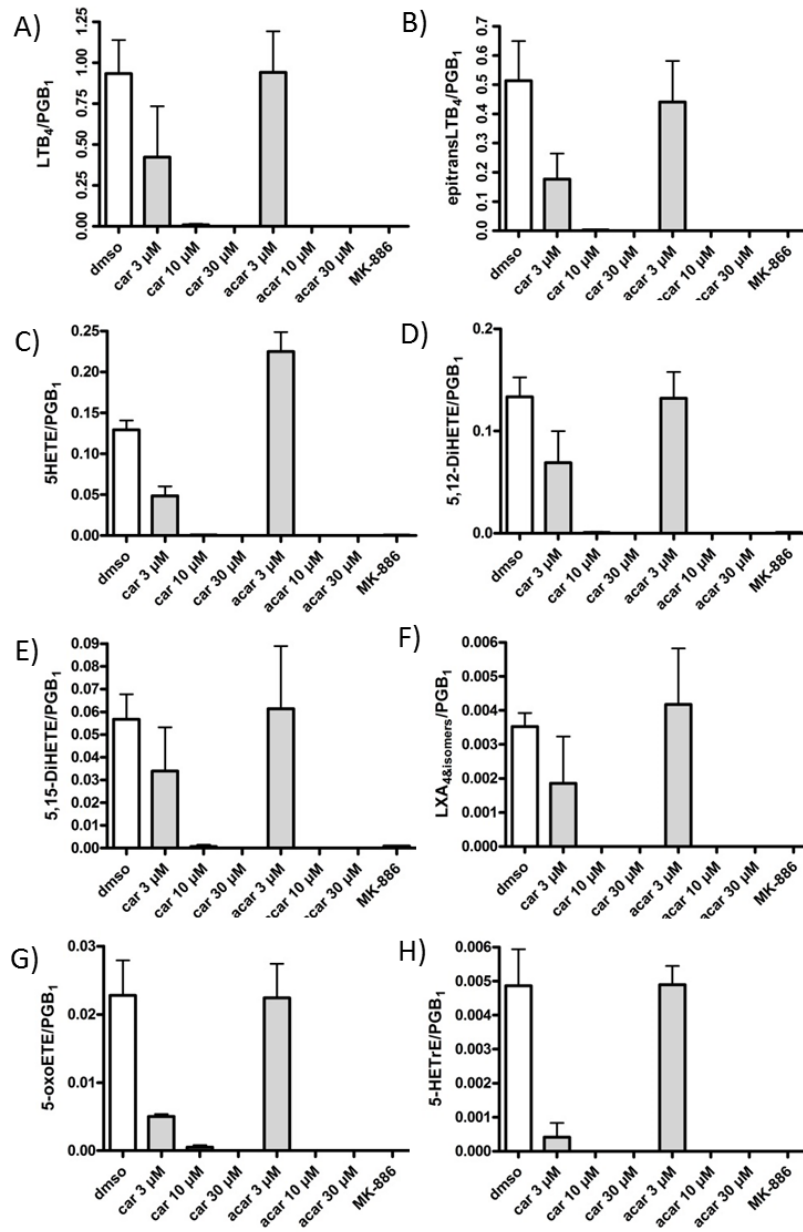


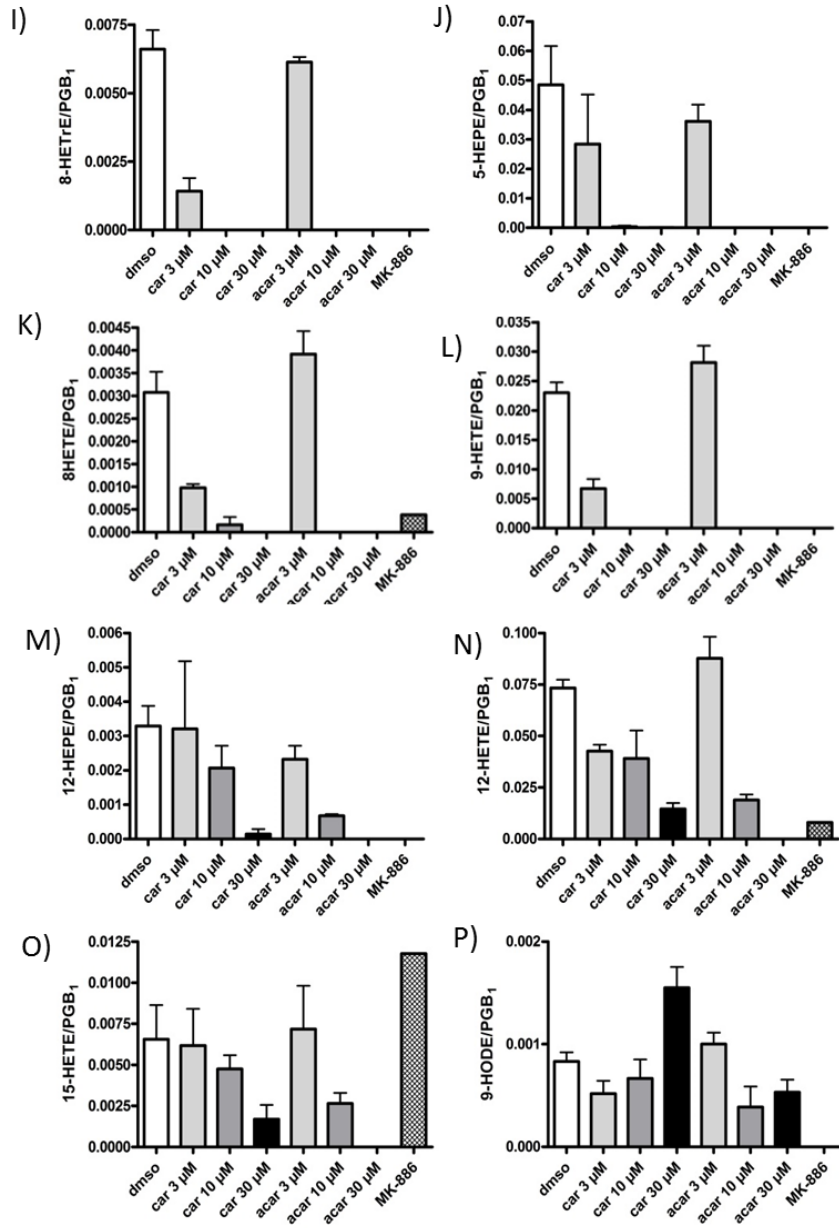
Figure 4.1.2.8 Concentration-response curves of carnosol and carnosic acid for the inhibition of 5-LOX activity. Data are given as means \pm SD, $n = 3$.

Moreover, they potently inhibited also 5-LOX¹⁰⁷ with IC₅₀ values of 0.29 \pm 0.03 and 0.81 \pm 0.05 μ M respectively, in cell-free system (Figure 4.1.2.8).¹¹⁴

In order to investigate whether or not the test compounds also inhibit the enzyme inside the cell and to quantify the production of arachidonic cascade metabolites we performed the lipid mediator profiling in PMNL and monocytes by UPLC-MS/MS.¹¹⁵ Freshly isolated neutrophils¹¹⁶ (5×10^6 /mL) were

preincubated with the test compounds (dissolved in DMSO) for 10 min at 37 °C, then were stimulated with 2.5 μM Ca²⁺-ionophore A23187 for 15 min at 37 °C, we stopped the reaction through the addition of 1 mL of methanol and the extraction of the eicosanoids were performed by SPE after the addition of 530 μM PBS/HCl and PGB₁ 100 ng/ml. The analysis of all the arachidonic cascade metabolites shows a significant effects on 5-LOX and COX metabolites production by carnosol and carnosic acid at 10 μM and 30 μM concentration, and on 12-LOX, 15-LOX and mPGES-1 metabolites production by carnosol and carnosic acid 30 μM (Figure 4.1.2.9).





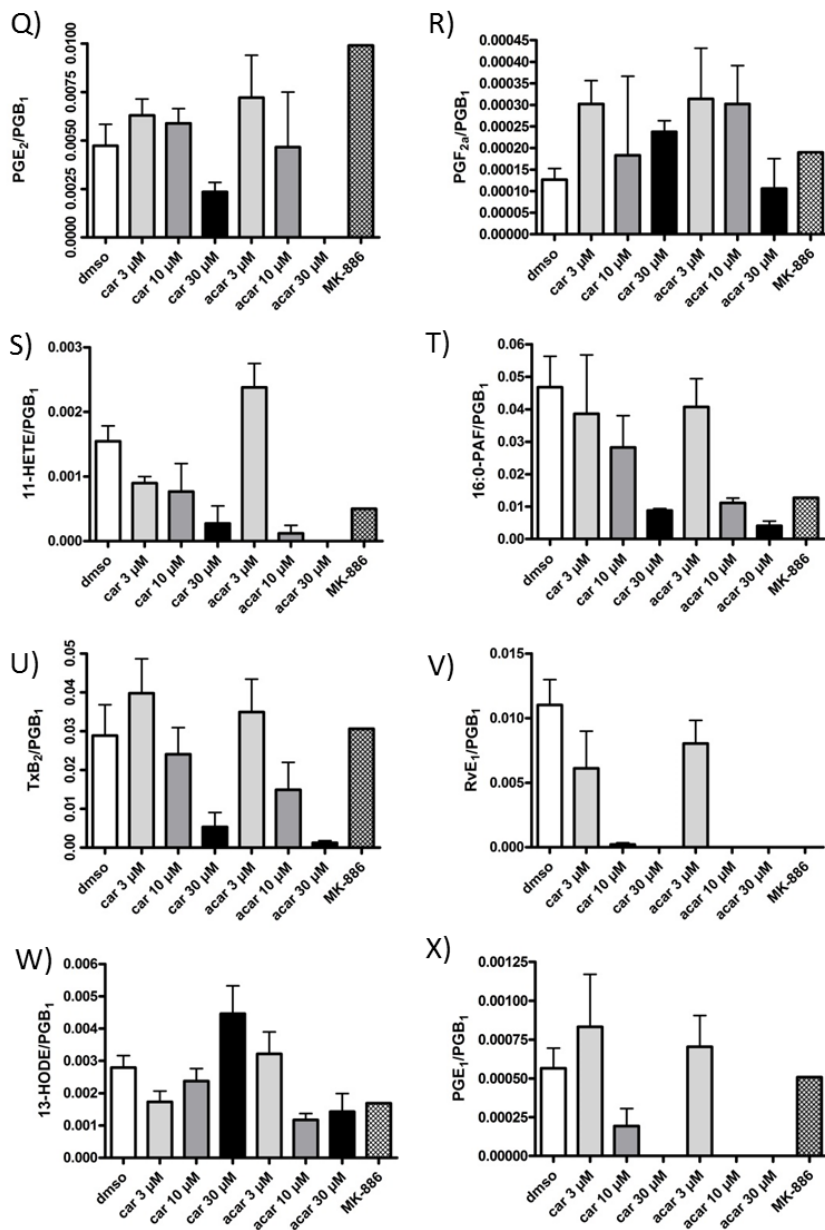
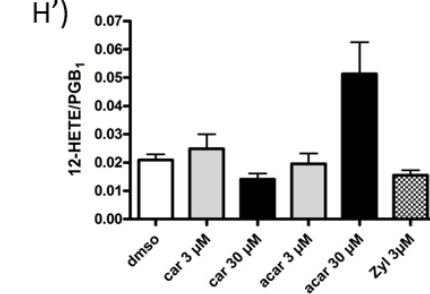
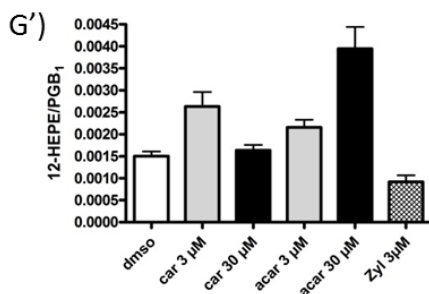
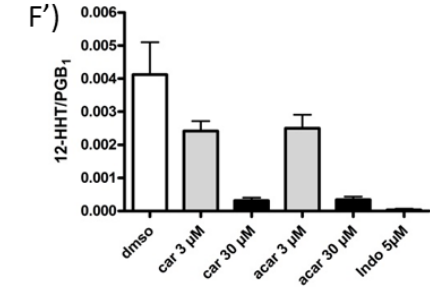
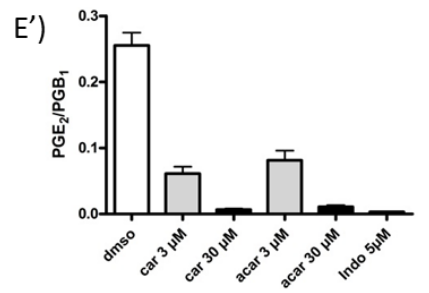
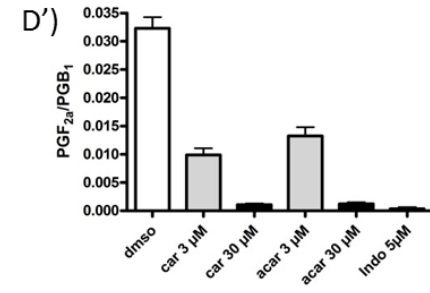
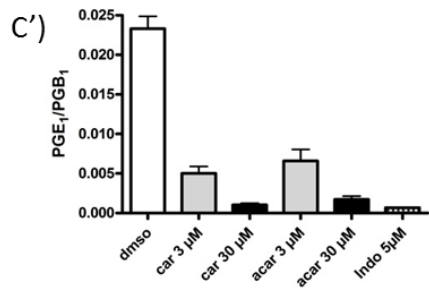
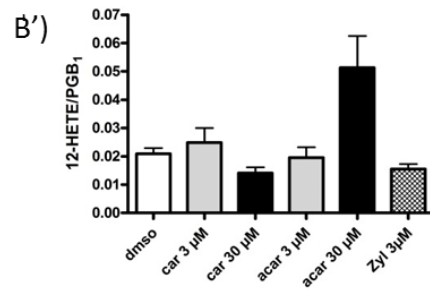
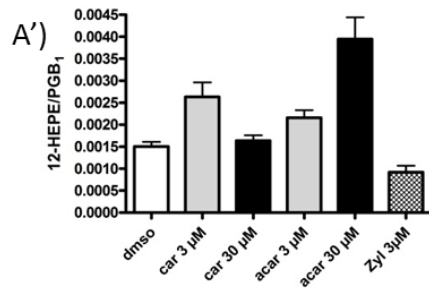


Figure 4.1.2.9 Effect of carnosol and carnosic acid at 3- 10- 30 μM on LTB₄ (A), epitransLTB₄ (B), 5HETE (C), 5,12-DiHETE (D), 5,15-DiHETE (E), LXA and isomers (F), 5-oxoETE (G), 5HETrE (H), 5HETrE (I), 5HEPE (J), 8HETE (K), 9HETE (L), 12HEPE (M), 12HETE (N), 15HETE (O), 9HODE (P), PGE₂ (Q), PGE_{2α} (R), 11HETE (S), 16:0-PAF (T), TxB₂ (U), RvE₁ (V), 13HODE (W), PGE₁ (X) production. Data are given as means ± SD, n = 3.

PBMC freshly isolated from buffy coats of human blood were plated in 170 cm² culture flask in RPMI culture medium (RPMI 1640 containing 100 U/mL penicillin, 100 mg/mL streptomycin, 2 mM L-glutamine and 2% (v/v) human serum) to let them adhere. After 1.5 h at 37 °C and 5% CO₂, monocytes were collected by scraping of the flask and 1.5×10⁶ /mL of monocytes were stimulated with LPS 10 ng/mL for 24 h in order to measure the production of mPGES-1 and COXs metabolites. Test compounds or vehicle were added 30 min before the stimulus, For measurement of eicosanoids levels supernatants were collected after centrifugation (2000 g, 4 °C, 10 min). Then extracted by SPE and analysed by UPLC-MS/MS. The analysis and the quantification of mPGES-1 and COXs metabolites shows significant effects on mPGES-1 and COXs metabolites production by carnosol and carnosic acid at 30 μM concentration, and an intermediate inhibition on them by carnosol and carnosic acid 3 μM (Figure 4.1.2.10).



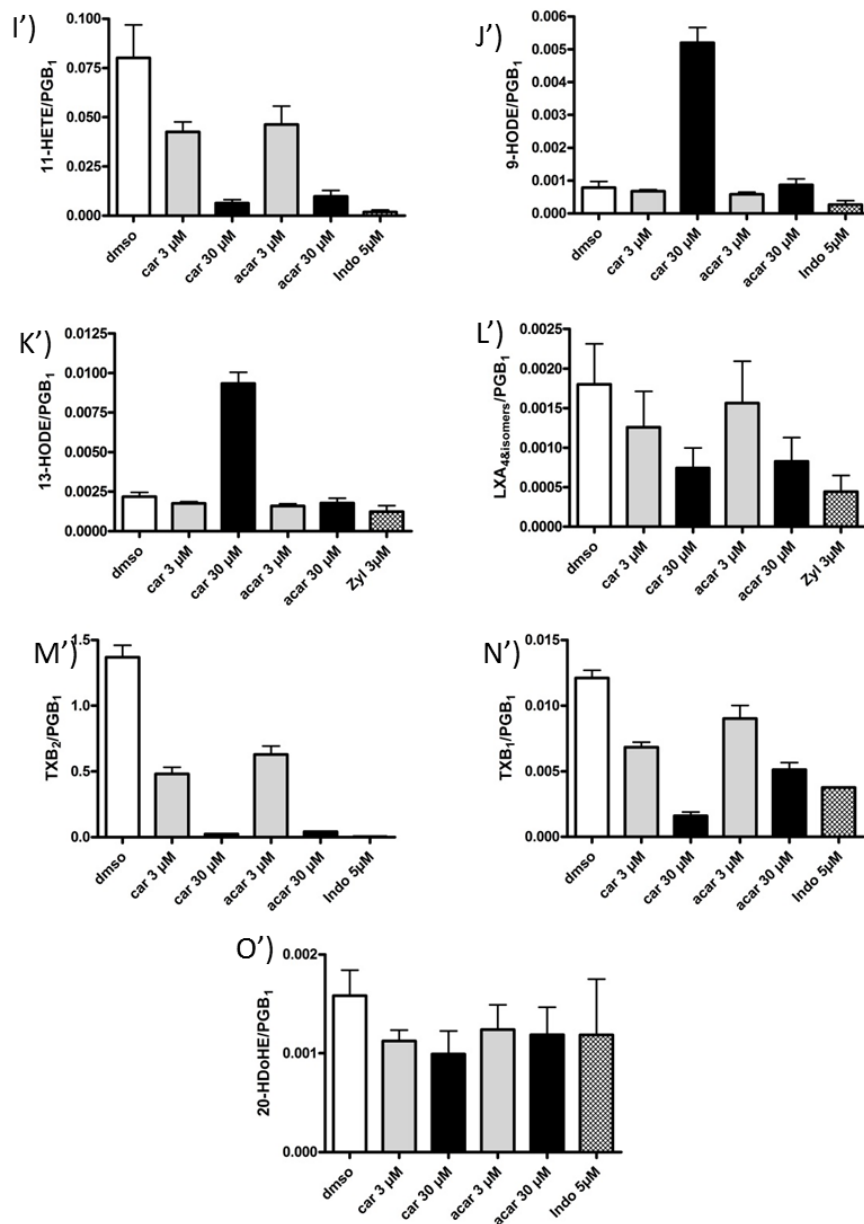


Figure 4.1.2.10 Effect of carnosol and carnosic acid at 3- 30 μM on 12HEPE (A'), 12HETE (B'), PGE₁ (C'), PGE_{2α} (D') PGE₂ (E'), 12HHT (F'), 12HEPE (G'), 12HETE (H'), 11HETE (I'), 9HODE (J'), 13HODE (K'), LXA and isomers (L'), TxB₁ (M'), TxB₂ (N'), 20HDdOe (O') production. Data are given as means ± SD, n = 3.

These results demonstrate that carnosol and carnosic acid present a significant inhibitory activity on arachidonic related metabolites, and that these

effects might contribute for the anti-nociceptive, anti-inflammatory and antitumoral property of others *Salvia spp.* containing these diterpenoids. In conclusion, our molecular docking studies have allowed the rationalization of the antinociceptive and anti-inflammatory effects of carnosol and carnosic acid associated to the inflammatory pain, which are related to the biological activity on some key enzymes involved in the arachidonic acid cascade such as mPGES-1, 5-LOX, COX-1 and COX-2. In fact, the multiple suppression might be superior over single inhibition in terms of efficacy as well as in terms of side effects.

4.3 The molecular mechanism of tanshinone IIA and cryptotanshinone in platelet anti-aggregating effects: an integrated study of pharmacology and computational analysis

Here, we utilized an integrated study of pharmacology and computational analysis to explain the molecular mechanism of tanshinone IIA and cryptotanshinone in platelet anti-aggregating effects.⁹² They are two pharmacologically active diterpenoids extracted from the roots of *Salvia milthiorriza* Bunge, a plant used in chinese traditional medicine for the treatment of some cardiovascular and cerebrovascular disease. Until now, the molecular mechanisms of action of these two diterpenoids on platelets are partially known. To clarify this aspect, our results demonstrate that cryptotanshinone is able to inhibit in a concentration dependent manner the rat platelet aggregation and also is endowed of G₁-coupled P2Y₁₂ receptor antagonist as demonstrated by docking studies. This computational method was also performed for tanshinone IIA demonstrating even for this diterpenoid an interaction with the same receptor.

The findings from our study enable a better understanding of tanshinone IIA and cryptotanshinone biological properties, which could ultimately lead to the

development of novel pharmaceutical strategies for the treatment and/or prevention of some cardiovascular disease.

It is well known that adenosine diphosphate (ADP) plays a key role in platelet activation. Aberrant activation of platelets by pathological factors is commonly associated with vascular disease and thrombosis.¹¹⁷ ADP activates platelets through two G-protein coupled receptors, the G_q-coupled P2Y₁ receptor and G_i-coupled P2Y₁₂ receptor.¹¹⁸ These receptors are targets for common anti-platelets agents such as aspirin and clopidogrel.¹¹⁹ However, the chronic use of these agents is limited because they can induce resistance or adverse effects on gastrointestinal tract¹²⁰ and, as often happens, drug toxicity may be increased when multiple antiplatelet drugs are used. In this context, new antiplatelet agents are greatly needed to increase the efficacy and reduce side effects. At nowadays, an increasing number of studies have been performed to search new agents from natural source and it is well know that some phytochemicals from plants have generated new drugs.^{121, 122, 123}

Tanshinone IIA (TIIA, **63** in Figure 4.1.3.1), from roots of *Salvia miltiorriza* Bunge (Lamiaceae) (also known as danshen), is an example of diterpenoid, studied *in vitro* and *in vivo*, able to inhibit platelet aggregation and to induce an increase of blood viscosity. We have previously demonstrated that these effects are mediated *via* the modulation of tubulin acetylation and inhibition of Erk-2 phosphorylation.¹²⁴ In our continuing studies on pharmacology of danshen constituents, here we explored the effect of cryptotanshinone (CRY, **64** in Figure 4.1.3.1), another major lipophilic constituent present in danshen, on platelet aggregation.^{125, 126, 127}

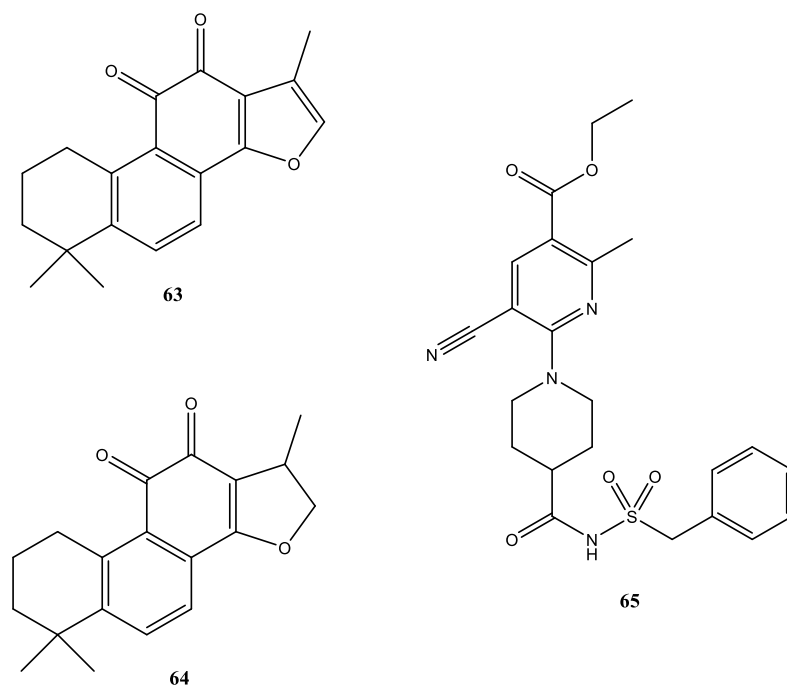


Figure 4.1.3.1 Molecular structure of tanshinone IIA (**63**), cryptotanshinone (**64**) and AZD1283 (**65**).

To this aim, we have tested in vitro the potential antiaggregant effect of **64** and simultaneously the interaction of **63** and **64** on the purinergic platelet receptor by a computational analysis. Tanshinone IIA (**63**), one of the lipophilic constituent present in danshen, is able to inhibit platelet aggregation and to induce an increase of blood viscosity *via* the modulation of tubulin acetylation and inhibition of Erk-2 phosphorylation. Here, we expand our previous observations and, by a molecular docking study, we investigated the interaction of **1** with the binding site of G-protein-coupled purinergic receptors P2Y₁₂R (PDB code: 4NTJ)¹²⁸ using AutodockVina software¹²⁹. P2Y₁₂R, is a target for the development of novel anti-platelet therapies being involved in the regulation of the platelet activation and thrombus formation.^{130, 131} In particular, in order to rationalize the binding mode of **1**, we have used the crystal structure of P2Y₁₂R in complex with ethyl 6-(4-((benzylsulphonyl)carbamoyl)piperidin-

l-yl)-5-cyano-2-methylnicotinate non-nucleotide antagonist (AZD1283, **65** in Figure 4.1.3.1)¹²⁸ as model receptor for our docking studies.

As already reported¹²⁸, **65**, a potent antagonist of the P2Y₁₂, makes a number of polar and hydrophobic contacts in the pocket 1 with side chains of amino-acids of the helices III-VII, mainly interacting with Tyr105, Phe252, Arg256, Tyr259, Leu276 and Lys280 (Figure 4.1.3.2), and adopting a different orientation with respect to the agonist.¹³² On these basis, we have analyzed the binding mode of **1** in the P2Y₁₂R in comparison with the co-crystallized antagonist **3**. From the analysis of this docking studies, even if **63** occupies the pocket 1 (helices III, IV and V), in analogy to the **65**, accounting for its antagonist activity, it poorly interacts with helices VI and VII (Figure 4.1.3.3) due to its smaller size compared to **65** (Figures 4.1.3.2 and 4.1.3.3).

In more details, **63** shows polar interactions with Asn159, Asn191 and Arg256, and it makes hydrophobic contacts with Val102, Phe252, Arg256 and Lys280. Furthermore, **63** establishes a weak hydrogen bond between oxygen at position 11 and the side chain of Cys194, and it forms π - π interactions with the side chains of Tyr105, as observed for **65**, and of Tyr109 (Figure 4.1.3.3).

In our continuing studies on pharmacology of danshen constituents, here we also explored the effect of **64**, another major lipophilic constituent present in danshen, on platelet aggregation.

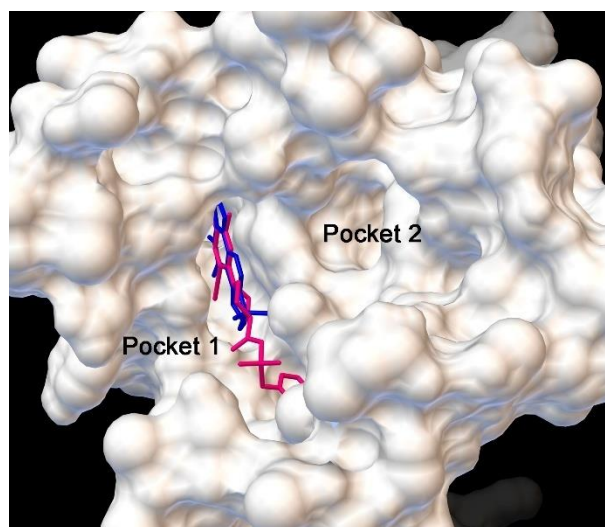


Figure 4.1.3.3 3D model of tanshinone IIA (colored by blue sticks) and AZD1283 (colored by fuchsia sticks) in the antagonist binding site of P2Y₁₂R (PDB code: 4NTJ).

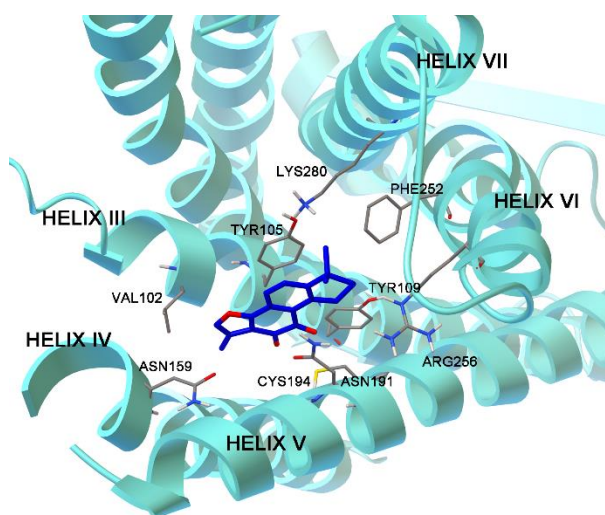


Figure 4.1.3.4 3D model of tanshinone IIA (colored by atom types: C blue, O red) into P2Y₁₂R binding site. Residues in the active site (pocket 1) are represented in sticks and balls (colored by atom types: C gray, N blue, O red, H white, S yellow).

Figure 4.1.3.4 shows a concentration-dependent inhibition of reversible platelet aggregation expressed as % of inhibition of AUC (Figure 4.1.3.4A) or amplitude (Figure 4.1.3.4B) induced by **64** (0.5, 5 and 50 μ M) added 1 min before the addition of ADP (3 μ M). **64** at concentration of 50 μ M displayed the

maximum inhibitory activity in terms of inhibition of AUC ($66.30 \pm 14.11\%$; $P < 0.01$) and amplitude ($31.00 \pm 7.09\%$; $P < 0.01$).

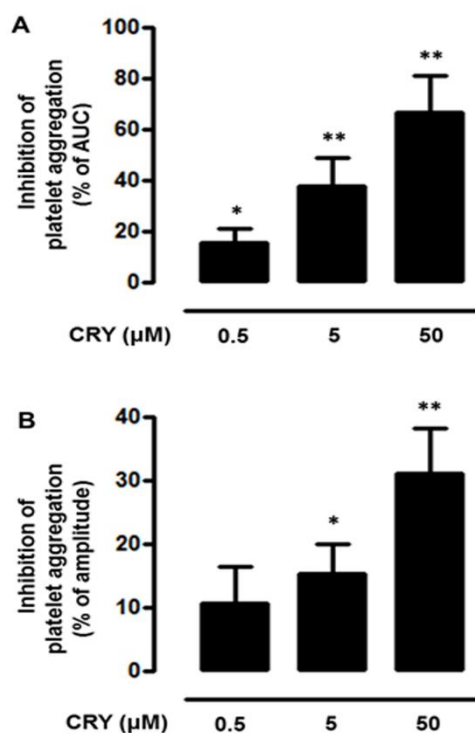


Figure 4.1.3.5 Concentration dependent effect of CRY on ADP-induced platelet aggregation. Rat PRP were incubated with CRY (0.5-50 μM) for 1 min, and then exposed to ADP (3 μM) to induce platelet aggregation. Percent (%) inhibition of aggregation was expressed in terms of AUC (A) or amplitude (B) calculated as the difference between the maximum value of aggregation in presence of ADP plus vehicle and the value obtained in the presence of ADP plus CRY. Data are expressed as mean \pm SEM. * $P < 0.05$ vs vehicle, ** $P < 0.01$ vs vehicle (one way ANOVA; $n=7$).

Moreover, considering the structural similarity of the **64** with **63** and its biological activity reported above, we have performed molecular docking studies of **2** with the P2Y₁₂R receptor (Figure 4.1.3.5). Cryptotanshinone shows the same polar interactions and hydrophobic interactions of **63** in the P2Y₁₂R binding site interacting with helices III, IV and V, and it displays an

additional hydrophobic interaction with VAL190 (Figure 4.1.3.6), accounting for the predicted similar energy of binding. The absence of the double bond at position 17 in **2**, in fact, does not affect its binding with P2Y₁₂R with respect to **63**, and according with the biological data, our docking results confirm its antiaggregant activity.

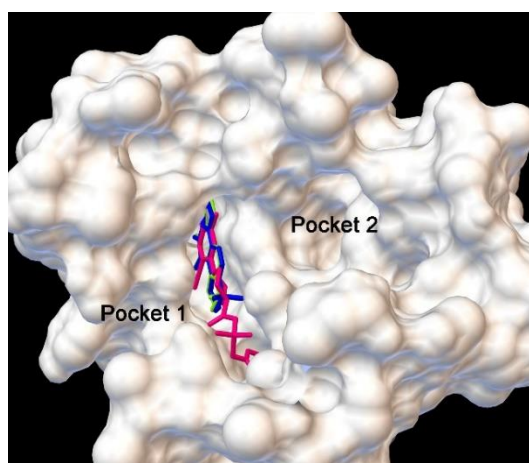


Figure 4.1.3.6 3D model of tanshinone IIA (colored by blue sticks), AZD1283 (colored by fuchsia sticks), and tanshinone II-A (colored by blue sticks) into P2Y₁₂R binding site.

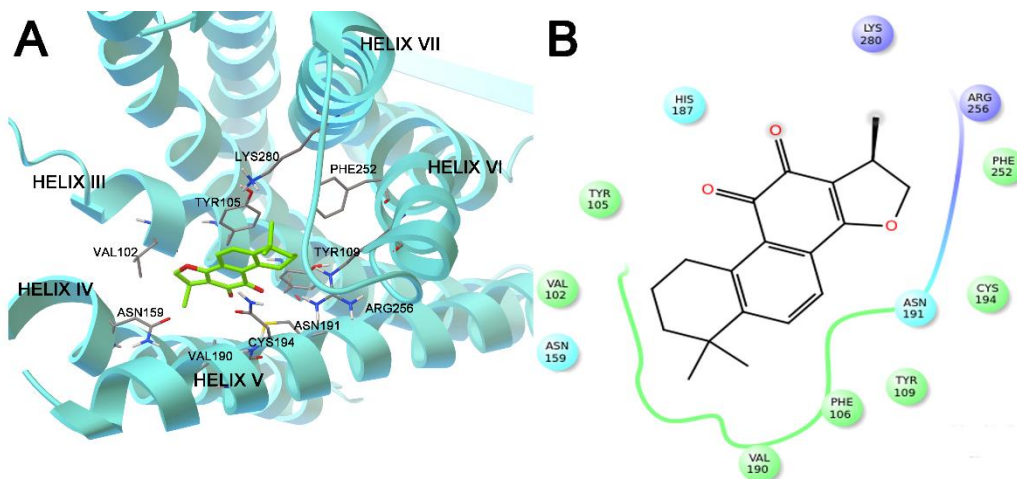


Figure 4.1.3.7(A) 3D model of cryptotanshinone (colored by atom types: C green, O red) in the binding site of P2Y₁₂R. Residues in the active site are represented in sticks and balls (colored by atom types: C gray, N blue, O red, H white). **(B)** 2D panel representing the

interactions between cryptotanshinone and residues in P2Y₁₂R binding site (charged residues are colored in violet, polar residues are colored in light blue, and hydrophobic residues are colored in green).

In conclusion, even if tanshinone IIA and cryptotanshinone show a relatively simple skeleton in comparison to the AZD1283, our docking results suggest that their established interactions with P2Y₁₂R are sufficient to rationalize the P2Y₁₂R antagonist activity of these two diterpenoids. The findings from our study enable a better understanding of **63** and **64** biological properties, which could ultimately lead to the development of novel pharmaceutical strategies for the treatment and/or prevention of some cardiovascular disease.

Furthermore, the tanshinones, such as tanshinone IIA and cryptotanshinone, and their derivatives, in fact, could be utilizable as lead compounds for future cancer and anti-inflammatory active molecules,¹³³ being able to inhibit the growth and proliferation of cancer cells, to induce cell cycle arrest and apoptosis, and to inhibit angiogenesis.

Indeed, tanshinone IIA shows both *in vitro* and *in vivo* biological effects comparable to those of pan-inhibitors, such as curcumin and oridonin, and interestingly, it interferes with the pathway of biosynthesis of PGE₂, in particular with the COX₂ receptor.^{133,134} On these bases, here we suggest the possible interaction of **63**, in analogy with **64**, with the microsomal prostaglandin E₂ synthase (mPGES-1). The inhibition, in fact, of these two diterpenoids on PGE₂ production by mPGES-1, could suggest a potential association of their anti-inflammatory and antiplatelet activity. Figure 4.3.8 clearly shows the good superimposition of the tanshinones skeleton with respect to LVJ in the groove B of mPGES-1 surface, even if the more potent inhibitor makes an optimal interactions with surface receptor.

On the other hand, tanshinoneIIA (TIIA) and cryptotanshinone (CRY) make interactions with the key aminoacids His53, Phe44, Tyr130, and glutathione (GSH) accounting for a potential inhibitory activity In conclusion, our docking calculations suggest that the pattern of interactions established with mPGES-1 is sufficient to suggest their biological activity in occupying the enzyme binding site (Figure 4.1.3.8).

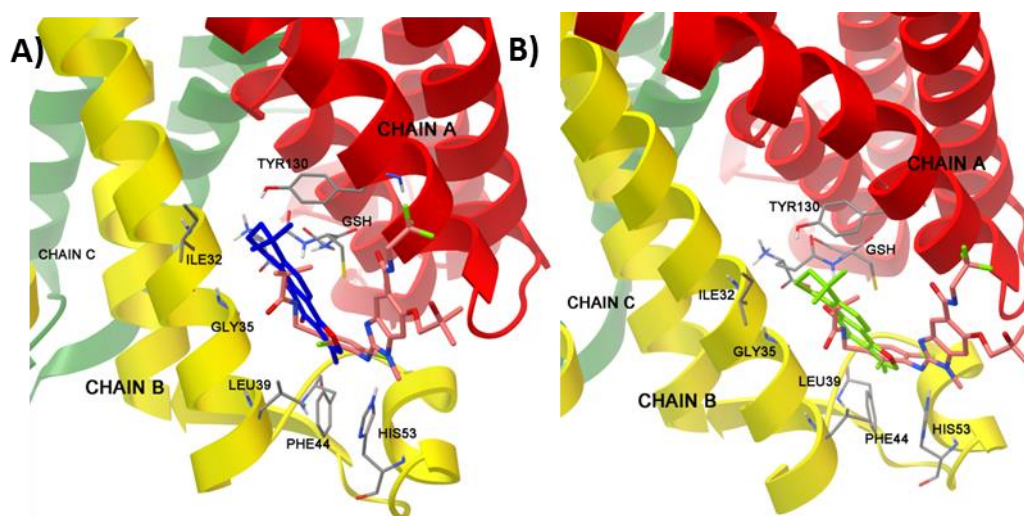


Figure 4.1.3.8 Superimposition of Tanshinones IIA (blue sticks, A) and cryptotanshinone (green sticks, B) with LVJ (light pink, A and B) in the mPGES-1 binding site.

-CHAPTER 5-

Structural Studies of Natural Products

5.1 QM/NMR integrated approach: a valid support to the determination of relative configuration of unknown molecules

Stereochemical features have a profound impact on a variety of molecular properties, such as chemical reactivity and catalytic, biological, and pharmacological activities. Many fundamental biological structures (protein, DNA, RNA), involved in cellular processes, are chiral. Drug-macromolecule interactions also depend on structural features of the ligand, such as conformation and configuration. Indeed, many bioactive compounds, involved in recognition process by a macromolecule, present stereocenters and often only one of two enantiomers can exert its biological activity. In light of the above considerations, full stereochemical knowledge of a given system is of fundamental importance in many different fields, spanning from chemical physics to biochemistry. For this reason, the assignment of the configurational pattern in chiral organic compounds containing more than one stereocenter is undoubtedly a key step of the structure elucidation process. The stereochemical analysis of compounds with well-defined conformational properties is presently fairly easy to accomplish, given the wealth of high-resolution NMR experiments useful in these kinds of studies. Typically, cyclic compounds with three to six-membered rings display a predictable conformational behaviour, thus allowing the knowledge of their configuration to be extracted from simple NMR parameters, such as proton-proton J-coupling values and/or nuclear Overhauser effect intensities. A much more challenging task is the assignment of relative (and hence absolute) configuration in the case of conformationally flexible systems, such as polysubstituted open chains and macrocyclic compounds. Quantum Mechanical (QM) methods are gaining increasing popularity in the structural study of medium to large sized molecules, including natural products. Structure validation protocols of organic compounds by QM

DFT calculations of NMR parameters (e.g. chemical shifts) may supply a new way to sort out difficult cases in the elucidation process, especially where NMR experimental data are difficult to interpret or can be misleading. Bifulco and co-workers has developed a protocol for the configurational assignment of organic molecules based on QM calculation of NMR properties such as ^{13}C chemical shift and J coupling constants. Quantum-mechanical ^{13}C chemical shift calculations methodology can be applied for the structure validation of natural products and for the determination of the configuration of medium weight low polar flexible compounds.^{164,165,135} In this chapter, we show the applicability of a combined QM/NMR approach for the determination of the relative configurations of seven diterpenoids through the calculation of ^{13}C and ^1H chemical shifts (cs) and the comparison with the related experimental data.¹³⁶

5.1.1. Giffonins J-P, Highly Hydroxylated Cyclized Diarylheptanoids from the Leaves of *Corylus avellana*, cultivar “Tonda di Giffoni”

The relative configurations of giffonins J-P (**66- 72**) were predicted by a combined QM/NMR approach through the calculation of ^{13}C and ^1H chemical shifts (cs). The cytotoxic activities of giffonin J-P were evaluated against U2Os and SAOs cell lines, derived from human osteosarcomas. They exhibited EC_{50} values higher than $150\ \mu\text{M}$ at 24–48 h, indicating the absence of cytotoxicity against both cell lines.

Corylus avellana L. (Betulaceae) is one of the most popular tree nuts on a worldwide basis, which may grow to 6 m high, exhibiting deciduous leaves that are rounded, 6–12 cm long, softly hairy on both surfaces, and with a double-serrate margin. The main products of *C. avellana* are kernels, nutritious food with a high content of healthy lipids, used by the confectionary industry,

consumed raw (with skin) or preferably roasted (without skin). Despite its wide cultivation for nuts collection, hazel leaves are also largely consumed as an infusion. They are used in folk medicine for the treatment of haemorrhoids, varicose veins, phlebitis and lower members' oedema, as consequence of its astringency, vasoprotective and anti-oedema properties and also for their mild antimicrobial effects. Antioxidant activity was reported for hazelnuts and leaves of *C. avellana*.

Herein, the isolation and the structural elucidation of two diaryl ether heptanoids (**66-67**) along with five new diaryl heptanoid (**68-72**) are described (Figure 5.1.1.1). The relative configurations of giffonins J-P (**66-72**) have been established by a combined QM/NMR approach, by a comparison of the experimental $^{13}\text{C}/^1\text{H}$ -NMR chemical shift data and the related predicted values. Furthermore, the cytotoxic activity of giffonins J-P (**66-72**) and curcumin, used as reference compound, has been evaluated against U2Os and SAOs cell lines, derived from human osteosarcomas.

Giffonins J-P structures were established by the extensive use of 1D and 2D-NMR experiments along with ESI-MS and HR-MS analysis. The relative configurations of the reported compounds **66-72** were assigned by a combined QM/NMR approach, comparing the experimental $^{13}\text{C}/^1\text{H}$ -NMR chemical shift data and the related predicted values, as previously applied and reported.^{176,164,161} We relied on this procedure, since the chemical shifts are the most diagnostic parameters of the local chemical and magnetic environment and the most reliably addressable by quantum chemical calculations.

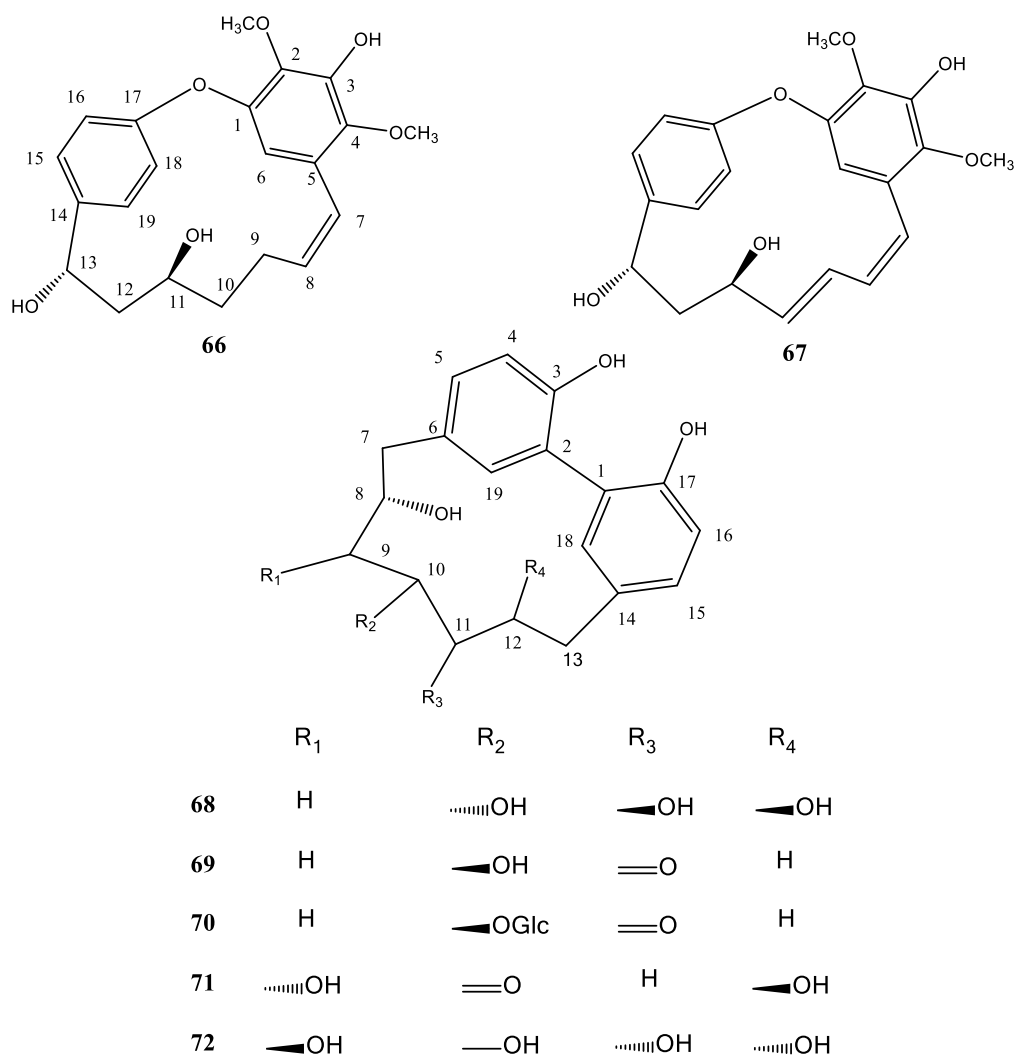


Figure 5.1.1.1 Molecular structures of giffonins (**66-72**).

For each considered compound, a proper sampling of the conformations was performed in order to attain a close agreement between calculated and experimental NMR parameters. For these reasons, an extensive conformational search at the empirical level (molecular mechanics, MM) for all the possible diastereoisomers of each investigated compound was carried out, combining Monte Carlo Molecular Mechanics (MCM), Low-Mode Conformational Sampling (LMCS), and Molecular Dynamics (MD) simulations (See

Experimental Section). Subsequently, the selected non-redundant conformers were further submitted to a geometry and energy optimization step at the density functional level (DFT) using the MPW1PW91 functional and 6-31G(d) basis set and IEFPCM for simulating the methanol solvent (Gaussian 09 software package). After the optimization of the geometries at the QM level, a visual inspection was performed in order to exclude further possible redundant conformers, and then those selected were used for the subsequent computation of the ^{13}C and ^1H NMR chemical shifts.

In details, the conformational analysis revealed many degrees of freedom in the heptanoid chains connecting the two phenyl moieties, determining different geometries to be accounted in the final Boltzmann distribution. Furthermore, similar conformers differing for the presence/absence of intramolecular H-bonds between the hydroxyl groups placed on adjacent carbons on the heptanoid chains were energetically weighted in the Boltzmann distribution according to the protic solvent (methanol) “continuum model” considered in the QM calculations. The diaryl moieties also affected the conformational sampling, leading to various conformers specifically differing for the dihedral angles between the two aromatic groups and their final arrangements on the heptanoid chain (Figure 5.1.1.2).

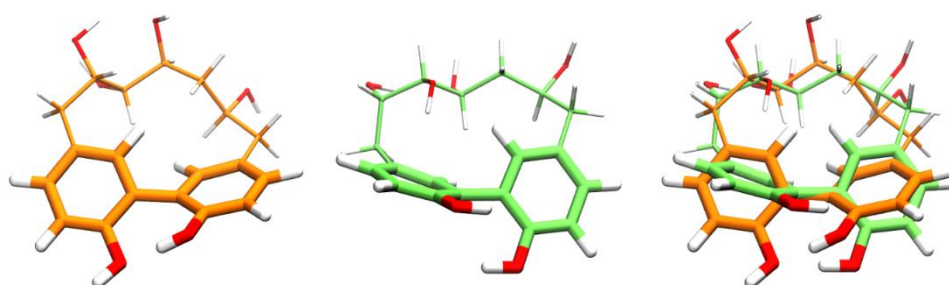


Figure 5.1.1.2 Two sampled conformations of **68f** in both separate and superimposed view modes, showing the flexibility of the heptanoid chain. The different relative arrangement of the diaryl moieties is highlighted using a higher thickness in the licorice representation.

Then, the ^{13}C and ^1H NMR chemical shifts for each investigated diastereoisomer were computed at the density functional level (DFT), using the MPW1PW91 functional and 6-31G (d,p) basis set and methanol IEFPCM. The specific contribution of each selected conformer was weighted on the final Boltzmann distribution according to the related energy. Aromatic ^{13}C and ^1H were scaled using benzene as reference compound, following the approach developed by Pellegrinet et al.,^{137,138} while the other atoms were scaled taking into account tetramethylsilane (TMS). Afterwards, for each atom of the investigated molecules, the comparison of the experimental and calculated ^{13}C and ^1H NMR chemical shifts was performed computing the $\Delta\delta$ parameter:

$$\Delta\delta = |\delta_{\text{exp}} - \delta_{\text{calc}}|$$

where, δ_{exp} (ppm) and δ_{calc} (ppm) are the $^{13}\text{C}/^1\text{H}$ experimental and calculated chemical shifts, respectively.

Finally, the relative configuration of each investigated compound was determined calculating and comparing the mean absolute errors (MAEs) for all the possible diastereoisomers:

$$\text{MAE} = \sum(\Delta\delta)/n$$

specifically defined as the summation through n of the absolute error values (difference of the absolute values between corresponding experimental and ^{13}C - ^1H chemical shifts), normalized to the number of the chemical shifts considered. In this way, the relative configurations of compounds **66-72**, shown in Table 5.1.1.1, were assigned selecting the related diastereoisomers showing the lowest $^{13}\text{C}/^1\text{H}$ MAE errors.

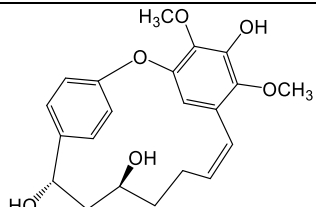
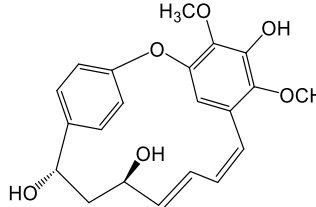
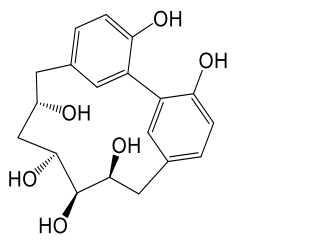
Moreover, three known flavonoid derivatives myricetin 3-O-rhamnopyranoside,¹ quercetin 3-O-rhamnopyranoside,¹ kaempferol 3-O-rhamnopyranoside,¹ and kaempferol 3-O-(4"-trans-p-coumaroyl)-rhamnopyranoside, have been also isolated from the leaves of *C. avellana*.

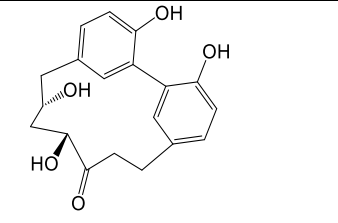
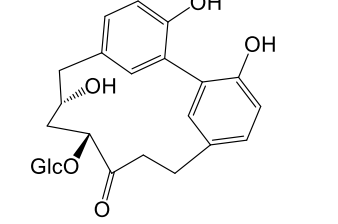
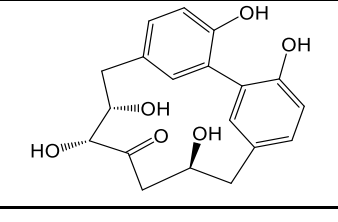
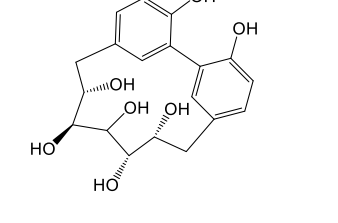
On the basis of the ability reported for the well known diarylheptanoid curcumin, a natural compound isolated from the rhizome of *Curcuma longa*, to

inhibit cell growth in malignant cells, the cytotoxic activity of compounds 1-7, myricetin 3-O-rhamnopyranoside, quercetin 3-O-rhamnopyranoside, kaempferol 3-O-rhamnopyranoside, kaempferol 3-O-(4''-trans-p-coumaroyl)-rhamnopyranoside and curcumin, used as reference compound, has been evaluated in two cancer cell lines, the U2Os and SAOs cells. The two cell lines have been selected based on the following criteria: 1) both cell lines have a common origin (human osteosarcoma) and they are resistant to apoptotic stimuli; 2) they are characterized by a different genetic background relatively to p53 gene, being SAOs p53 mutate and U2Os p53 wild-type; 3) both cell lines have been largely employed in previous studies to assess the biological activity of naturally occurring compounds. The obtained results showed that all tested compounds possess EC₅₀ values higher than 150 µM at 24-48 h, indicating the absence of cytotoxicity on both cell lines.

The present results suggest *C. avellana* leaves as a rich source of phenolic compounds, among which highly hydroxylated cyclized diarylheptanoids. Since the reported diarylheptanoid derivatives don't exert cytotoxic activity on the selected cancer cell lines, other investigations will be performed to evaluate the potential of these compounds as antioxidant agents, and to use the leaves of *C. avellana* as a source of functional ingredients for nutraceutical, herbal, and cosmetic formulations.

Table 5.1.1.1 ¹³C/¹H MAE (ppm)^a

	# of stereogenic centers	# of possible relative stereoisomer	Stereoisomer	Relative configuration	# of sampled conformers	¹³ C MAE (ppm)	¹ H MAE (ppm)	Proposed structure
66	2	2	66a	12S*,14S*	24	1.63	0.22	
			66b	12R*,14S*	25	1.73	0.28	
67	2	2	67a	12S*,14S*	19	1.85	0.25	
			67b	12R*,14S*	18	1.71	0.17	
68	4	8	68a	8S*,10R*,11R*,12R*	16	4.37	0.36	
			68b	8S*,10R*,11R*,12S*	17	2.77	0.34	
			68c	8S*,10R*,11S*,12R*	15	2.25	0.23	
			68d	8S*,10R*,11S*,12S*	17	2.05	0.34	
			68e	8S*,10S*,11R*,12R*	18	1.70	0.25	
			68f	8S*,10S*,11R*,12S*	15	1.37	0.16	
			68g	8S*,10S*,11S*,12R*	17	3.00	0.28	

			68h	8S*,10S*,11S*,12S*	18	3.07	0.21	
69	2	2	69a	8S*,10S*	27	2.62	0.30	
			69b	8S*,10R*	28	2.08	0.19	
70	2	2	70a	8S*,10S*	35	2.79	0.16	
			70b	8S*,10R*	34	2.50	0.14	
71	3	4	71a	8S*,9R*,12S*	18	3.21	0.31	
			71b	8S*,9R*,12R*	20	1.50	0.18	
			71c	8S*,9S*,12S*	18	2.06	0.23	
			71d	8S*,9S*,12R*	20	2.61	0.35	
72	4	8	72a	8S*,9R*,11R*,12R*	19	3.56	0.34	
			72b	8S*,9R*,11R*,12S*	22	2.40	0.31	
			72c	8S*,9R*,11S*,12R*	21	3.67	0.23	
			72d	8S*,9R*,11S*,12S*	22	3.57	0.24	
			72e	8S*,9S*,11R*,12R*	20	2.80	0.29	
			72f	8S*,9S*,11R*,12S*	21	2.98	0.23	

72g	8S*,9S*,11S*,12R*	19	2.28	0.18
72h	8S*,9S*,11S*,12S*	21	3.04	0.37

^a**MAE** = $\Sigma[|\delta_{\text{exp}} - \delta_{\text{calcd}}|]/n$, summation through n of the absolute error values (difference of the absolute values between corresponding experimental and ¹³C/¹H chemical shifts), normalized to the number of the chemical shifts. Values are reported for all the possible relative stereoisomers for each considered compounds. The predicted relative configurations are highlighted in green

-CONCLUSIONS-

In order to design and develop new synthetic and natural platforms targeting mPGES-1 and acting as anti-inflammatory and anti-cancer agents, we employed *in silico* strategies combined with the evaluation of the biological activities by means of *in vitro* experiments.

In particular, the computational aspects mainly regard the application and elaboration of screening methods, the analysis of structural determinants responsible of drug-macromolecule interaction and the design and development of new potent bioactive compounds by means of molecular docking calculations. For what concerns the biological part, the determination of PGE₂ synthase activity in microsomes of A549 cells, the determination of product formation by 5-LOX in the cell-based and cell-free assay, and the determination of eicosanoids production by LC-MS/MS in monocytes and polymorphonuclear leucocytes were performed at the Department of Pharmaceutical and Medicinal Chemistry of the Friedrich-Schiller University in Jena. This approach was successfully applied leading to the identification of new potent inhibitors for mPGES-1 enzyme.

Therefore, our studies were aimed to the discovery of new synthetic inhibitors targeting mPGES-1. The attention was focused on this target since it is involved in diverse levels and phases of tumor and inflammation process. In fact, in some types of cancer, inflammatory conditions are present before a malignant change occurs. Conversely, in other types of cancer, an oncogenic change induces an inflammatory microenvironment that promotes the development of tumors. Regardless of its origin, inflammation in the tumor microenvironment has many tumor-promoting effects. It aids in the proliferation and survival of malignant cells, promotes angiogenesis and metastasis, it subverts adaptive immune responses, and it alters responses to hormones and chemotherapeutic agents.

Thanks to the recently published crystal structures of mPGES-1 enzyme, the development of new inhibitors was obtained using fast computational methods.

Molecular docking technique was used for the rational design taking into account the analysis of ligand-target interactions and the actual synthetic possibilities. The X-ray structures of mPGES-1 in complex with LVJ inhibitor and more recently with four different inhibitors, provide us a good starting point providing a rationale for understanding the associated structure–activity relationships and a structural context for species-associated selectivity.

After an introduction regarding the derived-NSAIDs side effects determining the need of discovering new safe targets (such as mPGES-1), in the second chapter we reported the elucidation of new structural features of the triazole scaffold through docking calculations on the basis of the data arising from structure-based molecular docking experiments. In the course of previous studies, we identified a novel class of 1,4-disubstituted 1,2,3-triazoles that inhibited mPGES-1 in a cell-free assay with IC₅₀ values in the low μ M range. Afterwards, we performed a new structure drug design with the aim of investigating the influence of the ring-substituent topological position and simplifying the mPGES-1 inhibitor structure. The reported results led to the identification of compound **24** that showed efficient inhibitory activity and has proved the importance of halogen bonding as new key interaction useful for the design of this novel triazole derivatives as mPGES-1 inhibitors.

Moreover, we achieved the identification of different leads from a small synthetic library by means of *in silico* approaches. Docking results determined the selection of seven compounds that were able to inhibit mPGES-1. In particular, the compounds were tested on mPGES-1 and 5-LOX taking into account that dual inhibitors blocking both mPGES-1 and 5-LOX metabolic pathways of arachidonic acid are expected to possess clinical advantages over the selective inhibitors of enzyme. In particular, a good accordance between molecular modeling predictions and biological results was found; four of them displayed a considerable inhibition activity, while three of them showed also 5-LOX inhibitory activity. Two of these compounds (spiro[indoline-3,2'-

thiazolidine]-2,4'-dione and nitrofurans scaffolds) were further optimized to develop new possible mPGES-1 inhibitors. In this way, a series of commercially available building blocks were selected in order to decorate the selected scaffolds, with the aim of improving the potency and selectivity of the optimized ligands. Two compounds from spiro[indoline-3,2'-thiazolidine]-2,4'-dione series were identified displaying an increase of the inhibitory activity (mPGES-1 inhibition of 30% and 50% respectively) with respect to the lead compound, and further one compound from nitrofurans derivatives showing highest inhibitory activities with an IC_{50} of $1.37 \pm 0.7 \mu\text{M}$. The determination of the production of 5-LOX metabolites is ongoing.

At the end of the second chapter, we reported the identification of biphenylic scaffold as new synthetic platform targeting mPGES-1, which was carried out by virtual screening on the basis of a drug-receptor analysis, taking into account the more recent crystal structure of the enzyme⁷⁴ and using Autodock-Vina and Glide molecular modeling software. The rational design of this potential scaffold has guided the identification of 5 potent inhibitors of the enzyme, validated with biological assays. In particular, compounds **44** and **47** showed the strongest inhibitory activity with $IC_{50} = 0.26 \pm 0.05$ and $0.18 \pm 0.03 \mu\text{M}$, respectively. Due to the fact that the nitro groups can influence the cytotoxicity and the pharmacokinetic, two of them were further optimized to replace the nitro groups by more suitable residues, but causing the lack of inhibitory activity in enzymatic assay.

On the basis of the encouraging results regarding the identification of new synthetic platforms targeting mPGES-1, in the third chapter we reported the evaluation of the inhibitory activity of natural molecular platforms already recognized as mPGES-1 blocking agents. Accordingly, molecular docking was used to rationalize the binding modes of several compounds with known biological activities. As first point we reported the theoretical evaluation of a small library of natural molecules as potential mPGES-1 inhibitors that has led

to the identification of 12-O-methylsalvipestinoic acid as bioactive compounds. These compounds were then tested for inhibition of 5-LOX activity in a cell-based assay using PMNL and they did not affect the production of 5-LOX metabolites.

Another line of this project has regarded *in vivo* and *in vitro* biological evaluation of anti-inflammatory response of carnosol and carnosic acid and *in silico* analysis of their mechanism of action. The compounds were analyzed and a full rationalization of their binding mode was reported. The effects of these two compounds were mainly due to the inhibitory activity on arachidonic related metabolites production, and they might contribute to the anti-nociceptive, anti-inflammatory and antitumoral property of others *Salvia spp.* containing these diterpenoids. In conclusion, molecular docking and biological studies have allowed the rationalization of the molecular mechanism of carnosol and carnosic acid, which are related to the biological activity on some key enzymes involved in the arachidonic acid cascade such as mPGES-1, 5-LOX and COXs. In fact, the multiple suppression might be superior over single inhibition in terms of efficacy as well as in terms of side effects.

Another study has concerned the molecular mechanism of tanshinone IIA and cryptotanshinone in platelet anti-aggregating effects performing an integrated study of pharmacology and computational analysis in order to determinate the target responsible of their observed activity. Cryptotanshinone is able to inhibit the rat platelet aggregation in a concentration dependent manner and it also showed a G-coupled P2Y₁₂R receptor antagonistic activity as demonstrated by docking studies. This computational method was also employed for tanshinone IIA demonstrating also for this diterpenoid an interaction with the same receptor. Pharmacological and structure-activity relationship analysis have demonstrated that these natural diterpenoids are ligands of P2Y₁₂R.

Finally, the combination of NMR spectroscopy^{163b,139} and quantum mechanical calculation¹⁴⁰ (coupling constant, chemical shift) was successfully used in order to assign the relative configuration patterns of seven natural products giffonins J-P. These diterpenoids were isolated and extracted from the leaves of *Coryllus avellana*. Hence the relative configurations of the giffonins J-P were assigned by a combined QM/NMR approach, comparing the experimental ¹³C/¹H-NMR chemical shift data and the related predicted values.

Technical details about the employed computational techniques and regarding the biological evaluation and assay systems are reported in details in the appendix.

-APPENDIX A-

Experimental section

A.1 Molecular docking

Computational methodologies have become a crucial component in drug discovery, from virtual screening for hit identification to lead compound optimization. One key methodology is the molecular docking that consists in the prediction of ligand conformation and orientation within a targeted binding site. The molecular docking is based on the requirement that the 3D structure of the macromolecule is known. Many different programs have been developed, of which DOCK,¹⁴¹ FlexX,¹⁴² GOLD,¹⁴³ 120 Autodock,^{144,145,146} Autodock Vina,¹⁴⁷ and Glide122¹⁴⁸ are among the most popular. The mentioned tools are based on a range of different concepts, and each comes with its own set of strengths and weaknesses. One feature most docking programs share, however, is that they position a flexible ligand into a rigid binding site. Computational feasibility is the main reason for utilizing a rigid macromolecule in the docking calculations, as the number of freedom degrees that have to be considered grows exponentially with the number of accessible receptor conformations. Most molecular docking software have two key parts: (1) a search algorithm and (2) a scoring function.¹⁴⁹ For molecular docking to be useful in drug discovery, these key parts should be both fast and accurate. These two requirements are often in opposition to each other, requiring necessary compromises that commonly end in ambiguous results or failure.¹⁵⁰

The search algorithm samples different ligand orientations and conformations fitting the macromolecular binding site. This step is complicated by the number of freedom degrees contained in the small molecule, increasing the conformational space to sample. The search methods can be grouped in three categories: systematic methods, random or stochastic methods, and simulation methods. The systematic search algorithms try to explore all the degrees of freedom in a molecule, but they face the problem of huge number of generated conformations.¹⁵¹ The random methods (often called stochastic methods) operate by making random changes to either a single ligand or a

population of ligands. A newly obtained ligand is evaluated on the basis of a pre-defined probability function. Two popular random approaches are Monte Carlo and genetic algorithms. About simulations search methods, molecular dynamics is currently the most popular approach. However, molecular dynamics simulations are often unable to cross high-energy barriers within feasible simulation time periods, and therefore might only accommodate ligands in local minima of the energy surface.¹⁵² Therefore, an attempt is often made to simulate different parts of a protein–ligand system at different temperatures.¹⁵³ Another strategy for addressing the local minima problem is starting molecular dynamics calculations from different ligand positions. In contrast to molecular dynamics, energy minimization methods are rarely used as stand-alone search techniques, as only local energy minima can be reached, but often complement other search methods. The scoring function aims to evaluate the results of the search algorithm predicting the affinity for the biological target. This evaluation is very difficult because the binding process is governed by enthalpic and entropic factors and one or of them can predominate. Other elements can affect the scoring method, such as limited resolution of crystallographic targets, inherent flexibility, induced fit or other conformational changes that occur on binding and the participation of water molecules in macromolecule–ligand interactions. Three classes of scoring functions are currently applied: force field-based, empirical and knowledge-based scoring functions.

Molecular mechanics force fields usually quantify the sum of two energies, the macromolecule–ligand interaction energy and internal ligand energy (such as steric strain induced by binding). Most force field scoring functions only consider a single protein conformation, which makes it possible to omit the calculation of internal protein energy, which greatly simplifies scoring. The enthalpic contribution are essentially given by the electrostatic and Van der

Waals terms, and is some software (AutoDock, Gold) take into account the hydrogen bond formation between drug and biological target.

The van der Waals potential energy for the general treatment of non-bonded interactions is often modeled by a Lennard–Jones 12–6 function (Equation 1.1):

$$E_{VdW}(r) = \sum_{j=1}^N \sum_{i=1}^N 4\epsilon \left[\left(\frac{\sigma_{ij}}{r_{ij}} \right)^{12} - \left(\frac{\sigma_{ij}}{r_{ij}} \right)^6 \right]$$

Equation 1. 1

where ϵ is the well depth of the potential and σ is the collision diameter of the respective atoms i and j . The $\exp(12)$ term of the equation is responsible for small-distance repulsion, whereas the $\exp(6)$ provides an attractive term which approaches zero as the distance between the two atoms increases.

The Lennard–Jones 12–6 function is also used to describe the hydrogen bond in macromolecule-ligand complex, but compared to the Van der Waals function, is less smooth and angle dependent.

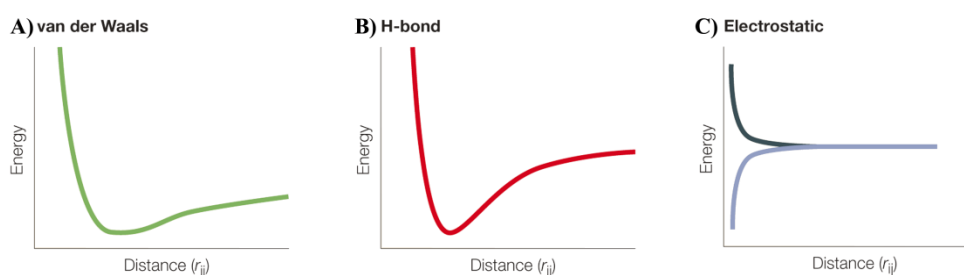


Figure 1. 5 Schematic representation of functions used to model pair-wise interactions that contribute to binding. Interactions are calculated as a function of the distance (r_{ij}) between two atoms i and j . a) van der Waals interaction given by a 12–6 Lennard–Jones potential (note the smoother attractive part of the potential compared to hydrogen bond term). B) hydrogen bond potential given by a ‘harder’ 12–10 Lennard–Jones potential. C) electrostatic potential for two

like (blue) or opposite (black) charges of same magnitude calculated using a distance dependent dielectric constant.

The electrostatic potential energy is represented as a summation of Coulombic interactions, as described in equation 1.2:

$$E_{Coul}(r) = \sum_{j=1}^{N_A} \sum_{i=1}^{N_B} \frac{q_i q_j}{4\pi\epsilon_0 r_{ij}}$$

Equation 1. 2

where N is the number of atoms in molecules A and B, respectively, and q the charge on each atom. The functional form of the internal ligand energy is typically very similar to the protein–ligand interaction energy, and also includes van der Waals contributions and/or electrostatic terms.

Empirical scoring functions work on the sum of several parameterized functions to reproduce experimental data. The design of empirical scoring functions is based on the idea that binding energies can be approximated by a sum of individual uncorrelated terms. The coefficients of the various terms are obtained from regression analysis using experimentally determined binding energies and X-ray structural information.

By using the knowledge-based scoring functions protein–ligand complexes are modeled using relatively simple atomic interaction-pair potentials. A number of atom-type interactions are defined depending on their molecular environment.

A.1.1. Autodock Vina: an Overview

There are numerous molecular docking software applications that utilize different searching and scoring algorithms and AutoDock Vina is currently one of the most cited of these applications,¹⁵⁴ especially in a virtual screening of a

compound libraries.¹⁵⁵ For the purposes of this project the software AutodockVina¹⁴⁷ and Glide have been used, where the differences between them are related to the speed, macromolecule sidechains flexibility, optimization of the free-energy scoring function based on a linear regression analysis, AMBER force field, larger set of diverse protein-ligand complexes with known inhibition constants; moreover the Lamarckian Genetic Algorithm (LGA) is a big improvement on the Genetic Algorithm, and both genetic methods are much more efficient and robust than SA in the new version of the software.

AutoDock Vina,¹⁴⁷ is a new open-source program for drug discovery, molecular docking and virtual screening, offering multi-core capability, high performance and enhanced accuracy and ease of use. Vina uses a sophisticated gradient optimization method in its local optimization procedure. The calculation of the gradient effectively gives the optimization algorithm a “sense of direction” from a single evaluation. In the spectrum of computational approaches to modeling receptor ligand binding molecular dynamics with explicit solvent, molecular dynamics and molecular mechanics with implicit solvent, molecular docking can be seen as making an increasing trade-off of the representational detail for computational speed.¹⁵⁶ Among the assumptions made by these approaches is the commitment to a particular protonation state of and charge distribution in the molecules that do not change between, for example, their bound and unbound states. Additionally, docking generally assumes much or all of the receptor rigid, the covalent lengths, and angles constant, while considering a chosen set of covalent bonds freely rotatable (referred to as active rotatable bonds here). Importantly, although molecular dynamics directly deals with energies (referred to as force fields in chemistry), docking is ultimately interested in reproducing chemical potentials, which determine the bound conformation preference and the free energy of binding. It is a qualitatively different concept governed not only by the minima in the

energy profile but also by the shape of the profile and the temperature.¹⁵⁷ Docking programs generally use a scoring function, which can be seen as an attempt to approximate the standard chemical potentials of the system. When the superficially physics-based terms like the 6–12 van der Waals interactions and Coulomb energies are used in the scoring function, they need to be significantly empirically weighted, in part, to account for this difference between energies and free energies.¹⁵⁷

The afore mentioned considerations should make it rather unsurprising when such superficially physics-based scoring functions do not necessarily perform better than the alternatives. This approach was seen to the scoring function as more of “machine learning” than directly physics-based in its nature. It is ultimately justified by its performance on test problems rather than by theoretical considerations following some, possibly too strong, approximating assumptions

The general functional form of the conformation-dependent part of the scoring function AutoDock Vina is designed to work with is:

$$c = \sum_{i < j} f_{t_i t_j}(r_{ij})$$

Equation 1. 3

where the summation is over all of the pairs of atoms that can move relative to each other, normally excluding 1–4 interactions, i.e., atoms separated by three consecutive covalent bonds. Here, each atom *i* is assigned a type *t_i*, and a symmetric set of interaction functions *f_{t_i-t_j}* of the interatomic distance *r_{ij}* should be defined.

This value can be seen as a sum of intermolecular and intramolecular contributions:

$$c = c_{inter} + c_{intra}$$

Equation 1. 4

The optimization algorithm attempts to find the global minimum of c and other low-scoring conformations, which it then ranks.

The predicted free energy of binding is calculated from the intermolecular part of the lowest-scoring conformation, designated as 1:

$$s_1 = g(c_1 - c_{intra1}) = g(c_{inter1})$$

Equation 1. 5

where the function g can be an arbitrary strictly increasing smooth possibly nonlinear function.

In the output, other low-scoring conformations are also formally given s values, but, to preserve the ranking, using c_{intra} of the best binding mode:

$$s_i = g(c_i - c_{intra1})$$

Equation 1. 6

For modularity reasons, much of the program does not rely on any particular functional form of f_{i-tj} interactions or g . Essentially, these functions are passed as a parameter for the rest of the code.

In summary the evaluation of the speed and accuracy of Vina during flexible redocking of the 190 receptor-ligand complexes making up the AutoDock 4 training set showed approximately two orders of magnitude improvement in speed and a simultaneous significantly better accuracy of the binding mode prediction. In addition, Vina can achieve near-ideal speed-up by utilizing multiple CPU cores. However, AutodockVina does not provide very good weight of the energetic contribution derived from the hydrogen bond and electrostatic interactions, especially when the metal ions are presents.

A.1.2. Glide: an Overview

Glide uses a hierarchical series of filters to search for possible locations of the ligand in the active-site region of the receptor. The shape and properties of the receptor are represented on a grid by several different sets of fields that provide progressively more accurate scoring of the ligand poses. Conformational flexibility is handled in Glide by an extensive conformational search, augmented by a heuristic screen that rapidly eliminates unsuitable conformations, such as conformations that have long-range internal hydrogen bonds. The second stage of the hierarchy begins by examining the placement of atoms that lie within a specified distance of the line drawn between the most widely separated atoms (the ligand diameter). This is done for a pre-specified selection of possible orientations of the ligand diameter. If there are too many steric clashes with the receptor, the orientation is skipped. Next, rotation about the ligand diameter is considered, and the interactions of a subset consisting of all atoms capable of making hydrogen bonds or ligand-metal interactions with the receptor are scored (subset test). If this score is good enough, all interactions with the receptor are scored. The scoring in these three tests is carried out using Schrödinger's discretized version of the ChemScore empirical scoring function. Only a small number of the best refined poses (typically 100-400) is passed on to the third stage in the hierarchy-energy minimization on the pre-computed OPLS-AA van der Waals and electrostatic grids for the receptor. Finally, the minimized poses are re-scored using Schrödinger's proprietary GlideScore scoring function. GlideScore is based on ChemScore, but includes a steric-clash term, adds buried polar terms devised by Schrödinger to penalize electrostatic mismatches, and has modifications to other terms:

$$\text{GScore} = 0.065 * \text{vdW} + 0.130 * \text{Coul} + \text{Lipo} + \text{Hbond} + \text{Metal} + \text{BuryP} + \text{RotB} + \text{Site}$$

The choice of best-docked structure for each ligand is made using a model energy score (E_{model}) that combines the energy grid score, the binding affinity

predicted by GlideScore, and (for flexible docking) the internal strain energy for the model potential used to direct the conformational-search algorithm.

It is important to underline in this phase of the studies description that the molecular docking methodology was used for the design and development of new molecular platforms with potential anticancer and anti-inflammatory activities as mPGES-1 (see chapter 3) inhibitors. In particular, for the elucidation of new structural features of the triazole scaffold we used the crystal structure PDBcode: 4AL1 (paragraph 3.1) and Glide software, for the rationalization of the binding mode of a small synthetic library (paragraph 3.2) and for the development of new libraries by a series of 71- 244 derivatives (paragraph 3.3) we used the crystal structure PDB code: 4AL1 and Autodock Vina software. In the structure-based rational drug design for the development of new potent mPGES-1 inhibitors we used the crystal structure PDBcode: 4YK5 (paragraph 3.4) and Autodock Vina software. Alongside this application, in this results description, the molecular docking was also used to rationalize the binding modes and the mechanism of action of a small pool of natural compounds as mPGES-1 (PDBcode: 4AL1, Autodock Vina) (paragraph 4.1), of carnosol and carnosic acids mPGES-1, COXs, 5-LOX (PDB code: 4AL1, 3N8X, 1CX2, 3O8Y respectively, Glide software) inhibitor (paragraph 4.2), of cryptotanshinone and tanshinone IIA inhibitors of P2Y₁₂R 1 (PDB code: 4NTJ, Glide software) (paragraph 4.3) (Chapter 4).

A.2 Biological evaluation and assay systems

In order to study the ability of the compounds to directly inhibit 5-LOX, a cell-free assay using purified human recombinant 5- LOX enzyme and arachidonic acid (20 mM) as the substrate was applied. To study the inhibitory potency on 5-LOX product formation in intact cells, human neutrophils stimulated with the Ca²⁺- ionophore A23187 together with exogenous AA (20 mM) were used. Regarding mPGES-1 to evaluate the PGE₂ production were

used microsomes of A549 cells stimulated with PGH₂ (final concentration, 20 μM). To determinate the eicosanoids production in intact cells, the analysis were assessed in PMNL stimulated with the Ca²⁺- ionophore A23187 20 mM and in monocytes stimulated by LPS in medium 5% FCS.

A.2.1. Induction of mPGES-1 and determination of PGE₂ synthase activity in microsomes of A549 cells

Preparation of A549 cells and determination of the activity of mPGES-1 was performed as described previously.¹⁰⁶ In brief, IL-1β-treated A549 cells overexpressing mPGES-1 were sonicated and the microsomal fraction was prepared by differential centrifugation at 10,000g for 10 min and at 174,000g. The resuspended microsomal membranes were preincubated with the test compounds or vehicle (DMSO). After 15 min, PGE₂ formation was initiated by addition of PGH₂ (final concentration, 20 μM). After 1 min at 4 °C, the reaction was terminated, and PGE₂ was separated by solid-phase extraction (RP-18 material) and analyzed by RP-HPLC as described. The solid phase extraction was performed with RP18-columns containing a polymeric reversed- phase. The sample was added after conditioning the column with 1 ml 100% Methanol and 1 ml H₂O. After washing the columns two times with 0,5 ml H₂O, eicosanoids were eluted with 300 μl 100% Methanol. The supernatant obtained after two centrifugation steps (15000 x g, 5 min, 4°C) was used for the RP-HPLC run.

A.2.2. Isolation of polymorphonuclear leukocytes and peripheral blood mononuclear cells from buffy coats

Human polymorphonuclear leukocytes (PMNL) and peripheral blood mononuclear cells (PBMC) were freshly isolated from whole warm venous blood, collected from adult female healthy volunteers at Universitatkilikum Jena, Institut fur Trasfusionsmedizin (Jena, Germany). Buffy coats were

diluted with 10 ml of PBS-dextran solution (5%, w/m), and stored at RT for 40 min to allow the erythrocytes precipitation. Then, 10 ml of lymphocyte separation medium were overlaid with 40 ml of the supernatant and centrifuged (2000 rpm, 20 min, RT and w/o brake) to separate the different cell types.

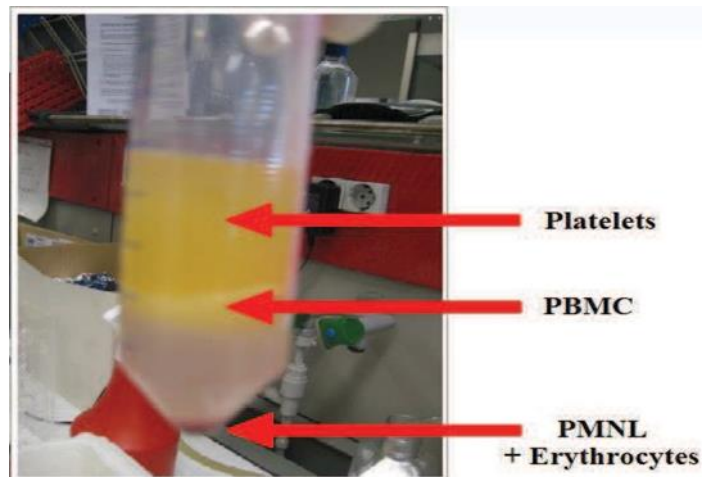


Figure A.3.1 Density Centrifugation (left to right)

The polymorphonuclear leukocytes are localized in the pellet fraction that was then washed with PBS and centrifuged (1200 rpm, 10 min, 4°C). The erythrocytes remaining in the pellet were lysed using ice-cold water, vortexing the suspension for 45 sec. This process was stopped by adding the fourfold amount of PBS to prevent the lysis of the leukocytes. The PMNL were washed again as described previously, diluted with PBS containing glucose (0.1%, w/v). The isolation procedure was strictly performed at 4°C.

PBMC are localized in the ring fraction that after collection, were washed 3 times with cold PBS; then monocytes were separated by adherence for 1 h at 37°C to culture flasks (2×10^7 cells/ml RPMI 1640 medium containing 2 mM l-glutamine and 50 µg/ml penicillin/streptomycin), which gave a purity of >85%, defined by properties of forward and side scatter of light and detection of the CD14 surface molecule by flow cytometry. Monocytes were finally

resuspended in ice-cold PBS plus 1 mg/ml glucose (PG buffer) or in PG buffer containing 1 mM CaCl₂ (PGC buffer).

A.2.3. Determination of product formation by 5-LOX in the cell-based assay by HPLC

For assays of intact cells stimulated with Ca²⁺-ionophore A23187, 5 × 10⁶ freshly isolated neutrophils were resuspended in 1 mL PGC buffer. After pre-incubation with the compounds (15 min, 37°C), 5-LOX product formation was started by addition of 1 mM CaCl₂ and 2.5 μM A23187 plus AA at the indicated concentrations respectively. After 10 min at 37°C, the reaction was stopped by addition of 1 mL of methanol. The 5-LOX metabolites formed were extracted and analysed by HPLC as described previously. 5-LOX product formation is expressed as ng of 5-LOX products per 10⁶ cells, which includes LTB₄ and all of its trans isomers, 5(S),12(S)-di-hydroxy-6,10-trans-8,14-cis-eicosatetraenoic acid (5(S),12(S)-DiHETE), and 5(S)-hydro(pero)xy-6-trans-8,11,14-cis-eicosatetraenoic acid (5-H(p)ETE). Cysteinyl LTs C₄, D₄ and E₄ were not detected, and oxidation products of LTB₄ were not determined.

A.2.4. Determination of product formation by 5-LOX in the cell-free assay by HPLC

Expression of 5-LOX was performed in *E. coli* JM 109 cells, transfected with pT3-5LO, and purification of 5-LOX was performed as described previously. In brief, cells were lysed by incubation in 50mM triethanolamine/HCl pH 8.0, 5 mM EDTA, soybean trypsin inhibitor (60 mg/ml), 1 mM phenylmethylsulfonyl fluoride (PMSF), and lysozyme (500 mg/ml), homogenized by sonication (3 15 s) and centrifuged at 19,000 g for 15 min. Proteins including 5-LOX were precipitated with 50% saturated ammonium sulfate during stirring on ice for 60min. The precipitate was collected by centrifugation at 16,000 g for 25 min and the pellet was suspended in 20ml

PBS containing 1 mM EDTA. After centrifugation at 100,000 g for 70min at 4°C, the 100,000 g supernatant was applied to an ATP-agarose column (Sigma A2767), and the column was eluted as described previously. Partially purified 5-LOX was immediately used for in vitro activity assays. Samples were preincubated with the test compounds or vehicle (0.1% DMSO) as indicated. After 10 min at 4 °C, samples were pre-warmed for 30 s at 37 °C, and 2 mM CaCl₂ plus 20 mM AA was added to start 5-LOX product formation. The reaction was stopped after 10 min at 37 °C by addition of 1 ml ice-cold methanol, and the formed metabolites were analyzed by HPLC as described. 5-LOX products include the all-trans isomers of LTB₄ as well as 5-HPETE and its corresponding alcohol 5-HETE.

A.2.5. Determination of eicosanoids production in PMNL and monocytes by UPLC-MS/MS

To determine the eicosanoids production in PMNL and monocytes, the analysis were assessed in PMNL stimulated with the Ca²⁺- ionophore A23187 and in monocytes stimulated by LPS. Freshly isolated neutrophils¹⁵⁸ (5 × 10⁶/mL) were preincubated with the test compounds (dissolved in DMSO) for 10 min at 37 °C, then were stimulated with 2.5 μM Ca²⁺-ionophore A23187 for 15 min at 37 °C, we stopped the reaction through the addition of 1 mL of methanol and the extraction of the eicosanoids were performed by SPE after the addition of 530 μM PBS/HCl and PGB₁ 100 ng/ml. PBMC freshly isolated from buffy coats of human blood were plated in 170 cm² culture flask in RPMI culture medium (RPMI 1640 containing 100 U/mL penicillin, 100 mg/mL streptomycin, 2 mM L-glutamine and 2% (v/v) human serum) to let them adhere. After 1.5 h at 37 °C and 5% CO₂, monocytes were collected by scraping of the flask and 1.5×10⁶ /mL of monocytes were stimulated with LPS 10 ng/mL for 24 h in order to measure the production of mPGES-1 and COXs metabolites. Test compounds or vehicle were added and 30 min before the

stimulus, For measurement of eicosanoids levels supernatants were collected after centrifugation (2000 g, 4 °C, 10 min). Then extracted by SPE and analysed by UPLC-MS/MS.

Ultra-performance liquid chromatography tandem mass spectrometry (UPLC-MS/MS) analyses were carried out on an Acquity UPLC BEH C18 column (1.7 μ m, 2.1 \times 50 mm, Waters, Milford, MA, USA) using an Acquity™ UPLC system (Waters) and a QTRAP 5500 Mass Spectrometer (AB Sciex, Darmstadt, Germany) equipped with a Turbo V™ Source and electrospray ionization (ESI) probe.

Cell products (4 μ l injection) were separated at a flow rate of 0.8 ml/min and a column temperature of 45 °C. The solvents for the mobile phase were water/acetonitrile (90/10; solvent A) and acetonitrile (solvent B) both acidified with 0.07% (v/v) formic acid. Isocratic elution at A/B=30% was performed for 2 min, and followed by a linear gradient to 70% B within 5 min. HPLC solvents were from VWR (Darmstadt, Germany).

Lipid mediators were detected by multiple reaction monitoring in the negative ion mode using a dwell time of 10 ms. The ion spray voltage was set to 4500 V, the heater temperature to 500 °C, the declustering potential to 50–120 eV, the entrance potential to 10 eV and the collision cell exit potential to 11–22 eV, the spray gas pressure to 50 psi, the Turbo V gas pressure to 80 psi and the curtain gas pressure to 20 psi.

Automatic peak integration was performed with Analyst 1.6 software (AB Sciex, Darmstadt, Germany) using IntelliQuan default settings. Data were normalized on the internal standard PGB1 and are given as percentage of positive control.

The reported method was optimized not for absolute quantification of eicosanoids, but for the analysis of mediator lipids production in PMNL and in THP-1 derived macrophage-like cells in different condition.

A.2.6. Induction and assessment of carrageenan-induced hyperalgesia

Acute inflammation was induced in the right hind paw by injecting subcutaneously (s.c.) 50µl of freshly prepared solution of 1% carrageenan. The left paw received 50µl of saline, which served as control. The response to inflammatory pain was determined by measuring the mechanical nociceptive pressure by the paw pressure test via a commercially available analgesiometer (Ugo Basile, Italy). The apparatus was set up to apply a force of 0-250 g, increasing from zero. The nociceptive threshold was taken as the end point at which mice vocalized or struggled vigorously. Carnosol and carnosic acid were administered subcutaneously (s.c.) in a dose dependent manner (1-100 µg/20µl) 30 min before 1% carrageenan (50µl; s.c.) into the dorsal hind paw of the mice and the pressure threshold was observed at 0.5, 1, 3 and 4h. The time selection was made based on the preliminary studies. A change in the hyperalgesic state was calculated as a percentage of the maximum possible effect (% MPE) from the formula: $[(P_2 - P_1) / (P_0 - P_1) \times 100]$, where P_1 and P_2 were the pre- and post-drug paw withdrawal thresholds respectively, and P_0 was the cut-off (250 g).

A.2.7. Formalin test

The procedure used has been previously described. Subcutaneous injection of a dilute solution of formalin (1%, 20 µl/paw) into the mice hind paw evokes nociceptive behavioral responses, such as licking, biting the injected paw or both, which are considered indices of pain. The nociceptive response shows a biphasic trend, consisting of an early phase occurring from 0 to 10 min after the formalin injection, due to the direct stimulation of peripheral nociceptors, followed by a late prolonged phase occurring from 20 to 40 min, which reflects the response to inflammatory pain. During the test, the mouse was placed in a Plexiglas observation cage (30 × 14 × 12 cm), 1 h before the formalin

administration to allow it to acclimatize to its surroundings. The total time (s) that the animal spent licking or biting its paw during the formalin-induced early and late phase of nociception was recorded. Carnosol and carnosic acid were administered subcutaneously (s.c.) (100 µg/20µl) 30 min before formalin injection (20µl; s.c.).

A.2.8. *In vitro* platelet aggregation assay

In vitro platelet aggregation was measured according to the turbidimetric method, using two-channel aggregometer (Chrono-Log, Corporation, Mod. 490, USA). Blood anticoagulated with 3.2% sodium citrate (1:9 citrate/blood, v/v) was withdrawn from male Wistar rats (anesthetized by enflurane) by cardiac puncture. Platelet-rich plasma (PRP) and platelet-poor plasma (PPP) were prepared as previously described (Maione et al., 2013, 2014). Briefly, PRP was obtained by centrifugation at 800 rpm for 15 min at 25 °C. PPP was prepared from the precipitated fraction of PRP by centrifugation at 2000 rpm for 20 min at 25 °C. PRP was adjusted to 3×10^8 platelets/ml. Next, 250 µl of PRP were incubated at 37 °C for 1 min in the cuvette with 20 µl of CRY solution at final concentration of 0.5, 5 and 50 µM. CRY-vehicle (0.3% DMSO in distilled water) was used as control. After incubation, platelet aggregation was induced by the addition of 20 µL ADP (3 µM). The maximum platelet aggregation rate was recorded within 10 min with continuous stirring at 37 °C. The light transmittance was calibrated with PPP. The percentage (%) of inhibition of platelet aggregation was calculated by the following formula: $[(X-Y)/X] \times 100\%$. X was the maximum aggregation rate of vehicle-treated PRP; Y was the maximum aggregation rate of sample-treated PRP and was expressed in terms of AUC (% of total response duration from reagent addition). Statistical analysis: all assays were repeated at least in triplicate and the results were expressed as mean \pm standard error of mean (SEM). Results were analyzed with one way analysis of variance (ANOVA), followed by

Bonferroni's test for multiple comparisons. In some cases, One Sample t-test was used to evaluate significance against the hypothetical zero value. The analysis was performed using GraphPad Prism Software version 4.0. P values less than 0.05 were considered significant.

A.2.9. Cell culture and viability assay

The U2Os and SAOs cell lines, derived from human osteosarcomas^{22,23} were maintained in Dulbecco's modified Eagle's medium (DMEM) supplemented with 10% fetal bovine serum (FBS; Life Technologies, Monza, Italy), 1% L-glutamine, 1% penicillin, 1% streptomycin (Life Technologies) at 37°C, in a 5% CO₂ humidified atmosphere and harvested at approximately 90% confluence.

A.3 Quantum Mechanical Calculation of NMR Parameters in the Stereostructural Determination of Natural Products

Many molecular properties of organic compounds, such as chemical reactivity and catalytic, biological, and pharmacological activities, are critically affected not only by their functional groups but also by their spatial position. Thus, the disclosure of the relative configuration has a great impact in the full understanding of their chemical behaviours. Different approaches to determine the exact structure and/or configuration of organic products have been devised.^{159,160,161} The total synthesis has played a primary role in the structural assignment and revision but its drawback is represented by the additional costs in terms of time and money. For these reasons, a series of new and more rapid methods that take advantage of the information deriving from nuclear magnetic resonance (NMR), circular dichroism (CD), X-ray crystallography, and mass spectrometry (MS), have shown to be a valid alternative to the classical chemical approach.

In this field, NMR spectroscopy is one of the most employed tool, since some NMR parameters (coupling constant, chemical shift (cs)) can provide

fundamental information on the configurational and conformational arrangement of organic molecules. For example, the $^3J_{\text{H-H}}$ coupling constants between protons separated by three bonds depend on the dihedral angles, following the well-known Karplus equation.¹⁶² Moreover, the Nuclear Overhauser Effect (NOE)¹⁶³ provides information of the 3D spatial arrangement of the nuclei, clarifying the geometrical information on the relative positions of the atoms in the analysed molecule. Thus, the evaluation of simple NMR parameters, such as proton-proton J -coupling values, chemical shifts, and/or nuclear Overhauser effect intensities allows to determine the configuration of cyclic compounds with three- to six-membered rings presenting a predictable conformational behaviour. Polysubstituted opened chains and macrocycles, constitute a more difficult cases of relative configurational assignment, because the stereochemical analysis is complicated by the geometrical uncertainty of such types of flexible systems.

For the above situations, different NMR-based methods, such as the quantum mechanical calculation of NMR parameters,^{161,164,165} has been proposed for the relative (and/or absolute) configurational assignment of organic molecules. In the last years, great advances have been made in developing QM methods of chemical interest able to predict molecular properties. In particular, the quantum mechanical calculations of NMR parameters have been used as an emerging strategy for the assignment of relative configuration of organic molecules, based on the high accuracy in the reproduction of experimental NMR properties achieved also at a low demanding level of theory.^{166,167} It is noteworthy that, besides the development and application of QM approach for structural studies, fast empirical methods have been devised to predict NMR chemical shifts.¹⁶⁸ These empirical methods are based on fast calculation algorithms¹⁶⁹ that can generate a set of possible structural hypotheses with the average deviation between calculated and experimental chemical shifts equal to $\delta = 1.8$ ppm for ^{13}C chemical shifts. Such

empirical NMR chemical shift predictions could be useful with large-sized molecules or in presence of very flexible compounds for which different conformers have to be considered in the more time consuming QM calculations. Moreover, these empirical methods can be applied as filter to narrow the number of stereoisomers to be accurately verified by other methods such as X-ray, total synthesis, QM approaches.

The ^{13}C -based protocol (Figure A.3.1), used in this project, consists of four fundamental steps: (a) conformational search and a preliminary geometry optimization of all the significantly populated conformers of each stereoisomer; (b) final geometry optimization of all the species at QM level; (c) GIAO (gauge including atomic orbital)¹⁷⁰ ^{13}C NMR calculations of all the so-obtained structures at QM level; (d) comparison of the Boltzmann averaged NMR parameter calculated for each stereoisomer with those experimentally measured for the compound under examination. This protocol could be used also for the prediction and comparison of ^1H NMR chemical shift data, and it has been devised for flexible systems considering the importance of the contribution of all significant conformers to predict a chemical-physical property and the theory level used to calculate the energy of the single geometrical isomers.^{164,165} Considering the simple case of a molecule with a couple of two adjacent stereocenters, the first step is to build two diastereoisomers by dedicated software.

Calculation Protocol for Rigid Molecular Frameworks

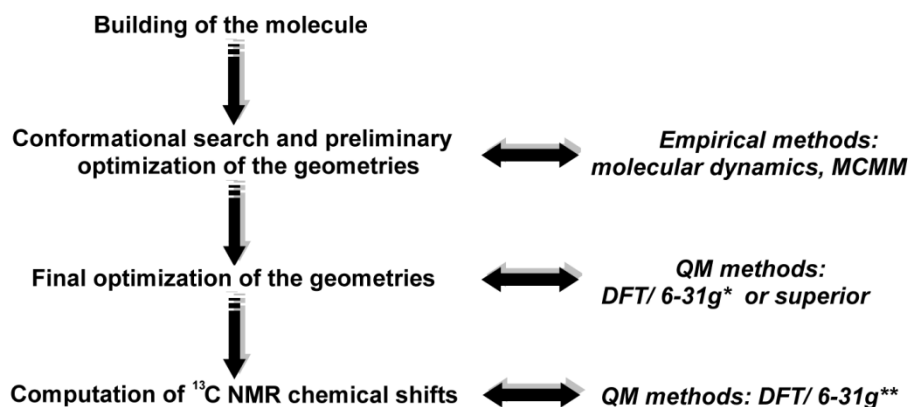


Figure A.3.1 Schematization of protocol used for the determination of relative configuration in organic compounds, based on ^{13}C calculation at QM level of theory.

The conformational sampling is performed at empirical theory level,¹⁷¹ generally through molecular dynamics (MD) or by Monte Carlo Multiple Minimum methods (MCMM).¹⁷²

A preliminary geometry optimization is run at empirical level (molecular mechanics, MM) or semi-empirical level (AM1,¹⁷³ PM3¹⁷⁴ or other) on all found conformers for each diastereoisomer, followed by a QM optimization step. On the so obtained geometries the $^{13}\text{C}/^1\text{H}$ NMR chemical shift for each stereoisomer is calculated and the theoretical data are extrapolated taking into account the Boltzmann-weighted average derived from the energies of the single conformers. The calculated values are compared with the experimental NMR data and the relative (or absolute) configuration is determined based on the best fit between theoretical and experimental data set given by one of the two structural hypothesis.

Following the same key steps described for $^{13}\text{C}/^1\text{H}$ -based protocol, the calculation of homo- and heteronuclear coupling constants can be carried out for the conformational and configurational studies of organic molecules. In

details, each global minimum conformer undergoes a full geometry optimization using the DFT theoretical level¹⁷⁵ and then, on the obtained geometries, the calculation of the J couplings is performed taking into account the contributions of the following interactions: Fermi contact (FC), paramagnetic spin-orbit (PSO), diamagnetic spin-orbit (DSO), and spin-dipole (SD). Based on the Boltzmann distribution of the conformers, the calculated J -coupling values are extrapolated and then compared to the experimental data set, suggesting the relative configuration of the examined compound. For large molecular systems, presenting many stereocenters, it is suggested that, given the prohibitive computational requirement for a simultaneous consideration of all combinations of the possible conformations and configurations, the molecule can be dissected into appropriately 2-C fragments prior to the J -coupling calculations,¹⁷⁶ as for the Murata's method. Each reduced subsystem is treated like an entire molecule: a geometry optimization step, followed by $^3J_{\text{H-H}}$ and $^{2,3}J_{\text{C-H}}$ calculations, is performed for each staggered rotamer. It is only one of the six calculated data sets that should display a satisfactory agreement with the experimental values. Differently from the original J -based approach proposed by Murata, for which it is impossible to distinguish the *antierythro* from the *antithreo* arrangement on the basis of the sole evaluation of the J coupling values, the quantitative analysis of the calculated vs the experimental data allows the relative configurational assignment for the right *anti* rotamer.

A.3.1. Computational details in determination of relative configuration of giffonins J-P

Maestro 9.6¹⁷⁷ was used to build the chemical structures of all possible relative diastereoisomers of compounds **66-72**. Optimization of the 3D structures was performed with MacroModel 10.2¹⁷⁷ using the OPLS force field¹⁷⁸ and the Polak-Ribier conjugate gradient algorithm (PRCG, maximum derivative less than 0.001 kcal/mol).

In particular, for compounds **66**, **67**, **69** and **70**, which have two stereo-chemical centers, two possible diastereoisomers were considered:

- **66a** (12S*,14S*), **66b** (12R*,14S*);
- **67a** (12S*,14S*), **67b** (12R*,14S*);
- **69a** (8S*,10S*), **69b** (8S*,10R*);
- **70a** (8S*,10S*), **70b** (8S*,10R*).

For compound **71**, possessing three stereo-chemical centers, four possible diastereoisomers were considered:

- **71a** (8S*,9R*,12R*), **71b** (8S*,9R*,12S*), **71c** (8S*,9S*,12R*) and **71d** (8S*,9S*,12S*).

Moreover, for compounds **68**, possessing four stereo-chemical centers, eight diastereoisomers were accounted:

- **68a** (8S*,10R*,11R*,12R*), **68b** (8S*,10R*,11R*,12S*), **68c** (8S*,10R*,11S*,12R*), **68d** (8S*,10R*,11S*,12S*), **68e** (8S*,10S*,11R*,12R*), **68f** (8S*,10S*,11R*,12S*), **68g** (8S*,10S*,11S*,12R*), **68h** (8S*,10S*,11S*,12S*);

For compound **72**, which has five stereo-chemical centers with one plane of symmetry, eight possible diastereoisomers were taken into account:

- **72a** (8S*,9R*,11R*,12R*), **72b** (8S*,9R*,11R*,12S*), **72c** (8S*,9R*,11S*,12R*), **72d** (8S*,9R*,11S*,12S*), **72e** (8S*,9S*,11R*,12R*), **72f** (8S*,9S*,11R*,12S*), **72g** (8S*,9S*,11S*,12R*), **72h** (8S*,9S*,11S*,12S*).

Starting from the obtained 3D structures, exhaustive conformational searches at the empirical molecular mechanics (MM) level with Monte Carlo Multiple Minimum (MCMM) method (50,000 steps) and Low mode Conformational Search (LMCS) method (50,000 steps) were performed, in order to allow a full exploration of the conformational space. Furthermore, molecular dynamic simulations were performed at 450, 600, 700, 750 K, with a time step of 2.0 fs, an equilibration time of 0.1 ns, and a simulation time of

10 ns. A constant dielectric term of methanol, mimicking the presence of the solvent, was used in the calculations to reduce artefacts.

For each diastereoisomer, all the conformers obtained from the previously mentioned conformational searches were minimized (PRCG, maximum derivative less than 0.001 kcal/mol) and compared. The “Redundant Conformer Elimination” module of Macromodel 10.2 was used to select non-redundant conformers, excluding the conformers differing more than 13.0 kJ/mol (3.11 kcal/mol) from the most energetically favored conformation and setting a 1.0 Å RMSD (root-mean-square deviation) minimum cut-off for saving structures.

Next, the obtained conformers were optimized at quantum mechanical (QM) level by using the MPW1PW91 functional and the 6-31G(d) basis set. Experimental solvent effects (CH₃OH) were reproduced using the integral equation formalism version of the polarizable continuum model (IEFPCM). After this step at the QM level, the new obtained geometries were visually inspected in order to remove further possible redundant conformers, and then those selected were accounted for the subsequent computation of the ¹³C and ¹H NMR chemical shifts, using the MPW1PW91 functional and the 6-31G(d,p) basis set and methanol IEFPCM. Final ¹³C and ¹H NMR spectra for each of the investigated diastereoisomers were built considering the influence of each conformer on the total Boltzmann distribution taking into account the relative energies. Furthermore, calibrations of calculated ¹³C and ¹H chemical shifts were performed following the multi-standard approach (MSTD).^{137,138} In particular, aromatic ¹³C and ¹H chemical shifts were scaled using benzene as reference compound. All the other ¹³C and ¹H calculated chemical shifts were scaled to TMS (tetramethylsilane).

All QM calculations were performed using Gaussian 09 software package.¹⁷⁹

References

- 1 Balkwill, F.; Mantovani, A. *Lancet* **2001**, *357*, 539–545.
- 2 Dvorak, H. F. *N. Engl J Med* **1986**, *135*, 1650–1659.
- 3 Dranoff, G. *Curr Opin Immunol* **2002**, *14*, 161–164.
- 4 Pardoll, D. M. *Nature Rev Immunol* **2002**, *2*, 227–238.
- 5 Philip, M.; Rowley, D.A.; Schreiber, H. *Semin Cancer Biol* **2004**, *14*, 433–9.
- 6 a) Coussens, L.M.; Werb, Z. *Nature* **2002**, *420*, 860–867; b) Okada, F. *Redox Rep* **2002**, *7*, 357–368; c) Yang, C. R.; Hsieh, S. L.; Ho, F. M.; Lin, W. W. *J Immunol* **2005**, *174*, 1647–1656; d) Nathan, C. *Nature* **2002**, *420*, 846–852.
- 7 Maiuri, M. C.; Tajana, G.; Iuvone, T.; De Stefano, D.; Mele, G.; Ribecco, M.T.; Cinelli, M. P.; Romano, M. F.; Turco, M. C.; Carnuccio, R. *Am J Pathol* **2004**, *165*, 115–26.
- 8 Levy, B. D.; Clish, C. B.; Schmidt, B.; Gronert, K.; Serhan, C. N. *Nat Immunol* **2001**, *2*, 612–619.
- 9 Hodge-Dufour, J.; Marino, M. W.; Horton, M. R.; Jungbluth, A.; Burdick, M. D.; Strieter, R. M.; Noble, P. W.; Hunter, C. A.; Puré, E.. *Proc Natl Acad Sci USA* **1998**, *95*, 13806–13811.
- 10 a) Savill, J.; Wyllie, A. H.; Henson, J. E.; Walport, M. J.; Henson, P. M.; Haslett, C. *J Clin Invest* **1989**, *83*, 865–875; b) Savill, J.; Fadok, V. A. *Nature* **2000**, *407*, 784–788; c) Savill, J.; Dransfield, I.; Gregory, C.; Haslett, C. *Nat Rev Immunol* **2002**, *2*, 965–75.
- 11 a) Fadok, V. A.; Bratton, D. L.; Konowal, A.; Freed, P. W.; Westcott, J. Y.; Henson, P. M. *J. Clin. Invest* **1998**, *101*, 890–898; b) McDonald, P. P.; Fadok, V. A.; Bratton, D.; O'Reilly, K. M.; Baglolle, C. J.; Phipps,

-
- R. P.; Sime, P. J. *J Immunol* **1999**, *163*, 6164–6172; c) Huynh, M.- L. N.; Fadok, V. A.; Henson, P. M. *J Clin Invest* **2002**, *109*, 41–50.
- 12 Macarthur, M.; Hold, G. L.; El-Omar, E. M. *Am J Physiol Gastrointest Liver Physiol* **2004**, *286*, G515–G520.
- 13 Berenblum, I. *Cancer Res* **1941**, *1*, 44–48.
- 14 Trosko, J. E. *Mol Carcinog* **2001**, *30*, 131–137.
- 15 Hanahan, D.; Weinberg, R. A. *Cell* **2000**, *100*, 57–70.
- 16 Aggarwal, B. B. *Cancer Cell* **2004**, *6*, 203–208.
- 17 Mantovani, A. *Nature* **2005**, *435*, 752–753.
- 18 Coussens, L. M.; Werb, Z. *Nature* **2002**, *420*, 860–867.
- 19 a) Martey, C. A.; Pollock, S. J.; Turner, C. K.; O'Reilly, K. M.; Bagloli, C. J.; Phipps, R. P.; Sime, P. J. *Am J Physiol Lung Cell Mol Physiol* **2004**, *287*, L981–991; b) Peek, Jr R. M.; Crabtree, J. E. *J Pathol* **2006**, *208*, 233–248; c) Castle, P. E.; Hillier, S. L., Rabe, L. K.; Hildesheim, A.; Herrero, R.; Bratti, M. C., Sherman M. E., Burk R. D., Rodriguez A. C., Alfaro M., Hutchinson M. L., Morales J., Schiffman M.. *Cancer Epidemiol Biomarkers Prev* **2001**, *10*, 1021–1027; d) Di Bisceglie, A. M. *Hepatology* **1997**, *26*, 34S–38S; e) Kanoh, K.; Shimura, T.; Tsutsumi, S.; Suzuki, H.; Kashiwabara, K.; Nakajima. T.; Kuwano, H. *Cancer Lett* **2001**, *169*, 7–14; f) Offersen, B. V.; Knap, M. M.; Marcussen, N.; Horsman, M. R.; Hamilton-Dutoit, S.; Overgaard, F. *Cancer* **2002**, *87*, 1422–1430; g) Garcea, G.; Dennison, A. R.; Steward, W. P.; Berry, D. P. *Pancreatology* **2005**, *5*, 514–529; h) Murphy, S. J.; Anderson, L. A.; Johnston, B. T.; Fitzpatrick, D. A.; Watson, P. R.; Monaghan, P.; Murray, L. J. *World J Gastroenterol* **2005**, *11*, 7290–7295; i) Mossman, B. T.; Kamp, D. W.; Weitzman, S. A. *Cancer Invest.* **1996**, *14*, 466–480; l) Okano, M.; Gross, T. G. *Pediatr Hematol Oncol* **2001**, *18*, 427–442; m) Vagefi, P. A.; Longo, W. E. *Clin Colorectal Cancer* **2005**, *4*, 313–319; m) Berwick, M.; Armstrong, B. K.; Ben-
-

-
- Porat, L.; Fine, J.; Krickler, A.; Eberle, C.; Barnhill, R. *J Natl Cancer Inst* **2005**, *97*, 195–199; n) Nelson, W. G.; De Marzo, A. M.; DeWeese, T. L.; Isaacs, W. B. *J Urol* **2004**, *172*, S6–11.
- 20 a) Balkwill, F.; Charles, K. A.; Mantovani, A. *Cancer Cell* **2005**, *7*, 211–217; b) Coussens, L. M.; Werb, Z. *Nature* **2002**, *420*, 860–867; c) Karin, M. *Nature*, **2006**, *441*, 431–436.
- 21 a) Koehne, C. H.; Dubois, R. N. *Semin Oncol* **2004**, *31*, 12–21; b) Flossmann, E.; Rothwell, P. M. *Lancet* **2007**, *369*, 1603–1613; c) Chan, A. T.; Ogino, S.; Fuchs, C. S. *N. Engl J Med* **2007**, *356*, 2131–2142.
- 22 Mantovani, A., Allavena, P., Sica, A.; Balkwill, F. *Nature* **2008**, *454*, 436–444.
- 23 Hanahan, D.; Weinberg, R. A. *Cell* **2000**, *100*, 57–70.
- 24 Kim, S.; Takahashi, H.; Lin, W. W.; Descargues, P.; Grivennikov, S.; Kim, Y.; Luo, J. L.; Karin, M. *Nature* **2009**, *457*, 102–106.
- 25 Maeda, H.; Akaike, H. *Biochemistry* **1998**, *63*, 854–65.
- 26 Fulton, A. M.; Loveless, S. E.; Heppner, G. H. *Cancer Res* **1984**, *44*, 4308–4311.
- 27 Pollard, J. W. *Nat Rev Cancer* **2004**, *4*, 71–78.
- 28 Hudson, J. D.; Shoaibi, M.A.; Maestro, R.; Carnero, A.; Hannon, G. J.; Beach, D. H. *J Exp Med* **1999**, *190*, 1375–82.
- 29 Petrenko, O.; Moll, U. M. *Mol. Cell.* **2005**, *17*, 225–36.
- 30 Chu, F. F.; Esworthy, R. S.; Chu, P. G.; Longmate, J. A.; Huycke, M. M.; Wilczynski, S.; Doroshov, J. H. *Cancer Res* **2004**, *64*, 962– 968.
- 31 Lin, E. Y.; Pollard, J. W. *Br. J Cancer* **2004**, *90*, 2053–2058.
- 32 Coussens, L. M.; Werb, Z. *J Exp Med* **2001**, *193*, F23–26.
- 33 a) Clark, W. H.; Elder, D. E.; Guerry, D., Braitman, L. E.; Trock, B. J.; Schultz, D.; Synnestvedt, M.; Halpern, A. C. *J Natl Cancer Inst* **1989**, *81*, 1893–1904; b) Clemente, C. G.; Mihm, M. C.; Bufalino, R.;

-
- Zurrída, S.; Collini, P.; Cascinelli, N. *Cancer* **1996**, *77*, 1303–1310; c) Naito, Y.; Saito, K.; Shiiba, K.; Ohuchi, A.; Saigenji, K.; Nagura, H.; Ohtani, H. *Cancer Res* **1998**, *58*, 3491–3494; d) Nakano, O.; Sato, M.; Naito, Y.; Suzuki, K.; Orikasa, S.; Aizawa, M.; Suzuki, Y.; Shintaku, I.; Nagura, H.; Ohtani, H. *Cancer Res* **2001**, *61*, 5132–5136; e) Zhang, L.; Conejo-García, J. R.; Katsaros, D.; Gimotty, P. A.; Massobrio, M.; Regnani, G.; Makrigiannakis, A.; Gray, H.; Schlienger, K.; Liebman, M. N.; Rubin, S. C.; Coukos, G. *Eng J Med* **2003**, *348*, 203–213; f) Dunn, G.; Bruce, A.; Ikeda, H.; Old, L.; Schreiber, R. *Nat. Immunol* **2002**, *3*, 991–998; g) Brigati, C.; Noonan, D. M.; Albini, A.; Benelli, R. *Clin Exp Metastasis* **2002**, *19*, 247–258; h) Tsung, K.; Dolan, J. P.; Tsung, Y. L.; Norton, J. A. *Cancer Res* **2002**, *62*, 5069–5075; i) Mihm, M.; Clemente, C.; Cascinelli, N. *Lab Invest* **1996**, *74*, 43–47.
- 34 Smyth, M. J.; Cretney, E.; Kershaw, M. H.; Hayakawa, Y. *Immunol Rev* **2004**, *202*, 275–293.
- 35 Khong, H.T.; Restifo, N. P. *Nat Immunol* **2002**, *3*, 999–1005.
- 36 Karin, M. *Nature* **2006**, *441*, 431–436.
- 37 Yu, H.; Kortylewski, M.; Pardoll, D. *Nature Rev Immunol* **2007**, *7*, 41–51.
- 38 a) Voronov, E.; Shouval, D. S.; Krelin, Y.; Cagnano, E.; Benharroch, D.; Iwakura, Y.; Dinarello, C. A.; Apte, R. N. *Proc Natl Acad Sci USA* **2003**, *100*, 2645–2650; b) Grivennikov, S.; Karin, M. *Cancer Cell* **2008**, *13*, 7–9; c) Szlosarek, P. W.; Balkwill, F. R. *Lancet Oncol* **2003**, *4*, 565–573; d) Langowski, J. L.; Zhang, X.; Wu, L.; Mattson, J. D.; Chen, T.; Smith, K.; Basham, B.; McClanahan, T.; Kastelein, R. A.; Oft, M. *Nature* **2006**, *442*, 461–465.
- 39 Aggarwal, B. B. *Nat Rev Immunol* **2003**, *3*, 745–56.
- 40 Balkwill, F. *Cytokine Growth Factor Rev* **2002**, *13*, 135–41.
- 41 Courtois, G.; Gilmore, T. D. *Oncogene* **2006**, *25*, 6831–6843.

-
- 42 a) Carbia-Nagashima, A.; Gerez, J.; Perez-Castro, C.; Paez-Pereda, M.; Silberstein, S.; Stalla, G. K.; Holsboer, F.; Arzt, E. *Cell* **2007**, *131*, 309–323; b) Mizukami, Y.; Jo, W. S.; Duerr, E. M.; Gala, M.; Li, J.; Zhang, X.; Zimmer, M. A.; Iliopoulos, O.; Zukerberg, L. R.; Kohgo, Y.; Lynch, M. P.; Rueda, B. R.; Chung, D. C. *Nature Med* **2005**, *11*, 992–997; c) Rius, J.; Guma, M.; Schachtrup, C.; Akassoglou, K.; Zinkernagel, A. S.; Nizet, V.; Johnson, R. S.; Haddad, G. G.; Karin, M. *Nature* **2008**, *453*, 807–811.
- 43 a) Greten, F. R.; Eckmann, L.; Greten, T. F.; Park, J. M.; Li, Z. W.; Egan, L. J.; Kagnoff, M. F.; Karin, M. *Cell* **2004**, *118*, 285–296; b) Pikarsky, E.; Porat, R. M.; Stein, I.; Abramovitch, R.; Amit, S.; Kasem, S.; Gutkovich-Pyest, E.; Urieli-Shoval, S.; Galun, E.; Ben-Neriah, Y. *Nature* **2004**, *431*, 461–466.
- 44 a) Garlanda, C.; Riva, F.; Veliz, T.; Polentarutti, N.; Pasqualini, F.; Radaelli, E.; Sironi, M.; Nebuloni, M.; Zorini, E. O.; Scanziani, E.; Mantovani, A. *Cancer Res* **2007**, *67*, 6017–6021; b) Xiao, H.; Gulen, M. F.; Qin, J.; Yao, J.; Bulek, K.; Kish, D.; Altuntas, C. Z.; Wald, D.; Ma, C.; Zhou, H.; Tuohy, V. K.; Fairchild, R. L.; de la Motte, C.; Cua, D.; Vallance, B. A.; Li, X. *Immunity* **2007**, *26*, 461–475.
- 45 Biswas, S. K.; Gangi, L.; Paul, S.; Schioppa, T.; Saccani, A.; Sironi, M.; Bottazzi, B.; Doni, A.; Vincenzo, B.; Pasqualini, F.; Vago, L.; Nebuloni, M.; Mantovani, A.; Sica, A. *Blood* **2006**, *107*, 2112–2122.
- 46 Saccani, A.; Schioppa, T.; Porta, C.; Biswas, S. K.; Nebuloni, M.; Vago, L.; Bottazzi, B.; Colombo, M. P.; Mantovani, A.; Sica, A. *Cancer Res* **2006**, *66*, 11432–11440.
- 47 Cha YI, Solnica-Krezel L, Dubois RN. *Dev Biol* **2006**; *289*, 263–272.
- 48 Bombardier C, Laine L, Reicin A, Shapiro D, Burgos-Vargas R, Davis B, Day R, Ferraz MB, Hawkey CJ, Hochberg MC, Kvien TK, Schnitzer TJ; *Engl J Med* **2000**; *343*, 1520–1528.

-
- 49 Nussmeier NA, Whelton AA, Brown MT, Langford RM, Hoelt A, Parlow JL, Boyce SW, Verburg KM. *N Engl J Med* **2005**; 352, 1081–1091.
- 50 Gislason GH, Jacobsen S, Rasmussen JN, Rasmussen S, Buch P, Friberg J, Schramm TK, Abildstrom SZ, Kober L, Madsen M, Torp-Pedersen C. *Circulation* **2006**; 113, 2906–2913.
- 51 Mukherjee D, Nissen SE, Topol EJ. *JAMA*. **2001**; 286, 954–959.
- 52 Van Rees BP, Sivula A, Thoren S, Yokozaki H, Jakobsson, PG, Offerhaus JA, Ristimäki A *Int J Cancer* **2003**; 107, 551–556.
- 53 Yucel-Lindberg T, Hallstrom T, Kats A, Mustafa M, Modeer T. *Inflammation* **2004**; 28, 89–95.
- 54 Mustafa M, Wondimu B, Yucel-Lindberg T, Kats-Hallstrom AT, Jonsson AS, Modeer T. *J Clin Periodontol* **2005**; 32, 6–11.
- 55 Wang M, Zukas AM, Hui Y, Ricciotti E, Pure E, Fitzgerald GA. *Proc Natl Acad Sci USA* **2006**; 103, 14507–14512.
- 56 Wu D, Mennerich D, Arndt K, Sugiyama K, Ozaki N, Schwarz K, Wei J, Wu H, Bishopric NH, Doods H. *Prostag Ot Lipid M* **2009**; 90, 21–25.
- 57 Wu D, Mennerich D, Arndt K, Sugiyama K, Ozaki N, Schwarz K, Wei J, Wu H, Bishopric NH, Doods H. *Prostag Leukotr Essent Fatty Acids*. **2009**; 81, 31–33.
- 58 Cheng Y, Wang M, Yu Y, Lawson J, Funk CD, Fitzgerald GA. *J Clin Invest* **2006**; 116, 1391–1399.
- 59 Von Rahden BH, Stein HJ, Hartl SA *Dis Esophagus*. **2008**; 21, 304–308.
- 60 Nardone G, Rocco A, Vaira D, Staibano S, Budillon G, Tatangelo F, Sciulli MG, Perna F, Salvatore G, Di Benedetto M, *J Pathol* **2004**; 202, 305–312.
- 61 Jang TJ. *Virchows Arch* **2004**; 445, 564–571.

-
- 62 Gudis K, Tatsuguchi A, Wada K *Hum Pathol* **2007**; 38, 1826–1835.
- 63 Nonaka K, Fujioka H, Takii Y, Abiru S, Migita K, Ito M, Kanematsu T, Ishibashi H *World J Gastroenterol* **2010**; 16, 4846–4853.
- 64 Kawata R, Hyo S, Araki M, Takenaka H. *Auris Nasus Larynx* **2010**; 37, 482–487.
- 65 Uematsu S, Matsumoto M, Takeda K, Akira S. *J Immunol* **2002**; 168, 5811–5816.
- 66 Naraba H, Yokoyama C, Tago N *J Biol Chem* **2002**; 277, 28601–28608.
- 67 Trebino CE, Stock JL, Gibbons CP *Proc Natl Acad Sci USA* **2003**; 100, 9044–9049.
- 68 Kamei D, Yamakawa K, Takegoshi Y *J Biol Chem* **2004**; 279, 33684–33695.
- 69 Jegerschöld, C.; Pawelzik, S. C.; Purhonen, P.; Bhakat, P.; Gheorghe, K. R.; Gyobu, N.; Mitsuoka, K.; Morgenstern, R.; Jakobsson, P. J.; Hebert, H. *Proc Natl Acad Sci USA* **2008**, 105, 11110–11115.
- 70 Xing L, Kurumbail RG, Frazier RB, Davies M. S., Fujiwara H., Weinberg R. A., Gierse J. K., Caspers N., Carter J. S., McDonald J. J., Moore W. M., Vazquez M. L. *J Comput Aided Mol Des* **2009**; 23, 13–24.
- 71 Hetu PO, Ouellet M, Falguyret JP, Ramachandran C, Robichaud J, Zamboni R, Riendeau D. *Arch Biochem Biophys* **2008**; 477, 155–162.
- 72 Sjögren, T.; Nord, J.; Ek, M.; Johansson, P.; Liu, G.; Geschwindner, S. *Proc Natl Acad Sci USA* **2013**, 110, 3806–3811.
- 73 Li, D.; Howe, N.; Dukkipati, A.; Shah, S. T.; Bax, B. D.; Edge, C.; Bridges, A.; Hardwicke, P.; Singh, O. M.; Giblin, G.; Pautsch, A.; Pfau, R.; Schnapp, G.; Wang, M.; Olieric, V.; Caffrey, M. *Cryst. Growth Des* **2014**, 14, 2034–2047.

-
- 74 Luz JG, Antonysamy S, Kuklish SL, Condon B, Lee MR, Allison D, Yu XP, Chandrasekhar S, Backer R, Zhang A, Russell M, Chang SS, Harvey A, Sloan AV, Fisher MJ. *J Med Chem* **2015**; 58, 4727-37.
- 75 Wu, T. Y.; Juteau, H.; Ducharme, Y.; Friesen, R. W.; Guiral, S.; Dufresne, L.; Poirier, H.; Salem, M.; Riendeau, D.; Mancini, J.; Brideau, C. *Bioorg Med Chem Lett* **2010**, 20, 6978–6982.
- 76 Cote, B.; Boulet, L.; Brideau, C.; Claveau, D.; Ethier, D.; Frenette, R.; Gagnon, M.; Giroux, A.; Guay, J.; Guiral, S.; Mancini, J.; Martins, E.; Massé, F.; Méthot, N.; Riendeau, D.; Rubin, J.; Xu, D.; Yu, H.; Ducharme, Y.; Friesen, R. W. *Bioorg Med Chem Lett* **2007**, 17, 6816–6820.
- 77 Riendeau, D.; Aspiotis, R.; Ethier, D.; Gareau, Y.; Grimm, E. L.; Guay, J.; Guiral, S.; Juteau, H.; Mancini, J. A.; Méthot, N.; Rubin, J.; Friesen, R. W. *Bioorg Med Chem Lett* **2005**, 15, 3352–3355.
- 78 Olofsson, K.; Suna, E.; Pelcman, B.; Ozola, V.; Katkevics, M.; Kalvins, I. International Patent Publication WO 2005/123673 A1, **2005**.
- 79 Chang, H. H.; Meuillet, E. J. *Future Med Chem* **2011**, 3, 1909-1934.
- 80 Mancini JA, Blood K, Guay J, gordon R, Claveau D, Chan CC *J Biol Chem* **2001**; 276, 4469–4475.
- 81 Riendeau D, Aspiotis R, Ethier D, Gareau Y.; Grimm E. L.; Guay J.; Guiral S.; Juteau H.; Mancini J. A.; Methot N.; Rubin J.; Friesen R. W. *Bioorg Med Chem Lett* **2005**; 15, 3352–3355.
- 82 Koeberle, A.; Werz, O. *Biochem Pharmacol* **2015**, 98, 1-5.
- 83 Koeberle, A.; Werz, O. *Curr Med Chem* **2009**, 16, 4274-4296.
- 84 Korotkova, M.; Jakobsson, P. J. *Basic Clin Pharmacol Toxicol* **2014**, 114, 64-69.
- 85 Gilbert, N.C.; Bartlett, S.G.; Waight, M.T.; Neau, D.B.; Boeglin, W.E.; Brash, A.R., Newcomer, M.E. *Science* **2011**, 331, 217-219.

-
- 86 Carter, G. W., Young, P. R., Albert, D. H., Bouska, J., Dyer, R., Bell, R. L., Summers, J. B., Brooks, D. W. *J Pharmacol Exp Ther* **1991**, *256*, 929–937.
- 87 Jakobsson, P. J.; Thorén, S.; Morgenstern, R.; Samuelsson, B. *Proc Natl Acad Sci USA* **1999**, *96*, 7220–7225.
- 88 Friesen, R. W.; Mancini, J. A. *J Med Chem* **2008**, *51*, 4059–4067.
- 89 Murakami, M.; Naraba, H.; Tanioka, T.; Semmyo, N.; Nakatani, Y.; Kojima, F.; Ikeda, T.; Fueki, M.; Ueno, A.; Oh, S.; Kudo, I. *J Biol Chem* **2000**, *275*, 32783–32792.
- 90 a) Nakanishi, M.; Gokhale, V.; Meuillet, E. J., Rosenberg, D. W. *Biochimie* **2010**, *92*, 660-664; b) Rådmark, O.; Samuelsson, B. *J Intern Med* **2010**, *268*, 5–14.
- 91 Chini, M. G.; Ferroni, C.; Cantone, V.; Dambrosio, P.; Varchi, G.; Pepe, A.; Fischer, K.; Pergola, C.; Werz, O.; Bruno, I.; Riccio, R.; Bifulco, G. *Med Chem Comm* **2015**, *6*, 75-79.
- 92 Maione, F.; Cantone, V.; Chini, M. G.; De Feo, V.; Mascolo, N.; Bifulco, G. *Fitoterapia* **2014**, *100C*, 174-178.
- 93 Masullo, M.; Cantone, V.; Cerulli, A.; Lauro, G.; Messano, F.; Russo, G. L.; Pizza, C.; Bifulco, G.; Piacente, S. *J Nat. Prod* **2015**, *78*, 2975-82.
- 94 Koeberle, A.; Werz, O. *Curr Med Chem* **2009**, *16*, 4274–4296.
- 95 De Simone, R.; Chini, M.G.; Bruno, I.; Riccio, R.; Mueller, D.; Werz, O.; Bifulco, G. *J Med Chem* **2011**, *54*, 1565–1575.
- 96 Chini, M. G.; De Simone, R.; Bruno, I.; Riccio, R.; Dehmb, F.; Weinigel, C.; Barz, D.; Werz, O.; Bifulco, G. *Eur. J Med Chem* **2012**, *54*, 311-323.
- 97 Congreve, M.; Chessari, G.; Tisi, D.; Woodhead A. J. *J Med Chem* **2008**, *51*, 3661-3680.
- 98 Shelke, S. V.; Cutting, B.; Jiang, X.; Koliwer-Brandl, H.; Strasser, D. S., Schwaradt, O.; Kelm, S.; Ernst, B. *Angew Chem Int Ed* **2010**, *49*, 5721–5725.

-
- 99 Nestler, H. P. *Curr. Drug Discovery Technol* **2005**, *2*, 1-12.
- 100 Sreeman, W.; Mamidyala, K.; Finn, M. G. *Chem Soc Rev* **2010**, *39*, 1252–126.
- 101 Moses, J. E.; Moorhouse, A. D. *Chem Soc Rev* **2007**, *36*, 1249–1262.
- 102 Rees, D. C.; Congreve, M.; Murray, C. W.; Carr, R. *Nat Rev Drug Discovery* **2004**, *3*, 660-672.
- 103 Kolb, H. C.; Sharpless, K. B. *DDT* **2003**, *8*, 1128-1137.
- 104 Sharpless, K. B.; Manetsch, R. *Expert Opinion on Drug Discovery* **2006**, *1*, 525-538.
- 105 Halgren, T. A.; Murphy, R. B.; Friesner, R. A.; Beard, H. S.; Frye, L. L.; Pollard, W. T.; Banks, J. L. *J Med Chem* **2004**, *47*, 1750.
- 106 Koeberle A, Siemoneit U, Buehring U, Northoff H, Laufer S, Albrecht W, Werz O. *J Pharmacol Exp Ther* **2008**, *326*, 975–982.
- 107 Fischer L, Szellas D, Radmark O, Steinhilber D, Werz O. *FASEB* **2003**, *17*, 949–951.
- 108 Bonito MC, Cicala C, Marcotullio MC, Maione F, Mascolo N. *Nat Prod Commun* **2011**, *6*, 1205-1215.
- 109 Giamperi L, Bucchini A, Bisio A, Giacomelli E, Romussi G, Ricci D. *Nat Prod Commun* **2012**, *7*, 201-202.
- 110 Bauer J, Kuehnl S, Rollinger JM, Scherer O, Northoff H, Stuppner H, Werz O, Koeberle A. *J Pharmacol Exp Ther* **2012**, *342*, 169-176.
- 111 Chae IG, Yu MH, Im NK, Jung YT, Lee J, Chun KS, Lee IS. *J Med Food*. **2012**, *15*, 879-886.
- 112 Bauer J, Kuehnl S, Rollinger JM, Scherer O, Northoff H, Stuppner H, Werz O, Koeberle A. *J Pharmacol Exp Ther*. **2012**, *342*, 169-176.
- 113 Villa C, Trucchi B, Bertoli A, Pistelli L, Parodi A, Bassi AM, Ruffoni B. *Int J Cosmet Sci* **2009**, *31*, 55-61.

-
- 114 Poeckel D, Greiner C, Verhoff M, Rau O, Tausch L, Hornig C, Steinhilber D, Schubert-Zsilavec M, Werz O. *Biochem Pharmacol* **2008**, 76, 91-97.
- 115 Kortz L, Dorow J, Ceglarek U. *J Chromatogr B*. **2014**, 1, 1-11
- 116 Schaible, A.M.; Traber, H.; Temml, V.; Noha, S.M.; Filosa, R.; Peduto, A. *Biochem Pharmacol* **2013**, 86, 476–486.
- 117 Davi G, Patrono C. *New Engl J Med* **2007**, 357, 2482–2494.
- 118 Kahner BN, Shankar H, Murugappan S, Prasad GL, Kunapuli SP. *J Thromb Haemostasis* **2006**, 4, 2317–2326.
- 119 Gaglia MAJr, Manoukian SV, Waksman P. *Am Heart J* **2010**, 160, 595–604.
- 120 Angiolillo DJ, Fernandez-Ortiz A, Bernardo E, Alfonso F, Macaya C, Bass TA *J Am Coll Cardiol* **2007**, 49, 1505–1516.
- 121 Bonito MC, Cicala C, Marcotullio MC, Maione F, Mascolo N. *Nat Prod Commun* **2011**, 6, 1205-1215.
- 122 Maione F, Cicala C, Musciacco G, De Feo V, Amat AG, Ialenti A. *Nat Prod Commun* **2013**, 8, 539-544.
- 123 Newman DJ, Cragg GM. *J Nat Prod* **2012**, 75, 311-335.
- 124 Maione F, De Feo V, Caiazzo E, De Martino L, Cicala C, Mascolo N. *J Ethnopharmacol* **2014**, 155, 1236-1242.
- 125 Chen W, Liu L, Luo Y, Odaka Y, Awate S, Zhou H *Cancer Prev Res* **2012**, 5, 778–787.
- 126 Feng H, Xiang H, Zhang J, Liu G, Guo N, Wang X. *J Biomed Biotechnol* **2009**; 78, 1-8.
- 127 Lee DS, Lee SH, Noh JG, Hong SD. *Biosci Biotechnol Biochem* **1999**, 63, 2236–2239.
- 128 Zhang J, Zhang K, Gao ZG, Paoletta S, Zhang D, Han GW *Nature* **2014**, 509, 115-118.
- 129 Trott O, Olson AJ. *J Comput Chem* **2010**, 31, 455-461.

-
- 130 Bach P, Boström J, Brickmann K, van Giezenb JJJ, Groneberg RD, Harvey DM. *Eur J Med Chem* **2013**, *65*, 360–375.
- 131 Jagroop IA, Burnstock G, Mikhailidis DP. *Platelets* **2003**, *14*, 15–20.
- 132 Zhang J, Zhang K, Gao ZG, Paoletta S, Zhang D, Han GW *Nature* **2014**, *509*, 119-122.
- 133 Chen X, Guo J, Bao J, Lu J, Wang Y. *Med Res Rev* **2014**, *34*, 768–794.
- 134 Kwak HB, Sun HM, Ha H, Kim HN, Lee JH, Kim HH *Eur J Pharmacol* **2008**, *601*, 30-37.
- 135 Della Monica, C.; Randazzo, A.; Bifulco, G.; Cimino, P.; Aquino, M.; Izzo, I.; De Riccardis, F.; Gomez-Paloma, L. *Tetrahedron Lett* **2002**, *43*, 5707-5710.
- 136 Chini, M. G.; Riccio, R.; Bifulco, G. *Magn Reson Chem* **2008**, *46*, 962-968.
- 137 Sarotti, A. M.; Pellegrinet, S. C. *J Org Chem* **2009**, *74*, 7254-7260.
- 138 Sarotti, A. M.; Pellegrinet, S. C. *J Org Chem* **2012**, *77*, 6059-6065.
- 139 Derome, A. E. *Modern NMR Techniques for Chemistry Research*; **1987**.
- 140 a) Hehre, W. J.; Radom, L.; Schleyer, P. V. R.; Pople, J. A. *Ab initio Molecular Orbital Theory*; Wiley: New York, **1986**; b) Nàray-Szabó, G.; Surján, P. R.; Ángyán, S. G. In *Applied Quantum Chemistry*; Reidel: Boston, 1897; c) van Gunsteren, W. F.; Berendsen, H. J. C. *Angew Chem Int Ed Engl* **1990**, *29*, 992-1023; d) Höltje, H. D.; Folkers, G. *Molecular Modeling Basic Principles and Applications*; Eds.; Mannhold, R.; Kubinyi H.; Timmerman, H., VCH: Weinheim New York, Vol. 5; e) Allinger, N. L.; Zhu, Z.-q. S.; Chen, K. *J Am Chem Soc* **1992**, *114*, 6120-6133; f) Allinger, N. L.; Rodriguez, S.; Chen, K. *Theochem* **1992**, *92*, 161-178; g) Weiner, P. K.; Kollman, P. A. *J Comp Chem* **1981**, *2*, 287-303; h) Weiner, S. J.; Kollman, P. A.; Case, D. A.; Singh, U. C.; Ghio, C.; Alagona, G.; Profeta, S.; Weiner,
-

-
- P. *J Am Chem Soc* **1984**, *106*, 765-784; i) Kollman, P. A.; Merz, K. M. *Acc. Chem Res* **1990**, *23*, 246-252.
- 141 Kuntz, I. D.; Blaney, J. M.; Oatley, S. J.; Langridge, R.; Ferrin, T. E. *J Mol Biol* **1982**, *161*, 269-288.
- 142 Rarey, M.; Kramer, B.; Lengauer, T.; Klebe, G. *J Mol Biol* **1996**, *261*, 470-489.
- 143 Jones, G.; Willett, P.; Glen, R. C.; Leach, A. R.; Taylor, R. *J Mol Biol* **1997**, *267*, 727-748.
- 144 Morris, G. M.; Goodsell, D. S.; Halliday, R. S.; Huey, R.; Hart, W. E.; Belew, R. K.; Olson, A. *J Comput Chem* **1998**, *19*, 1639-1662.
- 145 Huey, R.; Morris, G. M.; Olson, A. J.; Goodsell, D. S. *J Comput Chem* **2007**, *28*, 1145-1152.
- 146 Morris, G. M.; Huey, R.; Lindstrom, W.; Sanner, M. F.; Belew, R. K.; Goodsell, D. S.; Olson, A. *J Comput Chem* **2009**, *30*, 2785-2791.
- 147 Trott, O.; Olson, A. J. *J Comput Chem* **2010**, *31*, 455-461.
- 148 Friesner, R. A.; Banks, J. L.; Murphy, R. B.; Halgren, T. A.; Klicic, J. J.; Mainz, D. T.; Repasky, M. P.; Knoll, E. H.; Shelley, M.; Perry, J. K.; Shaw, D. E.; Francis, P.; Shenkin, P. S. *J Med Chem* **2004**, *47*, 1739-1749.
- 149 a) Halperin, I.; Ma, B.; Wolfson, H.; Nussinov, R. *Proteins* **2002**, *47*, 409-443; b) Kitchen, D. B.; Decornez, H.; Furr, J. R.; Bajorath, J. *Nat Rev Drug Discovery* **2004**, *3*, 935-949.
- 150 a) Verkhivker, G. M.; Bouzida, D.; Gehlhaar, D. K.; Rejto, P. A.; Arthurs, S.; Colson, A. B.; Freer, S. T.; Larson, V.; Luty, B. A.; Marrone, T.; Rose, P. W. *J Comput- Aided Mol Des* **2000**, *14*, 731-751; b) Watson, J. D.; Laskowski, R. A.; Thornton, J. M. *Curr Opin Struct Biol* **2005**, *15*, 275-284; c) Arakaki, A. K.; Zhang, Y.; Skolnick, J. *Bioinformatics* **2004**, *20*, 1087-1096; d) Park, H.; Lee, J.; Lee, S.

-
- Proteins* **2006**, *65*, 549-554, e) Hetenyi, C.; Van Der Spoel, D. *Protein Sci* **2002**, *11*, 1729-1737.
- 151 Leach, A. R. *Molecular Modelling: Principles and Applications*, Addison Wesley Longman Limited, Harlow, **1996**.
- 152 Brooijmans, N.; Kuntz, I. D. *Annu Rev Biophys Biomol Struct* **2003**, *32*, 335–373.
- 153 Di Nola, A.; Berendsen, H. J. C.; Roccatano, D. *Proteins* **1994**, *19*, 174–182.
- 154 Sousa, S. F.; Fernandes, P. A.; Ramos, M. J. *Proteins* **2006**, *65*, 15-26.
- 155 Park, H.; Lee, J.; Lee, S. *Proteins* **2006**, *65*, 549-554.
- 156 Gilson, M. K.; Zhou, H.-X.; *Annu Re Biophys Biomole Struct* **2007**, *36*, 21-42.
- 157 a) Gilson, M.; Given, J.; Bush, B.; McCammon, J. *Biophys J* **1997**, *72*, 1047-1069; b) Chang, C.-E. A.; Chen, W.; Gilson, M. K. *Proc Nat Acad Sci USA* **2007**, *104*, 1534-1539.
- 158 Schaible, A.M.; Traber, H.; Temml, V.; Noha, S.M., Filosa, R., Peduto, A. *Biochem Pharmacol* **2013**, *86*, 476–486.
- 159 Seco, J. M.; Quiñoà, E.; Riguera, R. *Chem. Rev.* **2004**, *104*, 17-117.
- 160 Nicolaou, K. C.; Snyder, S. A. *Angew Chem Int Ed Engl* **2005**, *44*, 1012-1044.
- 161 Bifulco, G.; Dambruoso, P.; Gomez-Paloma, L.; Riccio, R. *Chem Rev* **2007**, *107*, 3744-3779.
- 162 Karplus, M. *J Chem Phys* **1959**, *30*, 11-15.
- 163 Overhauser, A. W. *Phys Rev* **1953**, *92*, 411-415.
- 164 Barone, G.; Gomez-Paloma, L.; Duca, D.; Silvestri, A.; Riccio, R.; Bifulco, G. *Chem Eur J* **2002**, *8*, 3233-3329.
- 165 Barone, G.; Duca, D.; Silvestri, A.; Gomez-Paloma, L.; Riccio, R.; Bifulco, G. *Chem Eur J* **2002**, *8*, 3240-3245.

-
- 166 a) Cheeseman, J. R.; Trucks, G. W.; Keith, T. A.; Frisch, M. J. *J Chem Phys* **1996**, *104*, 5497-5509.
- 167 Cimino, P.; Duca, D.; Gomez-Paloma, L.; Riccio, R.; Bifulco, G. *Magn Reson Chem* **2004**, *42*, S26-S33.
- 168 a) Elyashberg, M.; Blinov, K.; Williams, A. *Magn Reson Chem* **2009**, *47*, 371–389; b) Elyashberg, M. E.; Blinov, K. A.; Williams, A. J. *Magn Reson Chem* **2009**, *47*, 333–341; c) Elyashberg, M.; Blinov, K.; Molodtsov, S.; Smurnyy, Y.; Williams, A. J.; Churanova, T. *J Chem Inf* **2009**, *3*, 1-26.
- 169 a) Elyashberg, M. E.; Williams, A. J.; Martin, G. E. *Prog NMR Spectrosc* **2008**, *53*, 1-104; b) Blinov, K. A.; Smurnyy, Y. D.; Churanova, T. S.; Elyashberg, M. E.; Williams, A. J. *Chemom Intell Lab Syst* **2009**, *97*, 91-97; c) Blinov, K. A.; Smurnyy, Y. D.; Elyashberg, M. E.; Churanova, T. S.; Kvasha, M.; Steinbeck, C.; Lefebvre, B. A.; Williams, A. J. *J Chem Inf Model* **2008**, *48*, 550-555; d) Smurnyy, Y. D.; Blinov, K. A.; Churanova, T. S.; Elyashberg, M. E.; Williams, A. J. *J Chem Inf Model* **2008**, *48*, 128-134.
- 170 a) Ditchfield, R. J. *Chem Phys* **1972**, *56*, 5688–5691; b) Wolinski, K.; Hinton, J. F.; Pulay, P. *J Am Chem Soc* **1990**, *112*, 8251–8260.
- 171 a) van Gunsteren, W. F.; Berendsen, H. J. C. *Angew Chem, Int. Ed.* **1990**, *29*, 992-1023; b) Höltje, H. D.; Sippl, W.; Folkers, G. *Molecular Modeling Basic Principles and Applications* (Eds.: R. Mannhold, H. Kubinyi, H. Timmerman), Wiley-VCH, Weinheim, New York, **2003**.
- 172 Chang, G.; Guida, W. C.; Still, W. C. *J Am Chem Soc* **1989**, *111*, 4379–4386.
- 173 Dewar, M. J. S.; Zoebisch, E. G.; Healy, E. F.; Stewart, J. J. P. *Am Chem Soc* **1985**, *107*, 3902–3909.
- 174 Stewart, J. J. P. *J Comput Chem* **1989**, *10*, 209-220.

-
- 175 P. Hohenberg, W. Kohn, *Phys. Rev. B* **1964**, *136*, 864-871; b) W. Kohn, L. J. Sham, *Phys Re A* **1965**, *140*, 1133-1138.
- 176 Bifulco, G.; Bassarello, C.; Riccio, R.; Gomez-Paloma, L. *Org Lett* **2004**, *6*, 1025–1028.
- 177 Schrödinger *LLC New York NY* **2013**.
- 178 Jorgensen, W. L.; Tiradorives, J. *JACS* **1988**, *110*, 1657-1666.
- 179 Frisch, M. J. T., G. W.; Schlegel, H. B.; Scuseria, G. E.; Robb, M. A.; Cheeseman, J. R.; Scalmani, G.; Barone, V.; Mennucci, B.; Petersson, G. A.; Nakatsuji, H.; Caricato, M.; Li, X.; Hratchian, H. P.; Izmaylov, A. F.; Bloino, J.; Zheng, G.; Sonnenberg, J. L.; Hada, M.; Ehara, M.; Toyota, K.; Fukuda, R.; Hasegawa, J.; Ishida, M.; Nakajima, T.; Honda, Y.; Kitao, O.; Nakai, H.; Vreven, T.; Montgomery, J. A., Jr.; Peralta, J. E.; Ogliaro, F.; Bearpark, M.; Heyd, J. J.; Brothers, E.; Kudin, K. N.; Staroverov, V. N.; Kobayashi, R.; Normand, J.; Raghavachari, K.; Rendell, A.; Burant, J. C.; Iyengar, S. S.; Tomasi, J.; Cossi, M.; Rega, N.; Millam, J. M.; Klene, M.; Knox, J. E.; Cross, J. B.; Bakken, V.; Adamo, C.; Jaramillo, J.; Gomperts, R.; Stratmann, R. E.; Yazyev, O.; Austin, A. J.; Cammi, R.; Pomelli, C.; Ochterski, J. W.; Martin, R. L.; Morokuma, K.; Zakrzewski, V. G.; Voth, G. A.; Salvador, P.; Dannenberg, J. J.; Dapprich, S.; Daniels, A. D.; Farkas, Ö.; Foresman, J. B.; Ortiz, J. V.; Cioslowski, J.; Fox, D. J. *Gaussian 09, Revision A.02*, Gaussian, Inc., Wallingford CT, **2009**.